

# Cosmic rays across the star-forming galaxy sequence. II: Stability limits and the onset of cosmic ray-driven outflows

Roland M. Crocker,<sup>1</sup><sup>★</sup> Mark R. Krumholz,<sup>1</sup> and Todd A. Thompson,<sup>2</sup>

<sup>1</sup>*Research School of Astronomy and Astrophysics, Australian National University, Canberra 2611, A.C.T., Australia*

<sup>2</sup>*Department of Astronomy and Center for Cosmology & Astro-Particle Physics, The Ohio State University, Columbus, Ohio 43210, U.S.A*

Accepted XXX. Received YYY; in original form ZZZ

## ABSTRACT

Cosmic rays (CRs) are a plausible mechanism for launching winds of cool material from the discs of star-forming galaxies. However, there is no consensus on what types of galaxies likely host CR-driven winds, or what role these winds might play in regulating galaxies’ star formation rates. Using a detailed treatment of the transport and losses of hadronic CRs developed in the previous paper in this series, here we develop a semi-analytic model that allows us to assess the viability of using CRs to launch cool winds from galactic discs. In particular, we determine the critical CR fluxes – and corresponding star formation rate surface densities – above which hydrostatic equilibrium within a given galaxy is precluded because CRs drive the gas off in a wind or otherwise render it unstable. We show that, for star-forming galaxies with lower gas surface densities typical of the Galaxy and local dwarfs, the locus of this CR stability curve patrols the high side of the observed distribution of galaxies in the Kennicutt-Schmidt parameter space of star formation rate versus gas surface density. However, hadronic losses render CRs unable to drive winds in galaxies with higher surface densities. Our results show that quiescent, low surface density galaxies like the Milky Way are poised on the cusp of instability, such that small changes to ISM parameters can lead to the launching of CR-driven outflows, and we suggest that, as a result, CR feedback sets an ultimate limit to the star formation efficiency of most modern galaxies.

**Key words:** hydrodynamics – instabilities – ISM: jets and outflows – radiative transfer – galaxies: ISM – cosmic rays

## 1 INTRODUCTION

This paper is the third in a series (Krumholz et al. 2020; Crocker et al. 2020a, hereafter Paper I) exploring the physics of relativistic cosmic ray (CR) transport, energy loss, and radiation in the interstellar media of star-forming galaxies, and, more importantly, the dynamical impact of CRs in such environments. In particular, our intention in this series is to investigate, in broad brush strokes, the potential importance of CRs as an agent of *feedback* in star-forming galaxies: What role, if any, do CRs have – as a function of environmental parameters – in establishing the remarkably low efficiency with which galaxies convert into stars the gas flowing out of the cosmic web and into their own interstellar media?

As discussed in Paper I and previously literature, CRs are a plausible agent of star formation feedback for a number of reasons: While this non-thermal particle population receives only a sub-dominant fraction,  $\sim 10\%$ , of the to-

tal kinetic energy liberated in supernova explosions, unlike the thermal gas (that receives most of the supernova energy), CRs lose energy to radiation very slowly. This means that, from their injection sites close to the midplanes of star-forming galaxies, CRs tend to disperse well out into these galaxies’ interstellar media<sup>1</sup>. Within the Milky Way disc, the CR energy density is near equipartition with the magnetic field and turbulent gas motions, implying CRs contribute significantly to establishing the vertical hydrostatic equilibrium of the gas (e.g., Bouldes & Cox 1990) and maintain, therefore, the conditions under which sustained, quiescent star-formation can proceed.

Moreover, given their soft effective equation of state<sup>2</sup>, CRs come to increasingly dominate the total energy density of a co-mingled astrophysical fluid of thermal and non-

<sup>1</sup> In fact, in many cases, including for the Milky Way, they may escape the galactic disc completely.

<sup>2</sup> That follows from the fact that the energetically dominant cosmic ray population is relativistic, i.e., adiabatic index  $\gamma_c \rightarrow 4/3$ .

<sup>★</sup> E-mail: rcrocker@fastmail.fm (RMC)

thermal particles that is suffering adiabatic losses under expansion in an outflow. Thus CRs can help sustain galactic winds by providing a distributed heating source via their non-adiabatic energy losses which, in this situation, are mostly mediated by the streaming instability (e.g., [Everett et al. 2008](#); [Zweibel 2017](#); [Ruszkowski et al. 2017](#)). Despite, however, the early recognition of their potential importance in driving winds ([Ipavich 1975](#); [Breitschwerdt et al. 1991](#); [Zirakashvili et al. 1996](#); [Ptuskin et al. 1997](#)), the possibility that CRs might generically be an important source of feedback in galaxy formation has only recently begun to receive much sustained attention, in either phenomenological (e.g., [Zirakashvili & Völk 2006](#); [Everett et al. 2008](#); [Samui et al. 2010](#); [Crocker et al. 2011](#); [Crocker 2012](#); [Lacki et al. 2011](#); [Hanasz et al. 2013](#); [Yoast-Hull et al. 2016](#)), or numerical models (e.g., [Jubelgas et al. 2008](#); [Wadepuhl & Springel 2011](#); [Uhlig et al. 2012](#); [Booth et al. 2013](#); [Salem & Bryan 2014](#); [Salem et al. 2016](#); [Pakmor et al. 2016](#); [Simpson et al. 2016](#); [Recchia et al. 2016, 2017](#); [Ruszkowski et al. 2017](#); [Pfrommer et al. 2017](#); [Chan et al. 2019](#); [Buck et al. 2019](#)). Even so, there remains significant disagreement in the literature about where and when CRs might be important: some authors conclude they are capable of driving galactic winds only off the most rapidly star-forming galaxies (e.g., [Socrates et al. 2008](#)), while others find they drive winds only in dwarfs, (e.g., [Jubelgas et al. 2008](#); [Uhlig et al. 2012](#)), and yet others that they do not drive winds by themselves at all, but can reheat and energise winds launched by other processes (e.g. [Ruszkowski et al. 2017](#)).

Thus, a first-principles effort to understand where and when CRs might be important, taking into account all the available observational constraints, seems warranted, and this is the primary goal of this and our previous paper. Having explored the theory and observational consequences of CR transport in the largely neutral gas phase from which star form ([Krumholz et al. 2020](#)), here and in our previous paper ([Paper I](#)), we seek to cut a broad swathe across the parameter space of star-forming galaxies, and determine where within this parameter space CRs might be important agents of feedback. We break this task down into two parts. [Paper I](#) addresses the question: What fraction of the total ISM pressure is typically supplied by CRs as a function of galaxy parameters? In other words: How important to the overall gas dynamics in typical star-forming galaxies can CRs be? In this paper we use the mathematical set-up of our previous papers to address a rather specific, follow-up question: What is the critical flux of cosmic rays above which a hydrostatic equilibrium within a given column of gas is precluded? In other words: At what point do cosmic rays – accelerated as a result of the star formation process itself – start to drive outflows in galaxies? We emphasise that we are not addressing the question of whether CRs can re-accelerate or re-heat winds that have been launched by other mechanisms, a question addressed by a number of previous authors as discussed above. Instead, we seek to determine under what conditions it becomes inevitable that the CRs themselves begin to lift neutral interstellar gas out of galactic discs, certainly rendering the neutral gas atmosphere unstable, and potentially giving rise to a cool galactic wind.

The remainder of this paper is structured as follows: in [Section 2](#) we briefly recap the mathematical setup of the problem and, in particular, write down the ordinary differen-

tial equation (ODE) system that describes a self-gravitating gaseous disc that maintains a quasi-hydrostatic equilibrium while subject to a flux of CRs injected at its midplane; in [Section 3](#) we present, describe, and evaluate the numerical solutions of our ODEs; in [Section 4](#) we consider the astrophysical implications of our findings for CR feedback on the dense, star-forming gas phase of spiral galaxies; we further discuss our results and summarise in [Section 5](#).

## 2 SETUP

### 2.1 Physical Model: Recapitulation

We provide a detailed description of the physical system we model in the companion paper ([Paper I](#)). In brief, our model is similar to one previously invoked by us in studies of radiation pressure feedback ([Krumholz & Thompson 2012, 2013](#); [Crocker et al. 2018a,b](#); [Wibking, Thompson, & Krumholz 2018](#)): an idealised 1D representation of a portion of a galactic disc with total gas mass per unit area  $\Sigma_{\text{gas}}$  and gas fraction  $f_{\text{gas}}$ , supported by a combination of turbulent motions with velocity dispersion  $\sigma$ , magnetic fields, and CR pressure, and confined by gravity. CRs (or radiation) are injected into this medium at the midplane with flux  $F_{c,0}$ . In the radiation context we have previously shown that, when the injected radiation flux exceeds a critical value, the system is destabilised and equilibrium becomes impossible. Numerical simulations confirm that radiation-driven winds are possible only in those systems for which equilibria do not exist. Here we are interested to determine whether a similar critical flux exists for CRs, since, if it does, that would suggest the circumstances under which it is possible for CRs to launch outflows of material out of galactic discs.

#### 2.1.1 Equations for transport and momentum balance

In [Paper I](#) we provide a detailed derivation of a pair of coupled ordinary differential equations (ODEs) that describe hydrostatic equilibrium and transport of CRs with losses. We present only a sketch of this development here for convenience, and refer readers to [Paper I](#) for the full derivation. We treat CRs in the relativistic, fluid dynamical limit whereby they behave as a fluid of adiabatic index  $\gamma_c = 4/3$ . Our ODEs express how the CR pressure and the gas column change as a function of our single variable,  $z$ , the height above the midplane. CRs are assumed to be injected by supernova explosions occurring solely in a thin layer near  $z = 0$ ; in the context of establishing a stability limit, this assumption turns out to be conservative (even though it is not realistic for most galaxies). We show in [Paper I](#) that the system can be described in terms of four dimensionless functions,  $s(\xi)$ ,  $r(\xi) = ds/d\xi$ ,  $p_c(\xi)$ , and  $\mathcal{F}_c(\xi)$ , which represent the dimensionless gas column, gas density, CR pressure, and CR flux as a function of dimensionless height  $\xi$ . These functions are prescribed by two equations. The first is the dimensionless CR transport equation,

$$\frac{\tau_{\text{stream}}}{\beta_s} \frac{d\mathcal{F}_c}{d\xi} = -\tau_{\text{abs}} r p_c + \tau_{\text{stream}} \frac{dp_c}{d\xi}, \quad (1)$$

where  $\tau_{\text{stream}}$ ,  $\tau_{\text{abs}}$ , and  $\beta_s$  are all defined below and

$$\mathcal{F}_c = -\frac{\beta_s}{\tau_{\text{stream}}} r^{-q} \frac{dp_c}{d\xi} \quad (2)$$

is the dimensionless CR flux expressed in the standard diffusion approximation (Ginzburg & Syrovatskii 1964)<sup>3</sup>, in which  $q$  specifies the running of the diffusion coefficient with density (i.e., the diffusion coefficient is proportional to  $\rho^{-q}$ ). The term on the LHS of equation 1 represents the gradient of the CR flux, while the two terms on the RHS represent, respectively, collisional and streaming losses of the CRs<sup>4</sup>. The coupled ODE expressing hydrostatic balance is

$$\frac{dp_c}{d\xi} + \phi_B \frac{dr}{d\xi} = -(1 - f_{\text{gas}})r - f_{\text{gas}}sr. \quad (3)$$

The terms in equation 3 are, from left to right, the pressure gradient due to CRs, the pressure gradient due to combined turbulence (treated as isotropic) plus magnetic support<sup>5</sup>, the gravitational acceleration due to stellar gravity, and the acceleration due to gas self-gravity.

The dimensionless variables are related to the physical quantities as follows. The dimensionless height is the physical height measured in units of the turbulent scale height:

$$\xi \equiv \frac{z}{z_*} \quad (4)$$

where

$$z_* \equiv \frac{\sigma^2}{g_*}, \quad (5)$$

(in which the turbulent velocity dispersion of the gas  $\sigma$  is assumed constant) and

$$g_* = 2\pi G \frac{\Sigma_{\text{gas}}}{f_{\text{gas}}}. \quad (6)$$

Similarly  $s(\xi)$  is the (dimensionless) fraction of the total half column contributed by gas in the height range from 0 to  $\xi z_*$ , and  $p_c(\xi)$  is the dimensionless CR pressure obtained by normalizing the dimensional CR pressure to the characteristic midplane pressure  $P_*$  (with related energy density  $u_* = (3/2)P_*$ ) given by

$$P_* = g_* \rho_* z_* = \rho_* \sigma^2 = \frac{\pi G}{f_{\text{gas}}} \Sigma_{\text{gas}}^2 \simeq 0.57 \frac{\Sigma_{\text{gas},1}^2}{f_{\text{gas}}} \text{ eV cm}^{-3}, \quad (7)$$

where we have defined  $\Sigma_{\text{gas},1} = \Sigma_{\text{gas}}/(10 M_\odot \text{ pc}^{-2})$  and

$$\rho_* \equiv \frac{\Sigma_{\text{gas}}}{2z_*} \quad (8)$$

is the characteristic matter density. The local density as a function of height is  $\rho_*(ds/d\xi)$ .

Other parameters appearing in the coupled ODEs are as follows: The coefficients  $\tau_{\text{abs}}$  and  $\tau_{\text{stream}}$  appearing on the RHS of equation 1 are, respectively, the optical depths of the gas column to CR absorption and scattering (see equation 9 and equation 10 below). In equation 3,  $\phi_B$  on the LHS lies in the range 0 to 2 and specifies the importance of magnetic effects in modifying the pressure due solely to gas turbulence

<sup>3</sup> Note that we can describe the process in terms of diffusion even if the microphysical transport process is predominantly streaming, as long as we are averaging over scales comparable to or larger than the coherence length of the magnetic field – see Krumholz et al. (2020) for further discussion.

<sup>4</sup> Note that here we assume that second-order Fermi reacceleration is negligibly small or actually zero; cf. Zweibel (2017).

<sup>5</sup> Note that we thus implicitly assume negligible thermal pressure.

(with values  $> 1$  indicating magnetic pressure support and values  $< 1$  indicating confinement by magnetic tension). We adopt  $q = 1/4$  and  $\phi_B = 73/72$  as fiducial values, but our results are only weakly sensitive to these choices – for further discussion see Paper I.

The cosmic ray optical depth parameters are given by

$$\tau_{\text{stream}} = \frac{\beta_s}{K_* \beta} \quad (9)$$

$$\tau_{\text{abs}} = \frac{1}{K_* \beta} \tau_{\text{pp}}. \quad (10)$$

where  $\beta_s \equiv v_s/c$  denotes the dimensionless CR streaming speed,  $\beta \equiv \sigma/c$  is the dimensionless ISM velocity dispersion, and  $K_*$  is the dimensionless midplane CR diffusion coefficient expressed in units of the effective diffusion coefficient for convective transport:

$$K_* = K_* \kappa_{\text{conv}}, \quad (11)$$

where

$$\begin{aligned} \kappa_{\text{conv}} &= \frac{z_* \sigma}{3} = \frac{\sigma^3 f_{\text{gas}}}{6\pi G \Sigma_{\text{gas}}} \\ &\simeq 3.8 \times 10^{26} \text{ cm}^2 \text{ s}^{-1} \sigma_1^3 f_{\text{gas}} \Sigma_{\text{gas},1}^{-1}, \end{aligned} \quad (12)$$

and we have defined  $\sigma_1 = \sigma/10 \text{ km s}^{-1}$ . Note that, as convection sets a lower limit to the rate of diffusion,  $K_* \geq 1$ . We apply this limit to all of the CR transport models we describe below. The  $\tau_{\text{pp}}$  parameter appearing in the definition of  $\tau_{\text{abs}}$  is the optical depth for “absorption” of cosmic rays via the hadronic collisions they experience in the limit of rectilinear propagation at speed  $c$  from the midplane to infinity through (half of the total) gas column  $\Sigma_{\text{gas}}$ :

$$\tau_{\text{pp}} = \frac{\Sigma_{\text{gas}}}{2\Sigma_{\text{pp}}} \quad (13)$$

where

$$\Sigma_{\text{pp}} \equiv \frac{\mu_p m_p}{3\eta_{\text{pp}} \sigma_{\text{pp}}} \simeq \frac{33 \text{ g cm}^{-2}}{(\eta_{\text{pp}}/0.5)(\sigma_{\text{pp}}/40 \text{ mbarn})} \simeq 1.6 \times 10^5 M_\odot/\text{pc}^2 \quad (14)$$

is the grammage required to decrease the CR flux by one e-folding; here  $m_p$  is the proton mass,  $\mu_p \simeq 1.17$  is the number of protons per nucleon for gas that is 90% H, 10% He by number,  $\eta_{\text{pp}}$  and  $\sigma_{\text{pp}}$  are the inelasticity and total cross-section for hadronic collisions experienced by relativistic CR protons.

The system formed by equation 1 and equation 3 is fourth-order, and thus requires four boundary conditions. Two of these apply to the density, and are

$$s(0) = 0 \quad (15)$$

$$\lim_{\xi \rightarrow \infty} s(\xi) = 1, \quad (16)$$

which amount to asserting that the gas half column is zero at the midplane, and that  $\lim_{z \rightarrow \infty} \Sigma_{\text{gas},1/2}(z) = 1/2 \Sigma_{\text{gas}}$ . The remaining two apply to the CR pressure and flux, and are

$$\frac{\tau_{\text{stream}}}{\beta_s} \mathcal{F}_c(0) = \frac{1}{K_* \beta} \frac{F_{c,0}}{F_*} \equiv f_{\text{Edd}}, \quad (17)$$

at  $\xi = 0$  and

$$\lim_{\xi \rightarrow \infty} \mathcal{F}_c = \lim_{\xi \rightarrow \infty} 4\beta_s p_c. \quad (18)$$

The first of these, equation 17, is set by the CR flux  $F_{c,0}$

entering the gas column; here  $F_* = cP_*$  is the scale flux for our non-dimensional system, and  $f_{\text{Edd}}$  is the Eddington ratio, which gives the ratio of the momentum flux carried by the CRs to that imparted by gravity. The second, [equation 18](#), asserts that the CR flux approach the value for free-streaming as  $\xi \rightarrow \infty$ . Again, we refer readers to [Paper I](#) for a full derivation of these conditions.

## 2.2 CR transport models

To complete the specification of the system, we require expressions for  $K_*$  and  $\beta_s$ , the normalised CR diffusion coefficient and streaming speed. These depend on the micro-physics of CR confinement, and here we consider the same three models for this process as in [Paper I](#). These are:

### 2.2.1 Streaming (fiducial case)

We are interested in the feedback effects of CRs on the (predominantly) neutral ISM, which at the midplane of a galactic disc constitutes  $\sim 50\%$  of the volume ([Dekel et al. 2019](#)), and close to 100% in the densest starbursts ([Krumholz et al. 2020](#)), and the vast majority of the mass. Thus our fiducial case is for CR transport through such a medium. As discussed in [Paper I](#) and shown in [Krumholz et al. \(2020\)](#), in such a medium strong ion-neutral damping prevents interstellar turbulence from cascading down to the small scales of CR gyroradii, which are the only scales that efficiently scatter CRs. Thus the only disturbances in the magnetic field with which CRs interact are those they themselves generate via the streaming instability. Thus CRs stream along field lines, but for the relatively low (but still relativistic) CR energies that dominate the CR energy budget, streaming instability limits the streaming speed to the ion Alfvén velocity of the medium,

$$v_{A,i} = \frac{\sigma}{\sqrt{2\chi}M_A}, \quad (19)$$

where  $M_A$  is the Alfvén Mach number of the Alfvénic turbulence modes in the ISM and  $\chi$  is the ionisation fraction by mass. For a dynamo-generated field  $M_A \approx 1-2$  ([Federrath et al. 2014; Federrath 2016, Paper I](#)), and astrochemical models show that the ionisation fraction  $\chi$  ranges from  $\sim 10^{-2}$  in Milky Way-like galaxies with relatively diffuse neutral media ([Wolfire et al. 2003](#)) to  $\sim 10^{-4}$  in dense starbursts [Krumholz et al. \(2020\)](#). On larger scales, the CR diffusion coefficient is therefore set by the combination of streaming at this speed along the field lines, and the random walk of the field lines themselves in the turbulence. For this model, we show in [Paper I](#) that

$$K_* = \frac{1}{\sqrt{2\chi}M_A} \quad (20)$$

$$\beta_s = \frac{\beta}{\sqrt{2\chi}M_A} \quad (21)$$

$$\tau_{\text{stream}} = M_A^3 \quad (22)$$

$$\tau_{\text{abs}} = \frac{\sqrt{2\chi}M_A^4}{\beta} \tau_{\text{pp}}, \quad (23)$$

and we use  $q = 1/4$  as our fiducial choice as introduced above<sup>6</sup>. For a given choice of  $M_A$  and  $\chi$ , and a galactic disc of specified  $\Sigma_{\text{gas}}$  and  $\sigma$  (which set  $\tau_{\text{pp}}$  and  $\beta$ , respectively), these expressions complete the specification of the system.

### 2.2.2 Scattering

Our second model is based on the premise that, although we are interested in feedback on the neutral ISM, ionised gas nevertheless fills  $\sim 50\%$  of the midplane volume in most galaxies ([Cox & Smith 1974; Dekel et al. 2019](#)), with the fraction rising as one goes away from the midplane, and thus CR transport might take place predominantly in the ionised phase of the ISM. Indeed, *in situ* observations suggest that such is the case for the local CR population seen at Earth (e.g., [Ghosh & Ptuskin 1983; Jones et al. 2001](#)). In this case CRs may still interact predominantly with their own self-generated turbulence, in which case we return to a situation much like the streaming model, except with  $\chi = 1$ . The more interesting possibility, therefore, is that, although CRs do stream at speed  $v_s = v_{A,i} = \sigma/\sqrt{2}M_A$ , they also scatter off turbulence that is part of the large-scale turbulent cascade in the ISM, and that this scattering is what sets the diffusion coefficient. In this case, we show in [Paper I](#) that transport coefficients are given by

$$K_* = \frac{1}{\beta} \left( \frac{G}{2f_{\text{gas}}} \right)^{p/2} \left( \frac{E_{\text{CR}}M_A}{e\sigma^2} \right)^p \quad (24)$$

$$\beta_s = \frac{\beta}{\sqrt{2}M_A} \quad (25)$$

$$\tau_{\text{stream}} = \frac{3\beta}{\sqrt{2}M_A^2} \left( \frac{E_{\text{CR}}}{e\sigma^2} \sqrt{\frac{G}{2f_{\text{gas}}}} \right)^{-p} \quad (26)$$

$$\tau_{\text{abs}} = \frac{3\tau_{\text{pp}}}{M_A} \left( \frac{E_{\text{CR}}}{e\sigma^2} \sqrt{\frac{G}{2f_{\text{gas}}}} \right)^{-p}. \quad (27)$$

Here  $E_{\text{CR}}$  is the CR energy (we adopt  $E_{\text{CR}} = 1 \text{ GeV} \equiv E_{\text{CR},0}$  as a fiducial choice),  $e$  is the elementary charge, and  $p$  is the index of the turbulent power spectrum –  $p = 1/3$  (corresponding to  $q = 1/6$ ) for a Kolmogorov spectrum, and  $p = 1/2$  (corresponding to  $q = 1/4$ , i.e., the fiducial value) for a Kraichnan spectrum, though which value of  $p$  we choose makes little difference to the qualitative results. As with the streaming model described above, for a particular choice of  $E_{\text{CR},0}$ ,  $p$ , and  $M_A$ , the above expressions allow us to compute the transport coefficients  $\beta_s$ ,  $\tau_{\text{stream}}$ , and  $\tau_{\text{abs}}$  for any choice of galactic disc parameters  $\Sigma_{\text{gas}}$  and  $\sigma$ . Compared to the streaming model, the scattering model generally predicts smaller streaming optical depths in all galaxies, and comparable diffusion rates and absorption optical depths in Milky Way-like galaxies. The models differ mainly in their predictions for denser and more rapidly star-forming galaxies, where the scattering model predicts slower transport and greater absorption optical depths than in the Milky Way

<sup>6</sup> This corresponds to the physical limit where the turbulent velocity dispersion is density independent, there is a local turbulent dynamo acting, and the ionization fraction becomes independent of the local gas density; while this latter is unlikely to hold strictly, as we have previously shown ([Paper I](#) and [Krumholz et al. 2020](#)), our results are not strongly dependent on  $q$  so long as  $0 < q < 1$ .

(due to stronger turbulence), while the streaming model predicts the opposite (due to the lower ionisation fraction in denser galaxies allowing faster CR streaming). We provide a more detailed comparison in [Paper I](#).

### 2.2.3 Constant diffusion coefficient

The third model we consider is a purely empirical one: The empirically-determined diffusion coefficient for  $\sim$ GeV CRs in the Milky Way is close to  $\kappa_{*,\text{MW}} \equiv 10^{28} \text{ cm}^2 \text{ s}^{-1}$  (e.g., [Ptuskin et al. 2006](#)) and, in this model, we simply assume  $\kappa$  in all galaxies is given by this value. We thus assume that CRs stream through a fully ionised medium, as in the scattering case, but we take the dimensionless diffusion coefficient to be  $K_* = \kappa_{*,\text{MW}}/\kappa_{\text{conv}}$ . The corresponding expressions for the dimensionless numbers entering the equilibrium equations are

$$K_* = \frac{6\pi G \Sigma_{\text{gas}} \kappa_{*,\text{MW}}}{f_{\text{gas}} \sigma^3} \quad (28)$$

$$\beta_s = \frac{\beta}{\sqrt{2} M_A} \quad (29)$$

$$\tau_{\text{stream}} = \frac{1}{\sqrt{2} M_A} \left( \frac{\kappa_{\text{conv}}}{\kappa_{*,\text{MW}}} \right) \quad (30)$$

$$\tau_{\text{abs}} = \frac{\tau_{\text{pp}}}{\beta} \left( \frac{\kappa_{\text{conv}}}{\kappa_{*,\text{MW}}} \right). \quad (31)$$

Since we can write down the convective diffusion coefficient  $\kappa_{\text{conv}}$  as a function of  $\Sigma_{\text{gas}}$  and  $\sigma$  (c.f. [equation 12](#)), this again represents a complete specification of the system.

## 3 THE COSMIC RAY EDDINGTON LIMIT

With this review of our dimensionless ODE system, and having dealt with the microphysics of CR transport, we are now in a position to address the basic question posed in this paper: under what conditions does it become impossible for a galactic disc forced by CRs from below to remain hydrostatic? To answer this question, we first describe a numerical method to identify this limit in the space of the dimensionless variables that characterise our system ([Section 3.1](#)), we use this method to obtain critical stability curves in this space ([Section 3.2](#)), and then we translate from the space of dimensionless variables to the space of observable galaxy properties ([Section 3.3](#)).

### 3.1 Numerical method

We must solve [equation 1](#) and [equation 3](#) numerically. Because the boundary conditions for the system, [equation 15](#) - [equation 18](#), are specified at different locations, the system forms a boundary value problem, which we solve using a shooting algorithm as follows: we have  $s(0) = 0$  from [equation 15](#), and we start with an initial guess for the mid-plane density  $r(0) = s'(0)$  and pressure  $p_c(0)$ . These choices together with [equation 17](#) allow us to compute the midplane CR pressure gradient  $p'_c(0)$ , so that we now have a set of four initial values at  $s = 0$  and can integrate outwards until  $s(\xi)$  and  $p_c(\xi)$  approach constant values at large  $\xi$ . In general our guess will not satisfy [equation 16](#), i.e.,  $s(\xi)$  will go to a value other than unity as  $\xi \rightarrow \infty$ . We therefore iteratively adjust

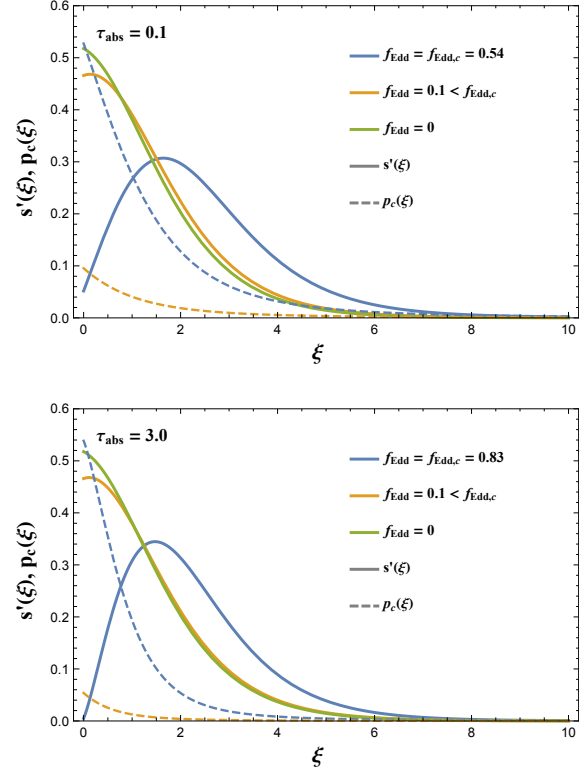


**Figure 1.** Profiles of (dimensionless) volumetric density  $r(\xi) = s'(\xi)$  (solid) and (dimensionless) CR pressure  $p_c(\xi)$  (dashed) for various representative cases as indicated in the legend. The upper panel is for  $\tau_{\text{abs}} = 0.1$ , the lower is for  $\tau_{\text{abs}} = 3.0$ ; otherwise, parameters common between the panels are  $q = 1/4$ ,  $\tau_{\text{stream}} = 1$ ,  $f_{\text{gas}} = 0.9$ ,  $\phi_B = 73/72$ . In both panels, the blue curves are evaluated for the critical  $f_{\text{Edd}}$  case and the yellow curves are for a sub-critical  $f_{\text{Edd}}$  value; the solid green curve is the density profile of a gas column supported purely by turbulence (with  $\phi_B = 73/72$ ). Note that because  $\sigma$  is constant,  $s'(\xi)$  is equivalent to the dimensionless turbulent pressure, and thus the ratio of solid and dashed curves of the same colour is also the ratio of turbulent to CR pressure.

$s'(0)$  while holding  $p_c(0)$  fixed, until [equation 16](#) is satisfied. In general, however, this choice will not obey [equation 18](#), i.e., the CR flux will not go to the correct value as  $\xi \rightarrow \infty$ . We therefore now iteratively adjust our guess for  $p_c(0)$ . We continue to iterate between our guesses for  $s'(0)$  and  $p_c(0)$  until the system converges and all boundary conditions are satisfied, or until convergence fails (see below).

A crucial feature of solutions to this system is that, as  $f_{\text{Edd}}$  increases at fixed  $\tau_{\text{abs}}$  and  $\tau_{\text{stream}}$ , the dimensionless midplane density  $s'(0)$  decreases monotonically, approaching zero at a finite value of  $f_{\text{Edd}}$ . We illustrate this behaviour for two example cases in [Figure 1](#). We refer to the value of  $f_{\text{Edd}}$  for which this occurs as the critical Eddington ratio,  $f_{\text{Edd},c}$ . No solutions exist for  $f_{\text{Edd}} > f_{\text{Edd},c}$ , and thus  $f_{\text{Edd},c}$  represents the largest Eddington ratio for which it is possible for a gas column through which CRs are forced to remain in equilibrium. Larger values of  $f_{\text{Edd}}$  necessarily render the system unstable. Mathematically, this manifests in that we



are unable to find values of  $s'(0)$  and  $p'_c(0)$  such that, when we integrate [equation 1](#) and [equation 3](#), the resulting solution satisfies the boundary conditions [equation 16](#) and [equation 18](#) as  $\xi \rightarrow \infty$ . The shooting method fails to converge.

We determine the value of the critical Eddington ratio  $f_{\text{Edd},c}(\tau_{\text{abs}}, \tau_{\text{stream}})$  as a function of  $\tau_{\text{abs}}$  and  $\tau_{\text{stream}}$  as follows. We start with a small value of  $f_{\text{Edd}}$ , for which a solution is guaranteed to exist because in the limit  $f_{\text{Edd}} \rightarrow 0$ , [equation 1](#) and [equation 3](#) are completely decoupled; the former just reduces to the equation for an isothermal atmosphere, and the latter to a nonlinear diffusion equation with losses, the analytic solution for which is given by [Krumholz et al. \(2020\)](#). We use the shooting procedure described above to obtain the numerical solution for this small value of  $f_{\text{Edd}}$ . We then progressively increase  $f_{\text{Edd}}$  and solve again, using the solution for the previous value as a starting guess. Eventually we reach a value of  $f_{\text{Edd}}$  for which the shooting method fails to converge, and no solution exists. Once we find this value, we iteratively decrease and increase  $f_{\text{Edd}}$  in order to narrow down the value  $f_{\text{Edd},c}$  for which a solution ceases to exist. We iterate in this manner until we have determined  $f_{\text{Edd},c}$  for a given  $\tau_{\text{abs}}$  and  $\tau_{\text{stream}}$  to some desired tolerance. [Figure 1](#) confirms that the value of  $f_{\text{Edd},c}$  we obtain by this procedure is indeed such that  $s'(0)$  is close to zero, although in practice how close we are able to push  $s'(0)$  to zero depends on the tolerances we use in our iterative solver – in the vicinity of  $f_{\text{Edd},c}$ , the value of  $s'(0)$  becomes exquisitely sensitive to  $f_{\text{Edd}}$ . This is visible in the upper panel of [Figure 1](#), where our solution for  $f_{\text{Edd}} \approx f_{\text{Edd},c}$  has  $s'(0) \approx 0.05$ , but if we increase  $f_{\text{Edd}}$  by even 1%, then solutions cease to exist entirely.

### 3.2 Critical curves

We show sample values of  $f_{\text{Edd},c}$  determined via the procedure described in [Section 3.1](#) in [Figure 2](#); the top panel shows  $f_{\text{Edd},c}$  as a function of  $\tau_{\text{abs}}$  for fixed  $\tau_{\text{stream}}$  at several values of  $f_{\text{gas}}$ , while the bottom panel shows  $f_{\text{Edd},c}(\tau_{\text{abs}})$  for fixed  $f_{\text{gas}}$  at several values of  $\tau_{\text{stream}}$ . Qualitatively, the behaviour of the solution with respect to  $\tau_{\text{abs}}$  is that, at small  $\tau_{\text{abs}}$ ,  $f_{\text{Edd},c}$  approaches a fixed,  $\mathcal{O}(1)$  value. At large  $\tau_{\text{abs}}$ , we find that  $f_{\text{Edd},c}$  begins to scale  $\propto \tau_{\text{abs}}$ . We also find that, at low  $\tau_{\text{abs}}$ , we have a rough scaling  $f_{\text{Edd},c} \propto \tau_{\text{stream}}$  scaling (cf. lower panel of [Figure 2](#)). Finally, we find that increasing  $f_{\text{gas}}$  renders the column less stable for other parameters held fixed; this is as expected given that gas self-gravity must vanish in the midplane.

We can understand the observed scalings of  $f_{\text{Edd},c}$  with  $f_{\text{gas}}$ ,  $\tau_{\text{abs}}$ , and  $\tau_{\text{stream}}$  via some straightforward analytic considerations. Of these,  $f_{\text{gas}}$  is the simplest. We note that, in the limit  $f_{\text{Edd}} \ll 1$ , the equation of hydrostatic balance ([equation 3](#)) has the usual solutions  $s'(\xi) = e^{-\xi/\phi_B}$  for  $f_{\text{gas}} = 0$  and  $s'(\xi) = \text{sech}^2(\xi/2\phi_B)$  for  $f_{\text{gas}} = 1$ ; at  $\xi = 0$ , these solutions have  $s' = 1/\phi_B$  and  $1/2\phi_B$ , respectively, so the density at the midplane is twice as high with  $f_{\text{gas}} = 0$  as with  $f_{\text{gas}} = 1$ . In between these limits, the midplane density scales as approximately  $1/[\phi_B(1 + f_{\text{gas}})]$ . Since the critical  $f_{\text{Edd}}$  corresponds to the point where  $s'(0) \rightarrow 0$ , we expect that configurations starting with a larger value of  $s'(0)$  at low  $f_{\text{Edd}}$  should have higher  $f_{\text{Edd},c}$ , as  $f_{\text{Edd},c} \propto s'(0)|_{f_{\text{Edd}} \ll 1}$ . This suggests a scaling  $f_{\text{Edd},c} \propto 1/[\phi_B(1 + f_{\text{gas}})]$ , which is consistent with our numerical results.

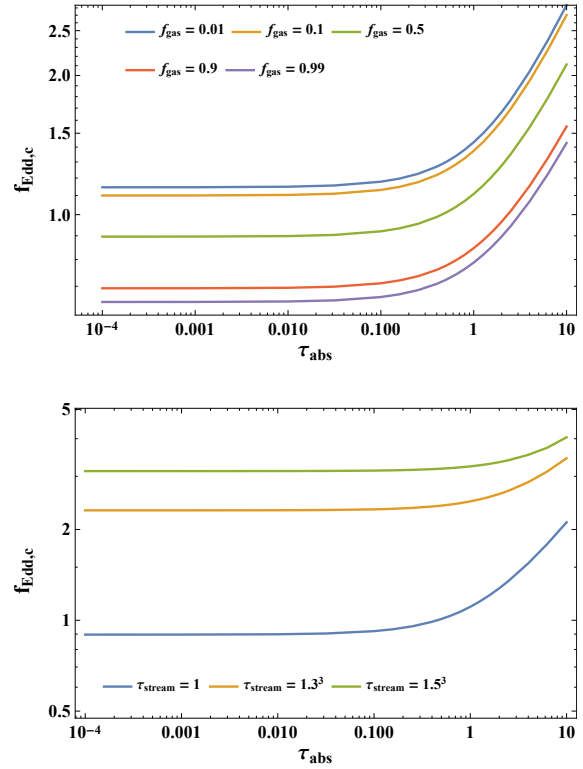


**Figure 2.** CR Eddington limit  $f_{\text{Edd},c}$  as a function of effective optical depth  $\tau_{\text{abs}}$ . **Upper panel:**  $f_{\text{Edd},c}$  versus  $\tau_{\text{abs}}$  at fixed  $\tau_{\text{stream}} = 1$  and for a range of gas fractions  $f_{\text{gas}}$  as indicated in the legend; a higher  $f_{\text{gas}}$  renders the column (somewhat) less stable (i.e., reduces  $f_{\text{Edd},c}$ ), while a higher  $\tau_{\text{abs}}$  renders the column *more* stable once we are in the optically thick regime (because hadronic collisions reduce the steady state CR pressure). **Lower panel:**  $f_{\text{Edd},c}$  as a function of  $\tau_{\text{abs}}$  for fixed  $f_{\text{gas}} = 0.5$  and a range of  $\tau_{\text{stream}}$  values as indicated in the legend; a higher  $\tau_{\text{stream}}$  renders the column more stable (again because losses – in this instance due to the streaming instability – reduce the steady state CR pressure).

The scalings for  $\tau_{\text{abs}}$  and  $\tau_{\text{stream}}$  require only slightly more consideration. We expect our system to approach the critical limit when the midplane CR pressure,  $P_c$ , becomes significant in comparison to the pressure required to keep the column in hydrostatic equilibrium,  $P_*$ . In steady state, the midplane CR pressure (or energy density, which differs just by a factor of 3), in turn, will be set by the product of the CR energy injection rate – set by star formation – and a dwell time  $t_c$  for CRs injected into the galaxy. Thus we have

$$\left(\frac{P_c}{P_*}\right)_{z=0} \sim \frac{(F_{c,0}/z_*)t_c}{P_*} = \frac{\sigma t_c}{z_*} K_* f_{\text{Edd}}, \quad (32)$$

where  $F_{c,0}$  is the energy injected per unit area, and we write the energy injected per unit volume as  $F_{c,0}/z_*$  under the assumption that the CRs are distributed over a height of order  $z_*$ . In the second step, we made use of [equation 17](#) to rewrite  $F_{c,0}$  in terms of the Eddington ratio.

The dwell time for a CR will be set by the minimum of

the time required for it to be lost to a collision,  $t_{\text{col}}$ , to have its energy sapped by streaming losses,  $t_{\text{stream}}$ , or to escape from the galaxy via diffusion,  $t_{\text{esc,diff}}$ :

$$t_c \sim \left( t_{\text{col}}^{-1} + t_{\text{stream}}^{-1} + t_{\text{esc,diff}}^{-1} \right)^{-1}. \quad (33)$$

We can rewrite each of the three ratios appearing inside the parentheses in the above equation in terms of our dimensionless parameters. The collisional loss time is (c.f. equation 11 of Paper I)

$$t_{\text{col}} \sim \frac{1}{c(\rho_*/\mu_p m_p)\sigma_{\text{pp}}\eta_{\text{pp}}} \sim \frac{1}{K_*\tau_{\text{abs}}} \left( \frac{z_*}{\sigma} \right), \quad (34)$$

where we have dropped factors of order unity, and in the second step we have made use of equation 10 and equation 13. Similarly, the streaming loss time is (c.f. equation 49 of Paper I)

$$t_{\text{stream}} \sim \frac{z_*}{v_s} \sim \frac{1}{K_*\tau_{\text{stream}}} \left( \frac{z_*}{\sigma} \right), \quad (35)$$

where in the second step we have used equation 9. Finally, the diffusive escape time is (c.f. equation 47 of Paper I)

$$t_{\text{esc,diff}} \sim \frac{z_*^2}{\kappa_*} \sim \frac{1}{K_*} \left( \frac{z_*}{\sigma} \right), \quad (36)$$

where we have used equation 11. Inserting these factors into equation 33 for  $t_c$ , and thence into equation 32, we find

$$\left( \frac{P_c}{P_*} \right)_{z=0} \sim f_{\text{Edd}} (1 + \tau_{\text{abs}} + \tau_{\text{stream}})^{-1}. \quad (37)$$

Thus if we expect the midplane ratio  $P_c/P_*$  to be of order unity when  $f_{\text{Edd}}$  is at the critical value, it follows immediately that

$$f_{\text{Edd,c}} \propto \frac{1 + \tau_{\text{abs}} + \tau_{\text{stream}}}{\phi_B(1 + f_{\text{gas}})}, \quad (38)$$

where we have now re-inserted the scaling with  $\phi_B$  and  $f_{\text{gas}}$  derived above. This is not, of course, an exact expression, but its scalings are qualitatively correct, as we have seen, and account for the following phenomena: CRs exert a pressure which is i) enhanced by the diffusive nature of their propagation (c.f. Socrates et al. 2008) – this leads to the constant term on the RHS – but attenuated by ii) their collisional and iii) their streaming losses; these lead to the  $\propto \tau_{\text{abs}}$  and  $\propto \tau_{\text{stream}}$  terms, respectively.

It will be convenient for the remainder of this paper to use our understanding of the scaling behaviour of  $f_{\text{Edd,c}}$  to derive an approximate analytic fit that we can use in lieu of the full, numerically-determined solution. We adopt the functional form given by equation 38, and after some numerical experimentation to find coefficients that minimise the error, we arrive at the approximate relationship

$$f_{\text{Edd,c}} \approx f_{\text{Edd,c,fit}} \equiv \frac{1}{2.4\phi_B(1 + f_{\text{gas}})} \left( 0.26 + \frac{\tau_{\text{abs}}}{2.5} + \frac{\tau_{\text{stream}}}{0.31} \right). \quad (39)$$

We plot the relative error in this fit, defined as

$$\text{rel. err.} \equiv \frac{|f_{\text{Edd,c}} - f_{\text{Edd,c,fit}}|}{f_{\text{Edd,c}}}, \quad (40)$$

in Figure 3. The figure demonstrates that our approximation is accurate to  $\lesssim 20$  percent for  $\tau_{\text{abs}} < 10$  and  $f_{\text{gas}} = 0.01\text{--}0.99$ .

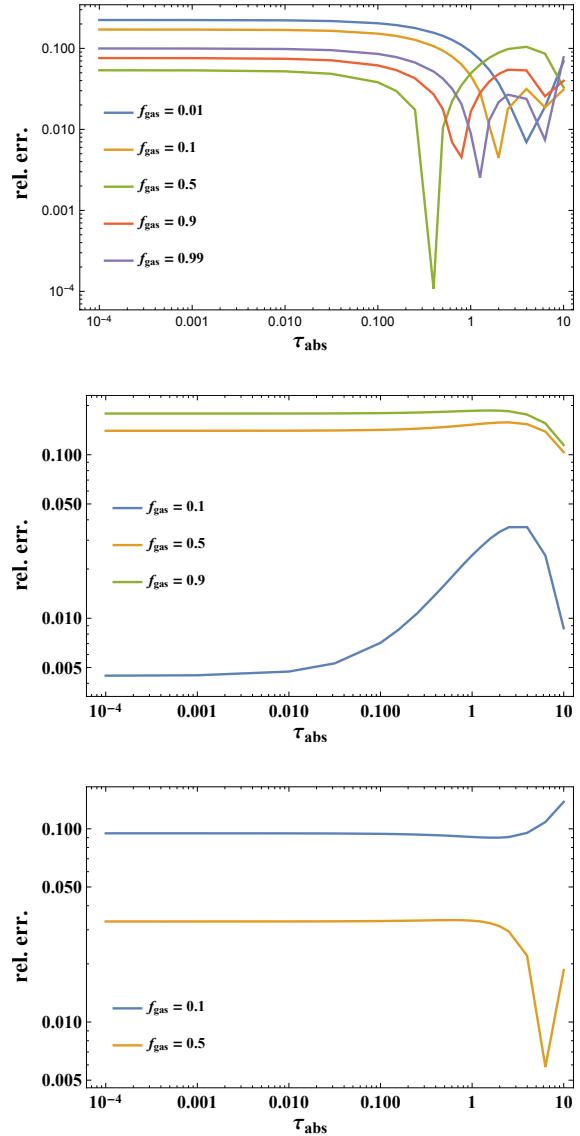


**Figure 3.** Relative error between the analytic approximation and the full numerically-determined CR critical Eddington ratio. From top to bottom, the panels are for  $\tau_{\text{stream}} = \{1^3, 1.3^3, 1.5^3\}$ ; gas fractions are as labelled in each panel's legend.

### 3.3 The cosmic ray stability limit for star-forming galaxies

The final step in our calculation is to translate our stability limit from dimensionless ( $f_{\text{Edd}}$ ,  $\tau_{\text{abs}}$ ,  $\tau_{\text{stream}}$ ) to the physical variables describing a star-forming galactic disc. In particular, we are interested in the highest star formation rate (since star formation produces supernovae that are the primary source of CRs) that a disc can sustain before it becomes unstable to the development of CR-driven outflows.

The conversion from dimensionless to physical variables is straightforward. Given a gas surface density  $\Sigma_{\text{gas}}$ , velocity dispersion  $\sigma$ , gas fraction  $f_{\text{gas}}$ , Alfvén Mach number  $M_A$ , and

either (depending on our choice of CR transport model) an ionisation fraction  $\chi$  or CR energy  $E_{\text{CR}}$ , we can compute the corresponding  $\tau_{\text{stream}}$  and  $\tau_{\text{abs}}$  values from [equation 22](#) and [equation 23](#) (for our fiducial streaming model), [equation 26](#) and [equation 27](#) (for the scattering transport model), or [equation 30](#) and [equation 31](#) (for the constant model). From these values plus  $f_{\text{gas}}$  we can compute the critical Eddington ratio  $f_{\text{Edd,c}}$  using either the numerical procedure outlined in [Section 3.1](#), or, with much less computational expense, our approximate fitting formula ([equation 39](#)).

We can obtain a corresponding star formation rate per unit area  $\dot{\Sigma}_\star$  from this as follows. First, following [Paper I](#), we write the CR flux as

$$F_{\text{C},0} = \epsilon_{\text{c},1/2} \dot{\Sigma}_\star, \quad (41)$$

where  $\epsilon_{\text{c},1/2}$  is the energy injected into CRs in each galactic hemisphere per unit mass of stars formed. We adopt a fiducial value  $\epsilon_{\text{c},1/2} \approx 5.6 \times 10^{47} \text{ erg } M_\odot^{-1}$ , which corresponds to assuming [Chabrier \(2005\)](#) initial mass function, that all stars with mass  $\geq 8 M_\odot$  end their lives as supernovae with total energy  $10^{51} \text{ erg}$ , and that 10% of this SN energy is eventually injected into CRs. Substituting [equation 41](#) into the definition of  $f_{\text{Edd}}$  ([equation 17](#)), we have

$$\begin{aligned} \dot{\Sigma}_\star &= \frac{F_\star}{\epsilon_{\text{c},1/2}} K_\star \beta f_{\text{Edd}} = \frac{\pi G}{\epsilon_{\text{c},1/2}} \frac{\Sigma_{\text{gas}}^2 \sigma}{f_{\text{gas}}} K_\star f_{\text{Edd}} \\ &= 4.9 \times 10^{-4} \frac{\Sigma_{\text{gas},1}^2 \sigma_1}{f_{\text{gas}}} K_\star f_{\text{Edd}} M_\odot \text{ pc}^{-2} \text{ Myr}^{-1}. \end{aligned} \quad (42)$$

By plugging our value of  $f_{\text{Edd,c}}$  into [equation 42](#), together with the appropriate value of  $K_\star$  for our chosen CR transport model ([equation 20](#), [equation 24](#), or [equation 28](#)), we obtain the critical star formation rate  $\dot{\Sigma}_{\star,\text{c}}$  above which galaxies become unstable to CRs.

In order to actually plot  $\dot{\Sigma}_{\star,\text{c}}$  versus  $\Sigma_{\text{gas}}$ , we require values of  $\sigma$ ,  $f_{\text{gas}}$ , and  $\chi$ , which vary systematically with  $\Sigma_{\text{gas}}$  on average (e.g., higher surface density galaxies tend to have higher velocity dispersion), but which are not single-valued functions of  $\Sigma_{\text{gas}}$  either. To avoid a proliferation of curves, we adopt the same strategy as in [Paper I](#): we interpolate between plausible values of these parameters as a function of  $\Sigma_{\text{gas}}$ . Specifically, we adopt

$$f_{\text{gas}}(\Sigma_{\text{gas}}) \equiv 0.11 \Sigma_{\text{gas},1}^{0.32} \quad (43)$$

$$\chi(\Sigma_{\text{gas}}) \equiv 0.013 \Sigma_{\text{gas},1}^{-0.79} \quad (44)$$

$$\sigma(\Sigma_{\text{gas}}) \equiv 8.5 \Sigma_{\text{gas},1}^{0.39} \text{ km/s}. \quad (45)$$

We emphasise that these are not intended to be accurate fits; they are simply intended to provide smooth functions we can use to reduce the multidimensional parameter space of  $\Sigma_{\text{gas}}$ ,  $\sigma$ ,  $f_{\text{gas}}$ , and  $\chi$  to a single dimension so that we can represent it on a plot.

With this understood, we plot  $\dot{\Sigma}_{\star,\text{c}}$  as a function of  $\Sigma_{\text{gas}}$  in [Figure 4](#). We show curves for the cases of i) our fiducial streaming model for CR transport (blue), ii) the alternative scattering (yellow), and iii) the case of constant  $\kappa$  (green); for all of these modes we show both results for both  $M_A = 2$  (solid) and  $M_A = 1$  (dashed). For any particular curve, the stable region is below and to the right, while the unstable region is above and to the left. [Figure 4](#) also shows a selection of observed galaxies culled from the literature (see [Paper I](#)

for details of the data compilation), with some particularly significant galaxies shown by the red points: the Milky Way datum (‘MW’), its Central Molecular Zone (CMZ), and the nearby starbursts NGC253, M82, and Arp 220, whose  $\gamma$ -ray emission we modelled in [Krumholz et al. \(2020\)](#).

## 4 IMPLICATIONS

[Figure 4](#) is the central result of this paper. Here we discuss its implications, and explore the physical origin of the result and its sensitivity to a variety of assumptions and parameter choices that we have made.

### 4.1 For which galaxies can CRs drive outflows from the star-forming ISM?

We start by examining our fiducial CR transport model, indicated by the blue lines in [Figure 4](#). An immediate conclusion we can draw is that, for physically-plausible scalings of the parameters, the CR stability curve patrols a region very close to the top of the occupied part of the  $(\Sigma_{\text{gas}}, \dot{\Sigma}_\star)$  plane for star-forming galaxies with low gas surface densities typical of the Galaxy and local dwarfs. This correspondence strongly suggests that CR feedback on the neutral gas may be an important mechanism in such galaxies: it might limit the ability of galaxies to make excursions above the locus where most of them like to be, or it might be responsible for launching winds and ejecting gas in galaxies that do wander upwards to higher star formation rates.

Conversely, it is evident that, at the higher gas surface densities encountered in local starbursts and high-redshift star-forming galaxies, *all* the critical curves (not just the one for our fiducial model) diverge away from the observed distribution of galaxies. This implies that CRs cannot drive winds in these systems (cf. [Paper I](#)). Mathematically, such a divergence must occur for the following reason: from [equation 42](#), for the range of  $\tau_{\text{abs}}$  for which  $f_{\text{Edd,c}} \sim \text{const}$  at fixed  $\tau_{\text{stream}}$  (cf. [Figure 2](#)) we have shown that the critical star formation rate surface density scales approximately as  $\dot{\Sigma}_{\star,\text{c}} \propto \tau_{\text{abs}}^2 \propto \Sigma_{\text{gas}}^2$ . On the other hand, the observed surface density of star formation rises with gas surface density with an index  $< 2$ . Physically, the divergence occurs because the high gas number densities in starburst systems kill CRs quickly, meaning that the energy density/pressure they represent cannot build up to be anything comparable to hydrostatic pressures (cf. [Lacki et al. 2011](#); [Thompson & Lacki 2013](#); [Crocker et al. 2020a](#)). On the other hand, such a situation constitutes a recipe for CR calorimetry, so these systems are expected – indeed, directly inferred, in a limited number of cases – to be good hadronic  $\gamma$ -ray sources (cf. [Torres et al. 2004](#); [Thompson et al. 2007](#); [Lacki et al. 2010, 2011](#); [Yoast-Hull et al. 2016](#); [Peretti et al. 2019](#); [Krumholz et al. 2020](#)).

### 4.2 Instability of galaxies under scattering

A second significant point that is evident from [Figure 4](#) is that, for the cases of both *constant* diffusivity and *scattering*, the critical curves cut well into the occupied region of parameter space for lower surface gas density galaxies; many such galaxies, including the Milky Way, are unstable under



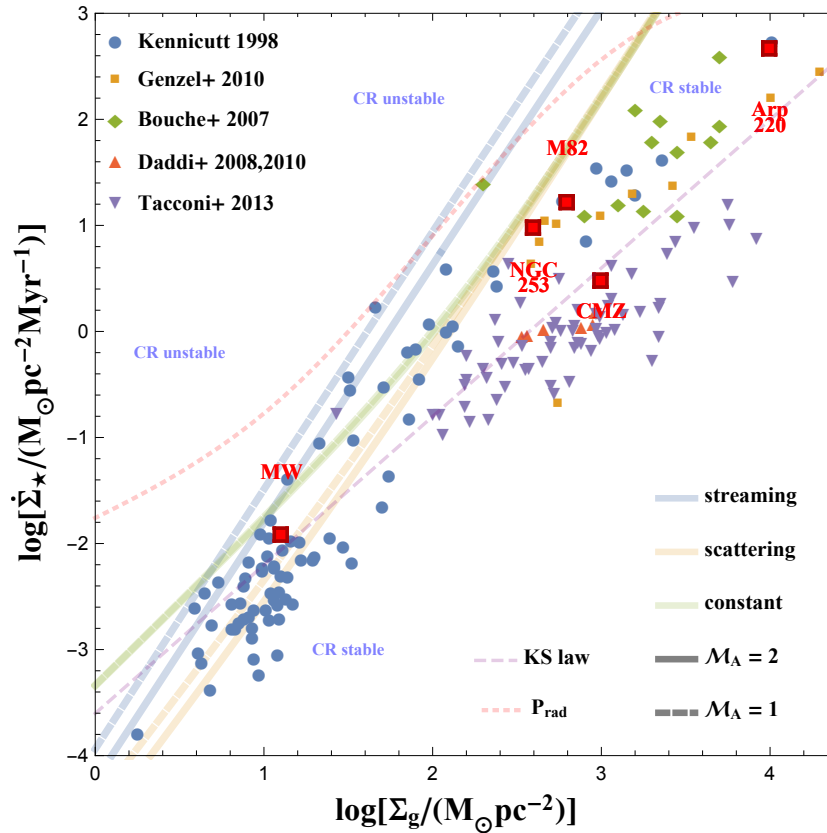


**Figure 4.** Thick coloured lines show critical stability curves  $\dot{\Sigma}_{*,c}$ , i.e., the star formation rate per unit area at which CR pressure precludes hydrostatic equilibrium, computed assuming one of three different CR transport modes as indicated (with streaming constituting our fiducial model), and for  $M_A = 2$  (solid) and  $M_A = 1$  (dashed) together with fiducial parameter choices for all models, and using the fits for  $f_{\text{gas}}$ ,  $\chi$ , and  $\sigma$  as a function of  $\Sigma_{\text{gas}}$  given by equation 43 - equation 45. The dashed, diagonal, purple line is the Kennicutt (1998) star formation scaling. The dotted red line is the critical star formation rate surface density obtained for radiation pressure feedback. This curve smoothly interpolates from the single-scattering case (adopting a critical Eddington ratio 0.6 on the basis of the calculation by Wibking, Thompson, & Krumholz (2018) and assuming a fixed flux-mean dust opacity per mass of dust+gas mixture of  $\kappa = 1000 \text{ cm}^2/\text{g}$ ) into the regime where the atmosphere is optically thick to FIR radiation due to the dust opacity (Crocker et al. 2018a) with a cross-over at  $\Sigma_{\text{gas}} \approx 10^3 \text{ M}_\odot/\text{pc}^2$  (and we have assumed a young,  $< 7 \text{ Myr}$  old, stellar population for the optically thick part of the curve). Finally, points show observations drawn from the following sources: local galaxies from Kennicutt (1998),  $z \sim 2$  sub-mm galaxies from Bouché et al. (2007), and galaxies on and somewhat above the star-forming main sequence at  $z \sim 1 - 3$  from Daddi et al. (2008, 2010b); Genzel et al. (2010); Tacconi et al. (2013). The red data points show the Solar neighborhood (‘MW’) and the Central Molecular Zone (‘CMZ’) of the Milky Way, and three, local starbursts whose  $\gamma$ -ray emission is modelled in Krumholz et al. (2020). The observations have been homogenised to a Chabrier (2005) IMF and the convention for  $\alpha_{\text{CO}}$  suggested by Daddi et al. (2010a); see Krumholz et al. (2012) for details.

this scenario. Since the constant model is not physically well-motivated, this is not particularly surprising; the more surprising result is for the scattering model. We remind readers that this model for CR transport applies in an environment where there is an extrinsic turbulence cascade that reaches down to the gyroradius scale of the energetically-dominant  $\sim \text{GeV}$  CRs. We have shown Krumholz et al. (2020) that this is not the case for the neutral medium that dominates the mass and forms the stars. On the other hand, the long-standing classical interpretation of the totality of the CR and diffuse gamma-ray emission phenomenology is that the spectrum of the Milky Way’s steady state, hadronic cosmic ray distribution is informed by exactly this process of scattering on extrinsic turbulence (e.g., Jones et al. 2001).

This is not necessarily a contradiction: unlike the situation for starbursts (Krumholz et al. 2020), the MW midplane ISM is not single phase. Rather, the filling factors of the dense, neutral phase and the more diffuse, ionised phase are similar in the midplane (Kalberla & Kerp 2009). Moreover, the ionised gas filling factor increases towards unity as we rise away from the midplane and individual SNRs or stellar cluster superbubbles form chimneys into the hot, ionised halo. Thus some – potentially large – fraction of CRs accelerated by SNR shocks in Milky Way-like conditions may never encounter a large grammage of matter in escaping the midplane, i.e., they experience an effective  $\tau_{\text{abs}} \ll 1$  and, incidentally, also  $\tau_{\text{stream}} \ll 1$  given that streaming losses are generically small, in relative terms, for the scattering mode.

These CRs – provided that the classical picture of scattering on an extrinsic turbulent cascade is roughly correct – will render the ionised gas column hydrostatically unstable. This applies for Milky Way conditions according to Figure 4. Of course, an assumption here is that the classical picture of scattering on extrinsic turbulence is essentially the correct one for the ionised phase, and this may not actually hold (e.g., Zweibel 2017; Blasi 2019). On the other hand, recognising that the ionised gas column for most low surface-density galaxies will only constitute some  $\lesssim 10\%$  of the total column, Figure 4 may actually tend to exaggerate stability with respect to cosmic ray feedback in the ionised phase for such galaxies.

In summary, as has long been recognised (Jokipii 1976; Ko et al. 1991; Breitschwerdt et al. 1991; Everett et al. 2008; Socrates et al. 2008), it is hard to escape the conclusions that for local galaxy conditions, CRs will likely drive winds in the ionised gas phase. This will lead to mass loss over cosmological timescales. However, none of these considerations preclude the existence of a hydrostatic equilibrium in the dense, neutral phase that allows it to sustain the star formation process. Overall, the picture we thus arrive at here is that there are effectively two transport regimes operating for CRs in Milky Way-like galaxies (according to the ISM phase within which CRs are propagating). Qualitatively this agrees with the long-standing argument (Ginzburg et al. 1980) that the correct interpretation of local CR phenomenology<sup>7</sup> is that there are distinct disc and halo CR propagation zones, with the halo diffusion coefficient significantly (i.e.,  $3\text{--}10\times$ ) larger than the disc one (while the characteristic matter density in the disc is, of course, substantially larger than that in the halo).

#### 4.3 The role of the Alfvénic Mach number

One of the important parameters that appears in our models is the Alfvénic Mach number of the turbulence. This parameter controls the streaming speed and thus the strength of streaming losses directly, and also affects the overall diffusion rate – weakly for the scattering or constant models, strongly for the streaming transport model. We have argued based on dynamo theory that  $M_A$  will always be in the range  $\sim 1\text{--}2$  in galactic discs (Federrath et al. 2014; Federrath 2016), but it is important to investigate to what extent our conclusions are dependent on this argument.

We first investigate this in the context of the streaming model, where the  $M_A$ -dependence is greatest. In Figure 5 we show critical stability curves for this model computed with various value of  $M_A$ . In the high  $M_A$  limit the stability curve becomes universal (i.e., independent of the transport mode) because the CR energy density is set purely by hadronic losses right across the range of gas surface density; the critical curve in this limiting case is shown as the dashed red

<sup>7</sup> Specific aspects of CR phenomenology that support the existence of a CR halo include i) the very low levels of CR anisotropy and ii) the difficulty encountered in otherwise reconciling CR age measurements obtained with unstable “clock” nuclei (like  $^{10}\text{Be}$ ) with the grammage encountered by typical  $\sim\text{GeV}$ + CRs as inferred from secondary to primary CR nuclei ratios.

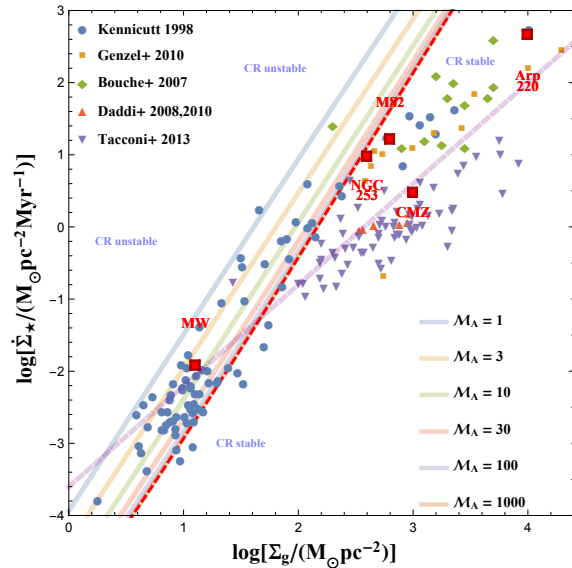


**Figure 5.** Critical stability curves for the streaming mode of CR transport with  $M_A$  as given in the legend. Parameters and data points are identical to those used in Figure 4, except for  $M_A$ . The red, dashed curve shows the stability curve in the high  $M_A$  limit, where it is completely determined by hadronic losses.

line in the figure. Note that, were ordinary, local disc galaxies operating in this limit, their neutral ISM phase would be unstable and driving a strong outflow, something that we do not observe. This implies, minimally, that magnetic fields in such galaxies are not too far below equipartition with respect to turbulent energy density (as expected in the case that a local turbulent dynamo is operating, and as we see directly in the Milky Way). More speculatively, it may be that gas motions induced by CRs in the case that the atmosphere is CR unstable help to drive magnetic fields towards equipartition at the lower surface gas density end of the distribution.

The difference between  $M_A = 1$  and 2 is far smaller for the scattering and constant models. This occurs because, for these modes, the streaming loss timescales are relatively long while the diffusive escape or collisional timescales are either mildly dependent or completely independent of  $M_A$ . The critical curves for the scattering and constant  $\kappa$  cases also become identical at high  $\Sigma_{\text{gas}}$ . This occurs because the collisional timescale formula is universal and collisional losses are solely responsible for setting the CR energy density in this regime. The streaming curve does not exhibit this behaviour because here streaming losses remain comparable to collisional losses even up to very high  $\Sigma_{\text{gas}}$ . The streaming case approaches the streaming and constant curves at high  $\Sigma_{\text{gas}}$  only in the limit  $M_A \gg 1$ .

#### 4.4 Unimportance of convective transport

On the basis of equation 42,  $\dot{\Sigma}_{*,c} \propto K_* f_{\text{edd},c}$ , so it might seem that we should expect that there should be clear structures in the critical curves where  $K_*$  becomes equal to unity

and the CR transport mechanism changes between convection and some other process. The  $K_* = 1$  regime occurs for  $\Sigma_{\text{gas}} \lesssim 10 M_\odot \text{ pc}^{-2}$  for the streaming transport model, and for  $\Sigma_{\text{gas}} \gtrsim 10^3 M_\odot \text{ pc}^{-2}$  for the starburst and scattering transport models, yet there are clearly no sharp features visible in the critical curves. Indeed, even if we explicitly ignore convection (i.e., we allow  $K_* < 1$  when computing  $\dot{\Sigma}_{*,c}$ ), we find critical curves that are essentially identical.

We can understand the reason for this both mathematically and physically. Mathematically, for a scattering or constant  $\kappa$  model of CR transport, the diffusive transport rate only becomes smaller than the convective rate in galaxies with very high surface densities. However, these galaxies also have  $\tau_{\text{abs}} \gg 1$ , and in this limit we have  $f_{\text{Edd},c} \propto \tau_{\text{abs}}$ . Since  $\tau_{\text{abs}} = \tau_{\text{pp}}/K_*\beta$ , we arrive at  $\dot{\Sigma}_* \propto \tau_{\text{pp}}/\beta$ , with no dependence on  $K_*$ ; this is why a sharp change in the value of  $K_*$  does not generate a corresponding sharp change in  $\dot{\Sigma}_*$ . Physically, the origin of this behaviour is that the only galaxies in which the rate of diffusive CR transport becomes smaller than the rate of convective transport are those with very high gas densities, and thus high  $\tau_{\text{abs}}$ . In these galaxies, the dominant CR loss process is no longer diffusive escape, it is pion production. In this regime, the rate of transport – diffusive or convective – is irrelevant to setting the CR energy density. Instead, the CR energy density is simply set by the competition between injection and pion loss, and it is the balance between these two processes that determines the location of the critical curve, the point at which the CR pressure becomes too high to permit hydrostatic balance.

For the streaming model, the transition to convective transport happens at low gas surface density. However, in these galaxies we also have  $\tau_{\text{stream}} \gtrsim 1$ , and thus  $f_{\text{Edd},c} \propto \tau_{\text{stream}}$ . Since  $\tau_{\text{stream}} \propto 1/K_*$ , the dependence of  $\dot{\Sigma}_*$  on  $K_*$  again disappears, and thus there is again no sudden change in the critical curve when we reach the convective limit. The physical origin of the behaviour in this place is that, for this transport model, CRs are lost primarily to streaming rather than to escape. We again therefore have a situation where the CR energy density is set by the balance between streaming and injection, a balance that does not depend on the effective diffusion coefficient.

#### 4.5 Cosmic rays versus radiation pressure as wind launching mechanisms

CRs are of interest as a feedback mechanism partly because they are much less efficiently lost to cooling than hot gas produced by SN explosions. However, a second appealing aspect of CR feedback is that CRs are “cool”, in that they can accelerate gas without the need for a shock, and thus naturally explain the presence of low-temperature species in galactic winds. It is therefore interesting to compare CRs to radiation pressure, which is another cool feedback mechanism. Radiation pressure can be delivered either by the direct stellar radiation field or by radiation that has been absorbed by dust and reprocessed into the infrared (cf. red dotted line in Figure 4 which interpolates between these limits). At galactic scales, the latter mechanism is only important in the densest starbursts (Thompson et al. 2005; Crocker et al. 2018a,b), precisely where we have shown that CR feedback is ineffective. The more interesting comparison is therefore in the

regime of low surface density galaxies, where direct, or “single scattering”, radiation pressure dominates (e.g., Scoville et al. 2001; Murray et al. 2005; Fall et al. 2010; Andrews & Thompson 2011; Thompson et al. 2015; Skinner & Ostriker 2015; Thompson & Krumholz 2016; Wibking, Thompson, & Krumholz 2018).

For a region of a galactic disc with areal star formation rate  $\dot{\Sigma}_*$ , the momentum per unit area per unit time delivered by the radiation field per hemisphere in the single scattering limit is

$$\dot{P}_{\text{ss}} = \frac{1}{c} \dot{\Sigma}_* \Phi_{1/2}, \quad (46)$$

where

$$\Phi_{1/2} \simeq 6.0 \times 10^{50} \text{ erg}/M_\odot \quad (47)$$

is the efficiency for conversion of gas mass into radiation (into one galactic hemisphere) via the star formation process (Kennicutt & Evans 2012). Note that we are assuming that all of the direct stellar radiation is absorbed. This is an upper limit, but cannot be wrong by a large factor, since, as pointed out by Andrews & Thompson (2011),  $\sim 1/3$  of the radiation momentum budget is in ionising photons, which will be absorbed even by a tiny column of neutral gas. By comparison, the momentum per unit area per unit time in the upward direction delivered by CRs into each hemisphere, integrating over the gas column, is

$$\dot{P}_c = -P_* \int_0^\infty \frac{dp_c}{d\xi} d\xi. \quad (48)$$

To evaluate the integral, we can make use of equation 1:

$$\begin{aligned} \int_0^\infty \frac{dp_c}{d\xi} d\xi &= \frac{1}{\tau_{\text{stream}}} \left[ \int_0^\infty \left( \tau_{\text{abs}} r p_c + \frac{\tau_{\text{stream}}}{\beta_s} \frac{d\mathcal{F}_c}{d\xi} \right) d\xi \right] \\ &= \frac{1}{\beta_s} [\mathcal{F}_c(\infty) - \mathcal{F}_c(0)] + \frac{f_{\text{Edd}} f_{\text{cal}}}{\tau_{\text{stream}}}, \end{aligned} \quad (49)$$

where

$$f_{\text{cal}} = \frac{\tau_{\text{abs}}}{f_{\text{Edd}}} \int_0^\infty r p_c d\xi \quad (50)$$

is the “calorimetric fraction”, i.e., the fraction of all CRs that are lost to pion production (c.f. equation 64 of Paper I), and  $\mathcal{F}_c(\infty)$  is the flux at  $\xi = \infty$ .

Therefore we find that the ratio of CR to single-scattering radiation momentum is

$$\begin{aligned} \frac{\dot{P}_c}{\dot{P}_{\text{ss}}} &= \left( \frac{\epsilon_{c,1/2}}{\Phi_{1/2}} \right) \frac{1}{\beta_s} \left[ 1 - f_{\text{cal}} - \frac{\mathcal{F}_c(\infty)}{\mathcal{F}_c(0)} \right] \\ &\simeq 9.3 \times 10^{-4} \frac{1}{\beta_s} \left[ 1 - f_{\text{cal}} - \frac{\mathcal{F}_c(\infty)}{\mathcal{F}_c(0)} \right] \\ &\simeq \frac{2.8}{v_{s,2}} \left[ 1 - f_{\text{cal}} - \frac{\mathcal{F}_c(\infty)}{\mathcal{F}_c(0)} \right] \end{aligned} \quad (51)$$

where  $v_{s,2} \equiv v_s/(100 \text{ km/s})$  and we have made use of equation 9, equation 17, equation 41 to simplify. This expression has a straightforward physical interpretation. The leading numerical factor of  $\approx 10^{-3}$  in the second line represents the ratio of energy injected into photons versus energy injected into CRs. The second term,  $1/\beta_s$ , which is always  $\gg 1$ , accounts for the fact that CRs transfer momentum to the gas much more efficiently than photons, due to the fact that

their propagation speed is limited to a value  $\ll c$  by scattering off Alfvén waves. Finally, the factor in square brackets just represents the reduction in CR momentum transfer due to loss of CRs by pion production (the  $f_{\text{cal}}$  term) and due to the escape of some fraction of the injected CRs from the disc without interaction (the  $\mathcal{F}_c(\infty)/\mathcal{F}_c(0)$  term). It approaches unity if all of the CR energy is lost to streaming, and becomes smaller if there is significant CR energy loss into other channels. This term can be evaluated numerically from our solutions, and, for the low surface density galaxies with which we are concerned here, is generally in the range  $\sim 0.1 - 1$  – see Section 4.3 of [Paper I](#).

The implication of [equation 51](#) is that CRs deliver more momentum to the gas than single-scattering radiation pressure if the CR streaming speed satisfies  $v_s \lesssim 100 \text{ km s}^{-1}$ ; the exact condition will depend on details such as the fraction of photon momentum that is actually absorbed, which is likely close to unity in spiral galaxies, but below unity in dust-poor dwarfs. Regardless of the exact numerical limit on  $v_s$ , the condition is certainly met if the CRs propagate through ionised gas, for which the streaming speed is nearly equal to the total gas Alfvén speed, which, for  $M_A \sim 1$ , is comparable to the  $\sim 10 \text{ km s}^{-1}$  velocity dispersion in the ISM. Thus in the scattering or constant  $\kappa_*$  CR propagation scenarios, CRs are more important than photons.

For our favoured streaming scenario, the question of whether CRs or photons are more important is more subtle because the streaming speed in this case is close to the ion Alfvén velocity, which, in a weakly-ionised medium, is much larger than the total Alfvén velocity or the velocity dispersion. Since we are concerned here with low surface density galaxies whose interstellar media are predominantly atomic, we expect the ionisation fraction  $\chi \sim 10^{-2}$  ([Wolffire et al. 2003](#)), and thus the ion Alfvén speed to be  $\approx 10$  times the bulk gas velocity dispersion. This suggests that CRs and single scattering radiation are of roughly comparable importance, and both may contribute to the launching of galactic winds in such galaxies (cf. [Figure 4](#)). CRs are probably somewhat more important than photons in low-metallicity dwarfs, where the absence of dust will render galaxies more transparent and thus reduce  $\dot{M}_{\text{ss}}$ , though only by a factor of  $\sim 3$  as noted above; on the other hand, it is possible that the equilibrium ionisation fraction is also slightly higher in low-metallicity dwarfs.<sup>8</sup> For denser galaxies whose interstellar media are largely molecular,  $\chi$  is smaller, and the ion Alfvén speed correspondingly larger. In these galaxies photons deliver more momentum than CRs; however, this changeover likely has little practical importance, since both direct photons and CRs are generally unimportant in these galaxies.

Finally, we note that our [equation 51](#) is somewhat different from the analogous expression (their equation 21) of [Socrates et al. \(2008\)](#). We discuss the reasons for this difference in [Appendix A](#).

<sup>8</sup> Also note that, though the (red, dashed)  $P_{\text{rad,ss}}$  line in [Figure 4](#) falls above the locus of points at low surface densities, [Thompson & Krumholz \(2016\)](#) argue that radiation pressure in a turbulent medium will be most important along low-column density sightlines not representative of the mean gas surface density.

## 5 CONCLUSIONS

In this paper we analyse the stability of the neutral, star-forming phase of galactic discs against cosmic ray (CR) pressure. We use an idealised model where such discs are taken to be plane-parallel slabs of gas confined by stellar and gas self-gravity, and supported by a combination of turbulent and CR pressure. Such a system is characterised primarily by three dimensionless numbers: the effective optical depths of the disc to CR absorption (via  $\pi$  production) and to CR streaming, and the CR Eddington ratio (defined by the ratio of the CR momentum flux to the gravitational momentum flux). The primary result of our analysis is that such a system possesses a stability limit: for a given effective optical depth, there exists a maximum CR Eddington ratio above which the system cannot remain hydrostatic. While the nature of the non-linear development of the resulting instability is uncertain, studies of the analogous instability driven by radiation suggests that the result is likely to be an outflow that removes mass until the system is driven back below the stability limit.

Given standard estimates for the efficiency with which SNe inject CRs into galaxies, together with characteristic numbers describing the magnetohydrodynamic turbulence in the ISM and a model for CR transport in a turbulent medium, we can translate our stability limit directly into a line in the space of gas surface density and star formation rate, the so-called Kennicutt-Schmidt (KS) plane. We find that the stability limit projected on to the KS plane is close to a line of slope 2, which, for our favoured model of CR transport closely matches the upper envelope of observed systems with the surface densities characteristic of modern spiral and dwarf galaxies,  $\Sigma_{\text{gas}} \lesssim 300 M_{\odot} \text{ pc}^{-2}$ . While a scaling  $\propto \Sigma_{\text{gas}}^2$  for the critical star formation rate density with gas surface density is generic to feedback mechanisms (e.g. [Andrews & Thompson 2011](#)), the fact that our calculation should have produced such a coincidence between the *normalization* of the critical curve and the upper range of the occupied KS parameter space is surprising: In the dimensionless parameter space of  $\tau_{\text{stream}}$ ,  $\tau_{\text{abs}}$ , and  $f_{\text{Edd}}$  that defines our system, the critical value of  $f_{\text{Edd}}$  above which the gas column is rendered hydrostatically unstable follows purely from the mathematical form of our ODEs. The only astrophysical inputs required to map this to the KS plane are then fundamental constants (e.g., the  $pp$  cross-section), quantities describing general physical processes that are unrelated to galaxies (e.g., the saturation field strength of turbulent dynamos), and quantities describing microphysical processes such as the conversion efficiency from supernova kinetic energy to CR energy. The only complex modeling needed is that required to estimate the ionization fraction, which is determined at least partly by the CRs themselves. Given these inputs, the overall similarity of the CR stability limit to the observed galaxy distribution seems unlikely to be a coincidence. We suggest that the star-forming gas in modern and/or low surface gas density galaxies is poised close to instability such that rather small changes in ISM parameters imply the launching of CR-driven outflows; CRs – possibly in concert with direct radiation pressure – thus define the upper limit to the star-formation efficiency of ordinary, star-forming disc galaxies.

In contrast, we find that galaxies with higher gas and



star formation surface densities lie well below the CR stability limit. This divergence between the CR stability line and the sequence occupied by observed galaxies has two related but distinct causes. The first is simply that the fundamental scaling that governs all considerations of feedback: the self-gravitational pressure of a galactic disc rises as the square of the gas surface density, whereas the available energy input from star formation, given that the observed index of the Kennicutt-Schmidt relation is  $< 2$ , rises more slowly. However, this alone would not be enough to prevent CRs from becoming significant at high surface densities, since, in the absence of loss mechanisms, CRs would also become increasingly well-confined in high surface density galaxies, and this would cause a superlinear rise in the CR pressure. Indeed, it was precisely this consideration that led [Socrates et al. \(2008\)](#) to conclude that CR feedback dominates in high surface-density galaxies. That it does not do so is due to the second factor that suppresses CR feedback in gas-rich galaxies: the increasing importance of hadronic losses. We show that the critical Eddington ratio above which CRs destabilise a galactic disc scales as the sum of the optical depths of a galactic disc to streaming and hadronic losses. While the former varies only weakly across the star-forming sequence, the latter becomes very large in high surface-density galaxies. Consequently, despite the fact that the discs are starburst galaxies that confine CRs quite well, hadronic losses prevent the CR energy density from building up to the point where CRs are able to launch outflows. Thus we conclude that CRs cannot be dynamically important in the star-forming ISM phase of these galaxies. Conversely, however, due to the importance of pion losses, these galaxies are good CR calorimeters and, therefore,  $\gamma$ -ray sources (cf. [Torres et al. 2004](#); [Thompson et al. 2007](#); [Lacki et al. 2010, 2011](#); [Yoast-Hull et al. 2016](#)).

In future work we intend to explore the consequences of the picture set out here and in [Krumholz et al. \(2020\)](#) and [Paper I](#) for understanding the far infrared–radio continuum correlation and the emerging far infrared– $\gamma$ -ray correlation, and to delimit the possible contribution of hadronic  $\gamma$ -ray emission from star-forming galaxies to the isotropic  $\gamma$ -ray flux as predicted by our model.

## DATA AVAILABILITY STATEMENT

No new data were generated or analysed in support of this research.

## ACKNOWLEDGEMENTS

This research was funded by the Australian Government through the Australian Research Council, awards FT180100375 (MRK) and DP190101258 (RMC and MRK). RMC gratefully acknowledges conversations with Felix Aharonian, Geoff Bicknell, Yuval Birnboim, Luke Drury, Alex Lazarian, Chris McKee, Christoph Pfrommer, Heinz Völk, and Siyao Xu. MRK and TAT acknowledge support from the Simons Foundation through the Simons Symposium Series “Galactic Superwinds: Beyond Phenomenology”, during which some aspects of this work were planned. TAT thanks

Brian Lacki and Eliot Quataert for discussions and collaboration. TAT is supported in part by National Science Foundation Grant #1516967 and NASA ATP 80NSSC18K0526.

## REFERENCES

- Abdo, A. A., Ackermann, M., Ajello, M., et al. 2010, *ApJ*, 709, L152
- Acero, F., Aharonian, F., Akhperjanian, A. G., et al. 2009, *Science*, 326, 1080
- Andrews, B. H., & Thompson, T. A. 2011, *ApJ*, 727, 97
- Beck, R. 2015, *A&ARv*, 24, 4
- Behroozi, P. S., Wechsler, R. H., & Conroy, C. 2013, *ApJ*, 762, L31
- Bell, A. R. 1978, *MNRAS*, 182, 147
- Bell, A. R. 2004, *MNRAS*, 353, 550
- Blasi, P. 2019, *Galaxies*, 7, 64
- Boettcher, E., Zweibel, E. G., Gallagher, J. S., III, & Benjamin, R. A. 2016, *ApJ*, 832, 118
- Booth, C. M., Agertz, O., Kravtsov, A. V., & Gnedin, N. Y. 2013, *ApJ*, 777, L16
- Bouché, N., Cresci, G., Davies, R., et al. 2007, *ApJ*, 671, 303
- Boulares, A., & Cox, D. P. 1990, *ApJ*, 365, 544
- Breitschwerdt, D., McKenzie, J. F., & Voelk, H. J. 1991, *A&A*, 245, 79
- Breitschwerdt, D., McKenzie, J. F., & Voelk, H. J. 1993, *A&A*, 269, 54
- Buck, T., Pfrommer, C., Pakmor, R., et al. 2019, arXiv e-prints, arXiv:1911.00019
- Chabrier, G. 2005, *The Initial Mass Function 50 Years Later*, 327, 41
- Chan, T. K., Kereš, D., Hopkins, P. F., et al. 2019, *MNRAS*, 488, 3716
- Cho, J., & Lazarian, A. 2002, *Phys. Rev. Lett.*, 88, 245001
- Cho, J., & Lazarian, A. 2003, *MNRAS*, 345, 325
- Ceverino, D., Klypin, A., Klimek, E. S., et al. 2014, *MNRAS*, 442, 1545
- Condon, J. J. 1992, *ARA&A*, 30, 575
- Cox, D. P., & Smith, B. W. 1974, *ApJ*, 189, L105
- Crocker, R. M., Jones, D. I., Aharonian, F., et al. 2011, *MNRAS*, 411, L11
- Crocker, R. M. 2012, *MNRAS*, 423, 3512
- Crocker, R. M., Krumholz, M. R., Thompson, T. A., & Clutterbuck, J. 2018 (**CKTC18**), *MNRAS*, 478, 81
- Crocker, R. M., Krumholz, M. R., Thompson, T. A., Baumgardt, H., & Mackey, D. 2018, *MNRAS*, 481, 4895
- Crocker, R. M., Krumholz, M. R., & Thompson, T. A. [**Paper I**]
- Crutcher, R. M. 1999, *ApJ*, 520, 706
- Daddi, E., Dannerbauer, H., Elbaz, D., et al. 2008, *ApJ*, 673, L21
- Daddi, E., Bournaud, F., Walter, F., et al. 2010, *ApJ*, 713, 686
- Daddi, E., Elbaz, D., Walter, F., et al. 2010, *ApJ*, 714, L118
- Davis, S. W., Jiang, Y. F., Stone, J. M., & Murray, N. 2014, *ApJ*, 796, 107
- Dekel, A., Sarkar, K. C., Jiang, F., Bournaud, F., Krumholz, M. R., Ceverino, D., & Primack, J. 2019, *MNRAS*, 4, 4753
- Domingo-Santamaría, E., & Torres, D. F. 2005, *A&A*, 444, 403
- Dorfi, E. A., & Breitschwerdt, D. 2012, *A&A*, 540, A77
- Drury, L. O., Markiewicz, W. J., & Voelk, H. J. 1989, *A&A*, 225, 179
- Drury, L. O. ’., & Strong, A. W. 2017, *A&A*, 597, A117
- Everett, J. E., Zweibel, E. G., Benjamin, R. A., et al. 2008, *ApJ*, 674, 258
- Faerman, Y., Sternberg, A., & McKee, C. F. 2017, *ApJ*, 835, 52
- Fall, S. M., Krumholz, M. R., & Matzner, C. D. 2010, *ApJ*, 710, L142
- Federrath, C. 2016, *J. Plasm. Phys.*, 82, 535820601



- Federrath, C., Schober, J., Bovino, S., & Schleicher, D. R. G. 2014, *ApJ*, 797, L19
- Fermi-LAT collaboration, et al. 2012, *ApJ*, 755, 164
- Fermi-LAT collaboration, et al. 2019, submitted to *ApJS*, arXiv:1902.10045
- Funk, S. 2015, *Annual Review of Nuclear and Particle Science*, 65, 245
- Gentry, E. S., Krumholz, M. R., Dekel, A., & Madau, P. 2017, *MNRAS*, 465, 2471
- Genzel, R., Tacconi, L. J., Gracia-Carpio, J., et al. 2010, *MNRAS*, 407, 2091
- Ghosh, A., & Ptuskin, V. S. 1983, *Ap&SS*, 92, 37
- Ginzburg, V. L., & Syrovatskii, S. I. 1964, *The Origin of Cosmic Rays*
- Ginzburg, V. L., Khazan, I. M., & Ptuskin, V. S. 1980, *Ap&SS*, 68, 295
- Hanasz, M., Lesch, H., Naab, T., et al. 2013, *ApJ*, 777, L38
- Heckman, T. M., Armus, L., & Miley, G. K. 1990, *ApJS*, 74, 833
- Heckman, T. M. 2002, *Extragalactic Gas at Low Redshift*, 254, 292
- Heintz, E., & Zweibel, E. G. 2018, *ApJ*, 860, 97
- Hill, A. S., Joung, M. R., Mac Low, M.-M., et al. 2012, *ApJ*, 750, 104
- Hillas, A. M. 2005, *JPGNP*, 31, 95
- Hopkins, P. F., Quataert, E., & Murray, N. 2011, *MNRAS*, 417, 950
- Ipavich, F. M. 1975, *ApJ*, 196, 107
- Jiang, Y.-F., & Oh, S. P. 2018, *ApJ*, 854, 5
- Jokipii, J. R. 1976, *ApJ*, 208, 900
- Jones, F. C., Lukasiak, A., Ptuskin, V., et al. 2001, *ApJ*, 547, 264
- Jubelgas, M., Springel, V., Enßlin, T., & Pfrommer, C. 2008, *A&A*, 481, 33
- Kafexhiu, E., Aharonian, F., Taylor, A. M., & Vila, G. S. 2014, *Phys. Rev. D*, 90, 123014
- Kalberla, P. M. W., & Kerp, J. 2009, *ARA&A*, 47, 27
- Kennicutt, R. C., Jr. 1998, *ApJ*, 498, 541
- Kennicutt, R. C., Jr., & Evans, N. J. E., II. 2012, *ARA&A*, 50, 531
- Kim, C.-G., & Ostriker, E. C. 2015, *ApJ*, 802, 99
- Ko, C. M., Dougherty, M. K., & McKenzie, J. F. 1991, *A&A*, 241, 62
- Kroupa, P. 2001, *MNRAS*, 322, 231
- Krumholz, M. R., & Dekel, A. 2010, *MNRAS*, 406, 112
- Krumholz, M. R., & Thompson, T. A. 2012, *ApJ*, 760, 155
- Krumholz, M. R., Dekel, A., & McKee, C. F. 2012, *ApJ*, 745, 69
- Krumholz, M. R., & Thompson, T. A. 2013, *MNRAS*, 434, 2329
- Krumholz, M. R., Kruijssen, J. M. D., & Crocker, R. M. 2017, *MNRAS*, 466, 1213
- Krumholz, M. R., Burkhardt, B., Forbes, J. C., & Crocker, R. M. 2018, *MNRAS*, 477, 2716
- Krumholz, M. R., Crocker, R. M., Xu, S., Lazarian, A., Rosevear, M. T., & Bedwell-Wilson, J. 2020, *MNRAS*, in press, (arXiv:1911.09774)
- Kulsrud, R. M. 2005, *Plasma physics for astrophysics / Russell M. Kulsrud*. Princeton, N.J.: Princeton University Press, c2005. (Princeton series in astrophysics),
- Lacki, B. C., Thompson, T. A., & Quataert, E. 2010, *ApJ*, 717, 1
- Lacki, B. C., Thompson, T. A., Quataert, E., Loeb, A., & Waxman, E. 2011, *ApJ*, 734, 107
- Lacki, B. C. 2013, arXiv:1308.5232
- Levermore, C. D., & Pomraning, G. C. 1981, *ApJ*, 248, 321
- Levermore, C. D. 1984, *J. Quant. Spectrosc. Radiat. Transfer*, 31, 149
- Martin, P. 2014, *A&A*, 564, A61
- Martizzi, D., Faucher-Giguère, C.-A., & Quataert, E. 2015, *MNRAS*, 450, 504
- McKee, C. F., & Ostriker, J. P. 1977, *ApJ*, 218, 148
- McKee, C. F., Parravano, A., & Hollenbach, D. J. 2015, *ApJ*, 814, 13
- Muratov, A. L., Kereš, D., Faucher-Giguère, C.-A., et al. 2015, *MNRAS*, 454, 2691
- Murray, N., Quataert, E., & Thompson, T. A. 2005, *ApJ*, 618, 569
- Nomoto, K., Tominaga, N., Umeda, H., et al. 2006, *Nuclear Phys. A*, 777, 424
- Paglionie, T. A. D., & Abrahams, R. D. 2012, *ApJ*, 755, 106
- Pakmor, R., Pfrommer, C., Simpson, C. M., & Springel, V. 2016, *ApJ*, 824, L30
- Parker, E. N. 1966, *ApJ*, 145, 811
- Peng, F.-K., Wang, X.-Y., Liu, R.-Y., Tang, Q.-W., & Wang, J.-F. 2016, *ApJ*, 821, L20
- Peretti, E., Blasi, P., Aharonian, F., et al. 2019, *MNRAS*, 487, 168
- Persic, M., Rephaeli, Y., & Arieli, Y. 2008, *A&A*, 486, 143
- Pfrommer, C., Pakmor, R., Simpson, C. M., & Springel, V. 2017, *ApJ*, 847, L13
- Protheroe, R. J., Ott, J., Ekers, R. D., et al. 2008, *MNRAS*, 390, 683
- Ptuskin, V. S., Voelk, H. J., Zirakashvili, V. N., et al. 1997, *A&A*, 321, 434
- Ptuskin, V. S., Moskalenko, I. V., Jones, F. C., et al. 2006, *ApJ*, 642, 902
- Recchia, S., Blasi, P., & Morlino, G. 2016, *MNRAS*, 462, 4227
- Recchia, S., Blasi, P., & Morlino, G. 2017, *MNRAS*, 470, 865
- Rosdahl, J., Schaye, J., Teyssier, R., & Agertz, O. 2015, *MNRAS*, 451, 34
- Ruszkowski, M., Yang, H.-Y. K., & Zweibel, E. 2017, *ApJ*, 834, 208
- Rybicki, G. B., & Lightman, A. P. 1979, *A Wiley-Interscience Publication*
- Salem, M., & Bryan, G. L. 2014, *MNRAS*, 437, 3312
- Salem, M., Bryan, G. L., & Corlies, L. 2016, *MNRAS*, 456, 582
- Samui, S., Subramanian, K., & Srikanth, R. 2010, *MNRAS*, 402, 2778
- Schlickeiser, R. 2002, *Cosmic ray astrophysics / Reinhard Schlickeiser, Astronomy and Astrophysics Library; Physics and Astronomy Online Library*. Berlin: Springer. ISBN 3-540-66465-3, 2002, XV + 519 pp.,
- Scoville, N. Z., Polletta, M., Ewald, S., et al. 2001, *Astronom. J.*, 122, 3017
- Skilling, J., 1971, *ApJ*, 170, 265
- Skinner, M. A., & Ostriker, E. C. 2015, *ApJ*, 809, 187
- Simpson, C. M., Pakmor, R., Marinacci, F., et al. 2016, *ApJ*, 827, L29
- Socrates, A., Davis, S. W., & Ramirez-Ruiz, E. 2008, *ApJ*, 687, 202-215
- Strong, A. W., Porter, T. A., Digel, S. W., et al. 2010, *ApJ*, 722, L58
- Tacconi, L. J., Neri, R., Genzel, R., et al. 2013, *ApJ*, 768, 74
- Tennekes, H., & Lumley, J. L. 1972, *First Course in Turbulence*, Cambridge: MIT Press, 1972,
- Thomas, T., & Pfrommer, C. 2019, *MNRAS*,
- Thompson, T. A., & Lacki, B. C. 2013, *Cosmic Rays in Star-forming Environments*, 283
- Thompson, T. A., Quataert, E., & Murray, N. 2005, *ApJ*, 630, 167
- Thompson, T. A., Quataert, E., Waxman, E., et al. 2006, *ApJ*, 645, 186
- Thompson, T. A., Quataert, E., & Waxman, E. 2007, *ApJ*, 654, 219
- Thompson, T. A., Fabian, A. C., Quataert, E., & Murray, N. 2015, *MNRAS*, 449, 147
- Thompson, T. A., & Krumholz, M. R. 2016, *MNRAS*, 455, 334
- Thornton, K., Gaudlitz, M., Janka, H.-T., & Steinmetz, M. 1998, *ApJ*, 500, 95

- Torres, D. F., Reimer, O., Domingo-Santamaría, E., et al. 2004, *ApJ*, 607, L99
- Tsang, B. T. H., & Milosavljević, M. 2015, *MNRAS*, 453, 1108–1120
- Uhlig, M., Pfrommer, C., Sharma, M., et al. 2012, *MNRAS*, 423, 2374
- VERITAS Collaboration, Acciari, V. A., Aliu, E., et al. 2009, *Nature*, 462, 770
- Vogelsberger, M., Genel, S., Springel, V., et al. 2014, *MNRAS*, 444, 1518
- Völk, H. J., Aharonian, F. A., & Breitschwerdt, D. 1996, *Space Sci. Rev.*, 75, 279
- Wadepuhl, M., & Springel, V. 2011, *MNRAS*, 410, 1975
- Wentzel, D. G. 1974, *ARA&A*, 12, 71
- Wibking, B. D., Thompson, T. A., & Krumholz, M. R. 2018, *MNRAS*, 477, 4665
- Wiener, J., Pfrommer, C., & Oh, S. P. 2017, *MNRAS*, 467, 906
- Wilson, C. D., Elmegreen, B. G., Bemis, A., et al. 2019, *ApJ*, 882, 5
- Wolfire, M. G., McKee, C. F., Hollenbach, D., et al. 2003, *ApJ*, 587, 278
- Xu S., & Lazarian A., 2017, *New Journal of Physics*, 19, 065005
- Yan, H., & Lazarian, A. 2008, *ApJ*, 673, 942
- Yoast-Hull, T. M., Gallagher, J. S., & Zweibel, E. G. 2016, *MNRAS*, 457, L29
- Zirakashvili, V. N., Breitschwerdt, D., Ptuskin, V. S., et al. 1996, *A&A*, 311, 113
- Zirakashvili, V. N., & Völk, H. J. 2006, *ApJ*, 636, 140
- Zweibel, E. G. 2013, *Physics of Plasmas*, 20, 055501
- Zweibel, E. G. 2017, *Physics of Plasmas*, 24, 055402

## APPENDIX A: COSMIC RAYS VERSUS RADIATION: COMPARISON TO THE RESULTS OF SOCRATES ET AL. (2008)

Our result for the ratio of CR to single-scattering radiation momentum imparted to the gas, [equation 51](#), is substantially different at first glance from that derived by [Socrates et al. \(2008\)](#). In this appendix we explain the reasons for this difference. Using our notation, the basic result from [Socrates et al.](#), their equation 21 is

$$\dot{\Pi}_c \sim \tau_{\text{CR}} \epsilon_{c,1/2} \dot{\Sigma}_*, \quad (\text{A1})$$

where  $\tau_{\text{CR}}$  is the effective optical depth of the galactic disc to CR scattering, which [Socrates et al.](#) argue is  $\sim 10^3$ . This expression differs from our [equation 51](#) in that dimensionless factor on the right hand side is  $\tau_{\text{CR}}$ , rather than  $[1 - f_{\text{cal}} - \mathcal{F}_c(\infty)/f_{\text{Edd}}]/\beta_s$ .

The difference in the two expressions can be explained by noting that the expression of [Socrates et al.](#) does not incorporate any loss mechanisms for CRs, either streaming or hadronic<sup>9</sup>. Thus they are here implicitly taking the limits  $\tau_{\text{abs}} \rightarrow 0$  and  $\tau_{\text{stream}} \rightarrow 0$ . We can first verify that, if we adopt the same limit, our results reduce to theirs. In this case we cannot use [equation 51](#) directly, because in this limit  $f_{\text{cal}} \rightarrow 0$ ,  $\mathcal{F}_c(\infty) \rightarrow f_{\text{Edd}}$ , and  $\beta_s \rightarrow 0$ , and thus the numerator and denominator of the equation both approach zero. However, for the case of zero losses, [equation 1](#) immediately implies

$d\mathcal{F}_c/d\xi = 0$ , so  $\mathcal{F}_c = \mathcal{F}_c(0) = f_{\text{Edd}}$  is constant. We then have, from [equation 2](#),

$$\int_0^\infty \frac{dp_c}{d\xi} d\xi = -f_{\text{Edd}} \int_0^\infty r^q d\xi = -f_{\text{Edd}} \frac{r(0)^{q+1}}{q+1}, \quad (\text{A2})$$

where  $q$  is the index describing the scaling of the diffusion coefficient with the ambient density and  $r(0)$  is the value of  $r$  at  $\xi = 0$ , and we have taken  $r \rightarrow 0$  as  $\xi \rightarrow \infty$ . The quantity  $r(0)^{q+1}/(q+1)$  is of order unity, and thus we recover, in dimensional terms

$$\dot{\Pi}_c \sim P_* f_{\text{Edd}}. \quad (\text{A3})$$

If we now rewrite  $f_{\text{Edd}}$  in terms of the injected CR flux  $F_{c,0}$  using [equation 17](#) and [equation 11](#), and dropping factors of order unity, we arrive at

$$\dot{\Pi}_c \sim F_{c,0} \frac{z_*}{K_*}. \quad (\text{A4})$$

The quantity  $\kappa_*/z_*$  has units of velocity, and can be thought of as the effective velocity which CRs diffuse, which is lower than the true microphysical velocity by a factor of  $\tau_{\text{CR}}$ . Thus if we further assume that CRs have a microphysical speed of  $c$  in between scatterings, then it immediately follows that

$$\dot{\Pi}_c \sim \tau_{\text{CR}} \frac{F_{c,0}}{c}, \quad (\text{A5})$$

which is exactly the [Socrates et al.](#) result.

With this understood, we can now explain why [Socrates et al.](#)'s results differ from our [equation 51](#). In the absence of losses, the CR pressure that can build up inside the disc is limited only by considerations of hydrostatic equilibrium. If one considers only CR transfer, then for a sufficiently small value of the CR diffusion coefficient  $\kappa_*$  (or its dimensionless analog  $K_*$ ), the Eddington ratio  $f_{\text{Edd}}$  can become arbitrarily large, allowing  $\dot{\Pi}_c$  to become similarly large. However, it is not self-consistent to retain the assumptions that  $\tau_{\text{stream}} \sim 0$  and  $\tau_{\text{abs}} \sim 0$  as  $K_* \rightarrow 0$  – from [equation 9](#) and [equation 10](#), we see that  $\tau_{\text{stream}}$  and  $\tau_{\text{abs}}$  both scale as  $1/K_*$ . Thus if a galactic disc has small  $K_*$ , possibly allowing a large CR pressure to build up, it necessarily also has large  $\tau_{\text{stream}}$  and  $\tau_{\text{abs}}$ , which reduce or counteract that buildup. Mathematically, this effect manifests in the fact that [equation 51](#) has a coefficient of  $[1 - f_{\text{cal}} - \mathcal{F}_c(\infty)/f_{\text{Edd}}]/\beta_s$ , which approaches [Socrates et al.](#)'s factor  $\tau_{\text{CR}}$  as  $\tau_{\text{abs}} \rightarrow 0$  and  $\tau_{\text{stream}} \rightarrow 0$ , but is smaller outside of these limits. Physically, the effect is that, if one attempts to confine CRs by making their diffusion slow, then at the same time this raises the importance of streaming and hadronic losses, which set limits on the extent to which the CR pressure can build up.

This paper has been typeset from a  $\text{\LaTeX}$  file prepared by the author.

<sup>9</sup> Note that [Socrates et al.](#) do consider CR losses elsewhere in their manuscript (see, for instance, their Appendix C).

# Cosmic Ray Feedback Bounds the Star Formation Efficiency of Spiral Galaxies

Roland M. Crocker,<sup>1\*</sup> Mark R. Krumholz,<sup>1</sup> and Todd A. Thompson,<sup>2</sup>

<sup>1</sup>*Research School of Astronomy and Astrophysics, Australian National University, Canberra 2611, A.C.T., Australia*

<sup>2</sup>*Department of Astronomy and Center for Cosmology & Astro-Particle Physics, The Ohio State University, Columbus, Ohio 43210, U.S.A*

Accepted XXX. Received YYY; in original form ZZZ

## ABSTRACT

Star formation proceeds inefficiently in galaxies. Moreover, in many galaxies – including the Milky Way – it is known or inferred that cosmic rays (CRs) provide a significant fraction of the total ISM pressure and therefore contribute to hydrostatic balance. Here we develop a semi-analytic model for the potential dynamical effect of the flux of CRs, directly accelerated as a result of star formation itself, on the ISM gas column. We determine the critical CR fluxes – and corresponding star formation rate surface densities – above which hydrostatic equilibrium within a given galaxy is precluded because CRs drive the gas off in a wind or otherwise render it unstable. The locus of this CR stability curve patrols the high side of the observed distribution of galaxies in the Kennicutt-Schmidt parameter space of star formation rate versus gas surface density for galaxies with  $\Sigma_{\text{gas}} \lesssim 10^{2.5} M_{\odot}/\text{pc}^2$ . We thus conclude that CR feedback sets an ultimate limit to the star formation efficiency of most ‘ordinary’ galaxies. At the higher surface densities pertinent to star burst systems, however, pionic losses imply that CRs are dynamically unimportant on global scales.

**Key words:** hydrodynamics – instabilities – ISM: jets and outflows – radiative transfer – galaxies: ISM – galaxies: star clusters

arXiv:2006.15821v1 [astro-ph.GA] 29 Jun 2020

\* E-mail: rcrocker@fastmail.fm (RMC)

## 1 INTRODUCTION

The formation of galaxies is a remarkably inefficient process. Matter flows into galaxies through the cosmic web, becoming part of the interstellar medium and eventually forming stars. However, galaxies convert at most 10% of this gas to stars per orbit, and at least some galaxies eject more mass into galactic winds than they successfully convert to stars. Despite extensive exploration in the literature of two plausible agents to curb star formation – the hot gas produced in supernova explosions and starlight emitted by young, bright stars – the identity of the mechanism responsible for this inefficiency remains one of the enduring mysteries of astrophysics. Our goal in this paper is to explore another plausible feedback agent: the relativistic cosmic rays (CRs) that supernovae produce along with hot gas.

Supernovae eventually deposit  $\sim 10\%$  of their kinetic energy into these particles, which then disperse out to suffuse the interstellar medium; within our own Galaxy, the CR energy density of the Galactic disc is near equipartition with the magnetic field and turbulent gas motions, and CRs therefore contribute significantly to the vertical hydrostatic equilibrium of gas in the Milky Way (Boulares & Cox 1990). Unlike the thermal gas that receives most of the supernova energy, CRs lose energy to radiation very slowly. This means that they are potentially important as an agent of feedback despite only receiving a fraction of the supernova energy budget. However, despite early pioneering work (Ipavich 1975; Breitschwerdt et al. 1991, 1993), the possibility that CRs might be an important source of feedback in galaxy formation has only recently begun to receive sustained attention, in either observations and analytic models (e.g., Everett et al. 2008; Samui et al. 2010; Crocker et al. 2011; Crocker 2012; Lacki et al. 2011; Hanaasz et al. 2013; Yoast-Hull et al. 2016), or in simulations (e.g., Jubelgas et al. 2008; Wadepuhl & Springel 2011; Uhlig et al. 2012; Booth et al. 2013; Salem & Bryan 2014; Salem et al. 2016; Pakmor et al. 2016; Simpson et al. 2016; Recchia et al. 2016, 2017; Ruszkowski et al. 2017; Pfrommer et al. 2017; Chan et al. 2019; Buck et al. 2019).

Observational knowledge of the importance of CRs in galaxies other than our own is rather limited. The well-known far infrared-radio correlation (Condon 1992) indicates a correlation between galaxies’ star formation rates and their leptonic CR populations, but since synchrotron luminosity depends not just on CR electron acceleration, but on complex factors such as the amplitude of the magnetic field and the local interstellar radiation field, it has proven challenging – albeit, not impossible (cf. Thompson et al. 2006; Lacki et al. 2010; Lacki 2013) – to draw strong conclusions about CR acceleration from radio observations. Radio observations directly constrain only leptonic CRs, whereas hadronic CRs carry the bulk of the CR energy density and pressure. Beyond the Milky Way, direct detection of  $\gamma$ -rays produced by the hadronic CRs that carry most of the energy has only recently become possible with the launch of the *Fermi*/LAT experiment and the development of the current generation of Imaging Air Cherenkov telescope arrays (e.g., Funk 2015). While there is now an established literature – first anticipating, more recently, contemplating (e.g., Völk et al. 1996; Zirakashvili et al. 1996; Torres et al. 2004; Domingo-Santamaría & Torres 2005; Thompson et al. 2007;

Persic et al. 2008; Lacki et al. 2011; Yoast-Hull et al. 2016) – the implications of the  $\gamma$ -ray detection of star-forming galaxies, the number of star-forming galaxies detected thus far is still  $< 10$  (e.g., VERITAS Collaboration et al. 2009; Acero et al. 2009; Abdo et al. 2010; Fermi-LAT collaboration 2012; ?, 2019), and such  $\gamma$ -rays signals as have been detected may, in any case, be polluted by contributions from various sources or processes other than a galaxy’s diffuse, hadronic CR population.

Given the paucity of direct observational constraints, exploration of CR feedback as a regulator of star formation is necessarily driven mostly by theory. However, there is vast disagreement in the theoretical literature about where and when CRs might be important, with some authors concluding they are capable of driving galactic winds only off the most rapidly star-forming galaxies (e.g., Socrates et al. 2008), others finding that they drive winds only in dwarfs, (e.g., Jubelgas et al. 2008; Uhlig et al. 2012), and yet others finding that they do not drive winds by themselves at all, but can reheat and energise winds produced by other processes (e.g. Ruszkowski et al. 2017). In simulations, the results seem to depend strongly on the exact prescription adopted for microphysical CR transport (e.g., Salem & Bryan 2014; Salem et al. 2016; Wiener et al. 2017; Buck et al. 2019).

The disagreements in the literature suggest that a first-principles effort to understand where and when CRs might be important, taking into account all the available observational constraints, seems warranted, and this is the primary goal of our paper. We seek to cut a broad swathe across the parameter space of star-forming galaxies, and determine where within this parameter space CRs might be important agents of feedback. [MRK: I deleted a block of text here; it’s commented out in the latex source] The remainder of this paper is structured as follows: In Section 2 we present the mathematical setup of our problem and, in particular, set out the ordinary differential equation (ODE) system that describes a self-gravitating gaseous disc that maintains a quasi-hydrostatic equilibrium while subject to a flux of CRs injected at its midplane; in Section 3 we present, describe, and evaluate the numerical solutions of our ODEs; in Section 4 we consider the astrophysical implications of our findings for CR feedback on the dense, star-forming gas phase of spiral galaxies; we further discuss our results and summarise in Section 5.

## 2 SETUP

### 2.1 Physical Model

The physical system that we consider here is similar to that modelled in the pioneering work of Socrates et al. (2008), and we have used in previous studies of radiation pressure feedback (Krumholz & Thompson 2012, 2013; Crocker et al. 2018a,b; Wibking, Thompson, & Krumholz 2018): an idealised 1D representation of a portion of a galactic disc consisting of a gas column confined by gravity through which radiation or CRs are forced from below. In the radiation context, we have shown that, when the injected radiation flux exceeds a critical value, the system is destabilised and equilibrium becomes impossible. Our immediate goal in this paper is to determine whether a similar critical flux exists for CRs.

Our approach also mirrors that in the radiation context: we write down the equations that describe energy and momentum balance for a gas column, and then determine numerically up to what maximum CR flux those equations admit solutions. Because we are interested in CR feedback as a mechanism for regulating star formation and perhaps ejecting star-forming gas from galaxies, we will specifically focus on the relatively dense, cool or cold, largely neutral (though, importantly, still partially ionised), and star-forming phase of the ISM gas that is to be found close to the midplane in spiral galaxies, rather than on gas in their ionised halos. Our focus on the neutral phase of the ISM will have important implications for CR transport mechanisms, as we discuss below.

### 2.1.1 Equations for transport and momentum balance

We work in 1-dimension,  $z$ , the height above the midplane<sup>1</sup>, and treat CRs in the fluid dynamical limit whereby they behave as a fluid of given adiabatic index  $\gamma_c$ ; below we adopt the relativistic limit and set  $\gamma_c = 4/3$ . CRs are injected by supernova explosions, which we approximate as occurring solely in a thin layer near  $z = 0$ .<sup>2</sup> Adopting, e.g., Eq. 30 from [Zweibel \(2017\)](#) (also cf. [Breitschwerdt et al. 1993](#), Eq. 5) to 1-dimension ( $\nabla \rightarrow d/dz$ ) and assuming a stationary configuration ( $\partial X/\partial t \rightarrow 0$  and  $v_{\text{gas}} \rightarrow 0$ ), but also now accounting for collisional energy losses of cosmic rays (not included in the equation written down by [Zweibel 2017](#)) we have the following equation for CR transport:

$$\frac{dF_c}{dz} = \frac{u_c}{t_F} - \frac{u_c}{t_{\text{col}}} + v_{A,x} \frac{dP_c}{dz}, \quad (1)$$

in which  $F_c = F_c(z)$  is the CR energy flux,  $u_c = u_c(z)$  is the CR energy density,  $P_c = P_c(z) = (\gamma_c - 1)u_c$  is the CR pressure,  $t_F$  and  $t_{\text{col}}$  are the timescales for second-order Fermi acceleration and collisional losses, respectively, and the final term on the RHS of [equation 1](#) describes exchange of energy between CRs and magnetic waves mediated by the streaming instability; depending on circumstances, in a partially ionised medium such as the one with which we are concerned,  $v_{A,x}$  might be either the Alfvén speed corresponding to the total mass density ( $v_{A,x} \rightarrow v_A$ ) or the density solely of the ions ( $v_{A,x} \rightarrow v_{A,i}$ ). We defer the question of which is the appropriate choice for the moment. In keeping with our assumption that all CR injection happens at  $z = 0$ , we do not include a source term in [equation 1](#); instead, we adopt a boundary condition that  $F_c$  takes on some particular non-zero value at  $z = 0$ .

<sup>1</sup> By symmetry, we can just treat the half-plane from vertical height  $z = 0$  to  $z \rightarrow \infty$ .

<sup>2</sup> As discussed in [Crocker et al. \(2018a\)](#) in the context of radiation, the assumption that all injection of photons / CRs happens in a layer that is much thinner than the gas scale height is a poor assumption for real galaxies. However, we are interested in determining the limit beyond which the force provided by CRs makes the scale height diverge, and as one approaches this limit the gas scale height does in fact become large compared to the injection scale height. Thus the assumption is a reasonable one for the purposes of determining the maximum CR flux, which is our goal.

The (quasi-)hydrostatic equilibrium condition gives us a second ODE:

$$\frac{d}{dz} (P_c + P_{\text{turb}} + P_B - 2P_{B_z}) = -\rho_{\text{gas}} g_z \quad (2)$$

Here  $P_{\text{turb}} = P_{\text{turb}}(z)$  is the non-thermal, dynamical (or ram) pressure associated with turbulent gas motions (see [Section 2.1.2](#)),  $P_B = |\mathbf{B}|^2/(8\pi)$  is the total magnetic field pressure,  $-2dP_{B_z}/dz = -(1/4\pi)d(|B_z|^2)/dz$  is the magnetic tension force in the vertical direction,  $\rho_{\text{gas}} = \rho_{\text{gas}}(z)$  is the volumetric gas density, and

$$g_z(z) = 4\pi G (\Sigma_{\text{gas},1/2}(z) + \Sigma_{\star,1/2}(z)). \quad (3)$$

is the magnitude of the acceleration in the vertical direction. This acceleration is due to a combination of stars and gas; the gas half-column integrated from the midplane to any height  $z$  is

$$\Sigma_{\text{gas},1/2}(z) = \int_0^z \rho_{\text{gas}}(z') dz', \quad (4)$$

while the stellar half-column is  $\Sigma_{\star,1/2}$ . Consistent with our treatment of CR injection, we assume the stars are in a thin layer near  $z = 0$ , so  $\Sigma_{\star,1/2}$  is constant for all  $z > 0$ . The total column of gas (that would be measured in observations) we denote (without the  $z$  argument) as

$$\Sigma_{\text{gas}} = \lim_{z \rightarrow \infty} 2\Sigma_{\text{gas},1/2}(z) \quad (5)$$

and the total stellar column is  $\Sigma_{\star} = 2\Sigma_{\star,1/2}$ . For future convenience, we also define the total gas fraction

$$f_{\text{gas}} = \frac{\Sigma_{\text{gas}}}{\Sigma_{\text{gas}} + \Sigma_{\star}}, \quad (6)$$

so the total surface mass density is

$$\Sigma_{\text{tot}} = \frac{\Sigma_{\text{gas}}}{f_{\text{gas}}}. \quad (7)$$

The next step in our calculation is to adopt models for the various terms appearing in [equation 1](#) and [equation 2](#); we proceed to do so in the remainder of this section.

### 2.1.2 Model for turbulence

Essentially all observed galaxies have velocity dispersions that are at least transsonic (e.g. [Krumholz et al. 2018](#)), so that turbulent pressure support is as or more important than thermal pressure. We must therefore adopt a model for turbulence. Given that this turbulence is injected at scales approaching the gas scale height and cascades down from there, we shall make the assumption that the turbulent velocity dispersion  $\delta v$  of the gas is constant. This position-independent turbulent velocity dispersion together with the local matter density sets the dynamical pressure within the gas column:

$$P_{\text{turb}}(z) = \frac{2}{3} u_{\text{turb}}(z) = \rho_{\text{gas}}(z) \delta v^2, \quad (8)$$

where  $u_{\text{turb}}$  is the turbulent energy density and  $\delta v^2 = \text{const}$  is the turbulent velocity dispersion.

Turbulence is important not just for the pressure it contributes, but also through CR transport, because, if a turbulent dynamo is operating, the turbulent energy density ultimately feeds into the CR diffusion coefficient through its



dependence on the magnetic field amplitude (e.g., because of the scaling of the scattering length with the gyroradius in fully-ionised gas or through the dependence of the streaming velocity on the Alfvén speed). We incorporate these considerations into our model as follows: First, we note that the natural outer or injection scale of the turbulence is the turbulent scale height in the galactic disc,  $z_* \simeq \delta v^2/g_*$ , where

$$g_* = 2\pi G \frac{\Sigma_{\text{gas}}}{f_{\text{gas}}} \quad (9)$$

is the characteristic acceleration due to the matter column. We therefore adopt as a fiducial value

$$l_{\text{out}} = z_* \equiv \frac{\delta v^2}{g_*}. \quad (10)$$

as the outer scale of the turbulence.<sup>3</sup> For future convenience we can also use this length scale to define a corresponding density scale

$$\rho_* = \frac{\Sigma_{\text{gas}}}{2z_*} = \frac{\pi G}{f_{\text{gas}}} \left( \frac{\Sigma_{\text{gas}}}{\delta v} \right)^2, \quad (11)$$

which is the characteristic density near the gas midplane.

Second, we note that, where they can be observed, magnetic field strengths tend to be such that they represent a roughly constant fraction of the energy density of the turbulence (e.g., [Crutcher 1999](#)); this is, of course, consistent with the picture that a local, turbulent dynamo is operating. Simulations confirm this picture (e.g., [Federrath et al. 2014](#); [Federrath 2016](#)). Given the assumption of a constant  $\delta v$  this implies a characteristic field strength that scales with density as  $B \propto \rho_{\text{gas}}^{1/2}$  or, put another way, an approximately constant Alfvénic Mach number. We henceforth assume this.

### 2.1.3 Model for CR collisional losses

The collisional loss time scale is

$$t_{\text{col}}(z) = \frac{1}{cn(z)\sigma_{\text{col}}\eta_{\text{col}}} \quad (12)$$

in which  $n(z)$  is the position dependent target nucleon density, and  $\sigma_{\text{col}}$  and  $\eta_{\text{col}}$  are the total cross-section and inelasticity of the relevant collisional loss process. Given that relativistic ions dominate the energy density for reasonable assumptions about the CR distribution<sup>4</sup>, and consistent with our earlier choice to set  $\gamma_c \rightarrow 4/3$ , we shall ignore the energetically sub-dominant, low energy, sub-relativistic cosmic ray population and treat the CRs in the relativistic limit. Given the relativistic CRs are close to or above the pion

<sup>3</sup> Note that, given our assumption the stars are distributed in a vanishingly thin sheet, this is the scale height of the gas distribution in the limit  $f_{\text{gas}} \rightarrow 0$ . In the opposite limit,  $f_{\text{gas}} \rightarrow 1$ , the scale height goes to  $2z_*$ .

<sup>4</sup> Specifically, we assume that the ions follow a power law distribution in (the absolute magnitude of the) momentum ([Bell 1978](#)),  $p$ , falling somewhat more steeply than  $p^{-2}$  as a result of first-order Fermi acceleration in combination with transport timescales that also decline with momentum. CR electrons, which suffer considerably more severe losses than ions, are expected (e.g., [Strong et al. 2010](#)) to constitute  $\lesssim$  few % of the total cosmic ray energy density for ISM conditions in star-forming galaxies.

production threshold, we shall consequently assume that CR collisional losses are dominated by hadronic processes (rather than Coulomb or ionising collisions which dominate for sub-relativistic CR ions). In this case for the cross-section and elasticity  $\sigma_{\text{col}}$  and  $\eta_{\text{col}}$  in [equation 12](#) we have (e.g., [Kafexhiu et al. 2014](#))

$$\sigma_{\text{col}} \rightarrow \sigma_{\text{pp}} \simeq 40 \text{ mbarn} \quad \text{and} \quad \eta_{\text{col}} \rightarrow \eta_{\text{pp}} \simeq 1/2. \quad (13)$$

Note that the hadronic collision cross-section is only weakly energy dependent above CR (proton) kinetic energies of  $T_c \sim \text{GeV}$ ; given that CR protons are expected to dominate the ‘target’ and ‘beam’ populations, we generically label these as ‘pp’, and we set the target density to  $n(z) = \rho_{\text{gas}}(z)/\mu_p m_p$ , where  $m_p$  is the proton mass and  $\mu_p \approx 1.17$  is the ratio of protons to total nucleons for a gas that is 90% H, 10% He by number. The proton loss time (at 10 GeV) works out to be approximately

$$\begin{aligned} t_{\text{col}} \simeq t_{\text{pp}} &\simeq 4.8 \times 10^4 n_3^{-1} \text{ yy} \\ &\simeq 1.0 \times 10^{10} \frac{f_{\text{gas}} \delta v_1^2}{\Sigma_{\text{gas},0}^2} \text{ yr}, \end{aligned} \quad (14)$$

where we have, for convenience, defined the scaling factors  $n_3 = n/(10^3 \text{ cm}^{-3})$  and  $\Sigma_{\text{gas},0} = \Sigma_{\text{gas}}/(M_{\odot} \text{ pc}^{-2})$ .

### 2.1.4 Model for CR transport and acceleration

[MRK: Rewriting this section; original text commented out]

The final model we must adopt is a description of how CRs interact with the magnetised turbulence in the ISM, which in turn will specify the CR flux,  $F_c$ , along with the terms describing second order Fermi-acceleration ( $t_F$ ) and Alfvén velocity  $v_{A,x}$  that determines the rate of energy exchange with the plasma due to streaming instability. We treat the flux in the standard diffusion approximation ([Ginzburg & Syrovatskii 1964](#)), whereby

$$F_c = -\kappa \frac{du_c}{dz}. \quad (15)$$

It is convenient to normalise  $\kappa$  to its minimum possible value, by writing

$$\kappa = K \kappa_{\text{conv}}, \quad (16)$$

where

$$\kappa_{\text{conv}} \simeq l_{\text{out}} \delta v \quad (17)$$

Here  $\kappa_{\text{conv}}$  is the ‘convective’ diffusion coefficient that would apply if we were to assume that CRs were perfectly frozen into the gas, and were mixed solely by passive advection in the gas turbulence ([Tennekes & Lumley 1972](#)). Since this a lower limit on the true diffusion coefficient, we have  $K \geq 1$ .

The value of  $K$ , and of  $t_F$  and  $v_{A,x}$ , depends on the ionisation state and other properties of the medium through which the CRs propagate. In the Milky Way and similar ‘normal’ star-forming galaxies, the midplane is roughly-evenly divided by volume between neutral and ionised material (e.g. [Dekel et al. 2019](#)), though neutral material dominates by mass; in more gas-rich and rapidly-star-forming galaxies, neutral material dominates by both mass and volume ([Krumholz et al. 2019](#)). Since we are interested in CR feedback on the star-forming gas, as our fiducial choice we

will adopt microphysical parameters appropriate for it. However, we also provide parameters suitable for a model of CRs in ionised gas, and we show below that the qualitative results we obtain do not depend strongly on which set of microphysical parameters we adopt.

**2.1.4.1 Neutral media** Our model for the neutral ISM is taken from [Krumholz et al. \(2019\)](#), and we refer readers to that paper for details of the calculation. Here we only summarise the most important results. In a predominantly neutral medium, strong ion-neutral damping cuts off the turbulent cascade in the ISM, and decouples ions from neutrals, at scales far larger than the gyroradii of  $\sim$ GeV CRs. Consequently, there is no Fermi acceleration because there is no mechanism to couple ISM turbulence to CRs ( $t_F \rightarrow \infty$ ), and the dissipation of CR energy via streaming instability occurs into Alfvén waves that propagate in the ions alone, and thus have speed

$$v_{A,x} = v_{A,i} = \frac{v_A}{\chi} = \frac{\delta v}{\sqrt{2}\chi M_A} \quad (18)$$

where  $\chi$  is the ionisation fraction by mass,  $M_A$  is the Alfvén Mach number of the turbulence in the ISM, and the factor two in the denominator of the last term arises from the assumption that Alfvénic modes carry half the turbulent energy. Following the review of turbulent dynamo simulations given in [Krumholz et al. \(2019\)](#), we adopt  $M_A = 2$  as our fiducial choice.

Since the external turbulence does not couple to CRs CR transport in such a medium occurs predominantly by CRs streaming along field lines at the ion Alfvén speed, coupled with the random walk of those field lines in the overall turbulence. The corresponding diffusion coefficient is

$$\kappa = v_{A,i} l_{\text{coh},B}, \quad (19)$$

where  $l_{\text{coh},B}$  is the coherence length of the magnetic field, which for a dynamo-generated field is

$$l_{\text{coh},B} \simeq \frac{l_{\text{out}}}{M_A^3} \quad (20)$$

Consequently, for this model, at the galactic midplane we have

$$K = K_* \simeq \frac{1}{\sqrt{2}\chi_* M_A^4}, \quad (21)$$

where here the subscript  $*$  indicates midplane values. The corresponding dimensional diffusion coefficient is

$$\begin{aligned} \kappa_* &\simeq 4.3 \times 10^{26} \frac{\delta v_1}{\sqrt{\chi_{*, -3}}} \frac{z_{*,2}}{\Sigma_{*, -3}} \left(\frac{M_A}{2}\right)^{-4} \text{ cm}^2 \text{ s}^{-1} \\ &\simeq 1.6 \times 10^{28} \frac{\delta v_1^3}{\sqrt{\chi_{*, -3}}} \frac{f_{\text{gas}}}{\Sigma_{\text{gas},0}} \left(\frac{M_A}{2}\right)^{-4} \text{ cm}^2 \text{ s}^{-1}, \end{aligned} \quad (22)$$

where we have defined  $\delta v_1 = \delta v/10 \text{ km s}^{-1}$ ,  $z_{*,2} = z_*/100 \text{ pc}$ , and  $\chi_{*, -3} = \chi_*/10^{-3}$ . The corresponding diffusive escape times are

$$\begin{aligned} t_{\text{esc,diff}} = \frac{z_*^2}{\kappa_*} &\simeq 3.5 \frac{z_{*,2}^2}{\delta v_1} \left(\frac{M_A}{2}\right)^4 \text{ Myr} \\ &\simeq 130 \frac{f_{\text{gas}}}{\Sigma_{\text{gas},0}} \frac{\delta v_1}{\Sigma_{\text{gas},0}} \left(\frac{M_A}{2}\right)^4 \text{ Myr}; \end{aligned} \quad (23)$$

note, cf. [equation 14](#), that while  $t_{\text{pp}} \propto \Sigma_{\text{gas}}^{-2}$ , from [equation 31](#) we have  $t_{\text{esc,diff}} \propto \Sigma_{\text{gas}}^{-1}$ , so collisional losses will always win out over diffusive escape at sufficiently high gas surface density (for other parameters held fixed).

While this description holds near the midplane, where the gas is predominantly neutral, it must break down at some point. As CRs diffuse up through the dominantly neutral gas layer and move into the galactic halo, they encounter gas that is progressively more rarefied, highly-ionised, and magnetic pressure-dominated, leading to a larger coherence length ([Beck 2015](#)). This transition is complex and poorly understood, and rather than developing a complex model for the plane-halo transition, we elect to follow [Krumholz et al. \(2019\)](#) by parameterising our ignorance: we assume that the diffusion coefficient  $\kappa$  scales with the density  $\rho$  as

$$\kappa = \kappa_* \left(\frac{\rho}{\rho_*}\right)^{-\beta}, \quad (24)$$

where the plausible range for the index  $\beta$  is  $\beta = 1/6 - 1/2$ . We adopt  $\beta = 1/4$  as a fiducial choice, but show below that our results are quite insensitive to  $\beta$ .

**2.1.4.2 Ionised media** For ionised media, there is a great deal of uncertainty about whether CRs are confined primarily by Alfvén waves that they themselves create via the streaming instability, or primarily by waves cascading from larger scales, or some combination of both (e.g., [Zweibel 2017](#), and references therein).

Before diving into the details of the specific model for CR transport through the neutral gas that we employ below, we pause to assure the reader that the results we shall derive are rather general and largely insensitive to the details of this model. Indeed, to the extent that it is accurate to describe CR transport in the diffusion approximation ([Ginzburg & Syrovatskii 1964](#)), we emphasize that our basic results will hold so long as the energy dependence of a diffusion coefficient  $\kappa$  is rather mild, its spatial dependence is such that, in regions of higher gas density, diffusion is slower, and its overall normalization is within an order of magnitude or so of the physical diffusion coefficient we derive below and present in [equation 29](#). This point is further discussed in [Section 4.2.1](#).

Thus to our particular model: this follows that presented in [Krumholz et al. \(2019\)](#), and we refer readers there for a thorough discussion and derivation; here we simply summarise the results of that paper of which we will make use here. The primary conclusion of [Krumholz et al. \(2019\)](#) is that, in the predominantly neutral phase of the ISM, the turbulent cascade does not reach the gyroradius scale of the energetically dominant  $\sim$ GeV CRs. Rather the microphysical magnetic field turbulence on which the CRs scatter is self-generated via the streaming instability, and this turbulence exists solely in the ions – its length and time scales are so small that collisions between neutrals and ions occur too infrequently to couple the two fluids together.

A first implication of this is that second-order Fermi acceleration is unimportant (i.e.,  $t_F \rightarrow \infty$ ), because, if the turbulent cascade does not reach the size scales with which CRs are resonant, there can be no transfer of energy between turbulence and CRs. Similarly, the velocity  $v_{A,x}$  that appears in the term describing CR energy dissipation via the streaming instability is the ion Alfvén speed  $v_{A,i}$  rather than

the total gas Alfvén speed  $v_A$ , since the waves generated by the streaming instability propagate solely in the ions. The two speeds are related by

$$v_{A,i} = \frac{v_A}{\sqrt{\chi}} \quad (25)$$

where  $\chi$  is the ionisation fraction by mass.

Second, because there is no source of turbulence transverse to the magnetic field lines (streaming instability only creates turbulence along field lines), CRs do not diffuse across field lines. Along field lines, they stream at a rate dictated by the balance between streaming excitation of magnetic waves and the ion-neutral damping of those waves. For the  $\sim$  GeV CRs that dominate the CR energy budget, the resulting streaming speed is close to  $v_{A,i}$  almost independent of CR energy. (We provide a discussion of energy dependence in [Appendix A](#).) Given this microphysical transport mechanism, one can describe the macroscopic transport process for CRs as one of streaming plus field line random walk (FLRW), which can be approximated as a diffusion process. The resulting flux is

$$F_c = -\kappa \frac{du_c}{dz}, \quad (26)$$

where the diffusion coefficient is ([Yan & Lazarian 2008](#); [Krumholz et al. 2019](#), and references therein)

$$\kappa = v_{A,i} l_{\text{coh,B}}, \quad (27)$$

where  $l_{\text{coh,B}}$  is the coherence length of the magnetic field. For a dynamo-generated magnetic field this is

$$l_{\text{coh,B}} \simeq \frac{l_{\text{out}}}{M_A^3} \quad (28)$$

where  $M_A$  is the Alfvénic Mach number. As discussed in [Krumholz et al. \(2019\)](#), for a dynamo-generated field, modern simulations suggest  $M_A \simeq 2$ , and we henceforth adopt this as our fiducial choice. This generates reference values for the diffusion coefficient near the midplane,

$$\begin{aligned} \kappa_* &\equiv \left( \frac{\delta v}{\sqrt{2}\chi_* M_A} \right) \left( \frac{l_{\text{out}}}{M_A^3} \right) \\ &\simeq 4.3 \times 10^{26} \frac{\delta v_1}{\sqrt{\chi_{*,3}}} \frac{z_{*,2}}{2} \left( \frac{M_A}{2} \right)^{-4} \text{ cm}^2 \text{ s}^{-1} \\ &\simeq 1.6 \times 10^{28} \frac{\delta v_1^3}{\sqrt{\chi_{*,3}}} \frac{f_{\text{gas}}}{\Sigma_{\text{gas},0}} \left( \frac{M_A}{2} \right)^{-4} \text{ cm}^2 \text{ s}^{-1} \end{aligned} \quad (29)$$

where  $\chi_*$  is the midplane ionization fraction, and we have defined the additional scaling factors for convenience:  $\delta v_1 = \delta v / 10 \text{ km s}^{-1}$ ,  $z_{*,2} = z_*/100 \text{ pc}$ , and  $\chi_{*,3} = \chi_*/10^{-3}$  [5].

While this description holds near the midplane, where the gas is predominantly neutral, it must break down at

<sup>5</sup> Note that, taking  $f_{\text{gas}} \rightarrow 0.1$  or so, the last approximation in equation 29, shows that our model for CR transport predicts a macroscopic diffusion coefficient very similar in scale to that determined empirically for  $\sim$  GeV CRs in the local Milky Way ( $\sim 3 \times 10^{27} \text{ cm}^2/\text{s}$  for  $\sim$  GeV CRs; e.g., [Gabici et al. 2007](#)). This is apparently by complete coincidence given the very different physics supposedly setting the diffusion coefficients in the neutral gas, on the one hand, and in the largely diffuse, ionised gas inside which locally-detected CRs apparently spend most of their time (cf. [Krumholz et al. 2019](#)).

some point. As CRs diffuse up through the dominantly neutral gas layer and move into the galactic halo, they encounter gas that is progressively more rarefied, highly-ionised, and magnetic pressure-dominated, leading to a larger coherence length ([Beck 2015](#)). This transition is complex and poorly understood, and rather than developing a complex model for the plane-halo transition, we elect to follow [Krumholz et al. \(2019\)](#) by parameterising our ignorance: we assume that the diffusion coefficient  $\kappa$  scales with the density  $\rho$  as

$$\kappa = \kappa_* \left( \frac{\rho}{\rho_*} \right)^{-\beta}, \quad (30)$$

where the plausible range for the index  $\beta$  is  $\beta = 1/6 - 1/2$ . We adopt  $\beta = 1/4$  as a fiducial choice, but show below that our results are quite insensitive to  $\beta$ .<sup>6</sup> See [Krumholz et al. \(2019\)](#) for a detailed discussion of arguments for different scaling choices.

The escape time works out to be

$$\begin{aligned} t_{\text{esc,diff}} &\sim \frac{z_*^2}{\kappa} \\ &\simeq 3.5 \times 10^6 \frac{z_{*,2}^2}{\delta v_1} \left( \frac{M_A}{2} \right)^4 \text{ year} \\ &\simeq 1.3 \times 10^8 \frac{f_{\text{gas}}}{\Sigma_{\text{gas},0}} \frac{\delta v_1}{2} \left( \frac{M_A}{2} \right)^4 \text{ year}; \end{aligned} \quad (31)$$

note, cf. equation 14, that while  $t_{\text{pp}} \propto \Sigma_{\text{gas}}^{-2}$ , from equation 31 we have  $t_{\text{esc,diff}} \propto \Sigma_{\text{gas}}^{-1}$ , so collisional losses will always win out over diffusive escape at sufficiently high gas surface density (for other parameters held fixed).

## 2.2 Non-dimensionalisation

We have now specific models for all terms appearing in the transport and hydrostatic balance equations. Our next step is to non-dimensionalise the equations and, in the process, extract the key dimensionless numbers that govern the system. We have already defined characteristic values  $g_*$ ,  $z_*$ , and  $\rho_*$  for the gas acceleration, scale height, and density. Other natural scales follow immediately: the characteristic midplane pressure  $P_*$  (with related energy density  $u_* = (3/2)P_*$ ) is given by

$$P_* = g_* \rho_* z_* = \rho_* \delta v^2 = \frac{\pi G}{f_{\text{gas}}} \Sigma_{\text{gas}}^2, \quad (32)$$

and the associated flux required if the pressure is carried by a collection of relativistic particles in the free-streaming limit

$$F_* = cP_* = \frac{\pi G c}{f_{\text{gas}}} \Sigma_{\text{gas}}^2. \quad (33)$$

We now proceed to non-dimensionalise our system by

<sup>6</sup> It is also worth noting that  $\beta = 1/4$  is also the expected density dependence of the CR diffusion coefficient in the case of externally-driven turbulence with a Kraichnan spectrum in a fully ionised medium; for a Kolomogorov spectrum  $\beta = 1/6$ . However, in these cases, the diffusion coefficient is energy-dependent, unlike the case we examine in the main text.

defining the non-dimensional variables

$$\xi = \frac{z}{z_*} \quad s(\xi) = \frac{\Sigma_{\text{gas}, 1/2(z)}|}{\rho_* z_*} \Big|_{z=z_* \xi} \\ p_c(\xi) = \frac{P_c(z)}{P_*} \Big|_{z=z_* \xi} \quad \mathcal{F}_c(\xi) = \frac{F_c(z)}{F_*} \Big|_{z=z_* \xi}. \quad (34)$$

Here  $\xi$ ,  $s$ , and  $p_c$  are the dimensionless height, gas (half) column, cosmic ray pressure, and flux;  $ds/d\xi$  is the dimensionless gas density. Changing to these variables, the CR transport equation, [equation 1](#), becomes

$$\frac{d\mathcal{F}_c}{d\xi} = 3 \frac{z_*}{ct_{\text{F}}} p_c - 3 \frac{z_*}{ct_{\text{col}}} p_c + \beta_{A,i} \frac{dp_c}{d\xi} \quad (35)$$

where  $\beta_{A,i}$  is the ion Alfvén speed normalised to  $c$ . Note in passing that the physical density satisfies

$$\rho(z) = \rho_* \frac{ds}{d\xi} \Big|_{\xi=z/z_*}. \quad (36)$$

We next non-dimensionalise our model expressions for the CR flux and source/sink terms. Making use of [equation 26](#) - [equation 30](#), the dimensionless flux is

$$\mathcal{F}_c = - \left( \frac{v_{A,i} l_{\text{coh},B}}{z_* c} \right) \left( \frac{ds}{d\xi} \right)^{-\beta} \frac{dp_c}{d\xi}. \quad (37)$$

We will find it convenient in what follows to write the dimensionless ratio that appears in the first set of parentheses as the product of two terms. We define  $\beta_{A,i} = v_{A,i}/c$  as the CR propagation velocity normalised to  $c$ , and we define

$$\tau_s \equiv \frac{z_*}{l_{\text{coh},B}} = M_A^3 \quad (38)$$

as the scattering optical depth of the gas column. The latter identification arises from the fact that a diffusion coefficient can generically be written as  $\kappa \sim v\lambda$ , where  $v$  is the characteristic velocity of the diffusing particles (in this case  $v_{A,i}$ ) and  $\lambda$  is the their mean free path (in this case  $l_{\text{coh},B}$ ). With this identification, we can see that  $\tau_s$  is simply the ratio of the gas scale height to the CR scattering mean free path, and the dimensionless flux is

$$\mathcal{F}_c = - \frac{\beta_{A,i}}{\tau_s} \left( \frac{ds}{d\xi} \right)^{-\beta} \frac{dp_c}{d\xi}. \quad (39)$$

Following the same approach for the collisional loss term, [equation 12](#), we have

$$\frac{z_*}{ct_{\text{col}}} = \frac{\eta_{\text{pp}} \sigma_{\text{pp}} \Sigma_{\text{gas}}}{\mu_p m_p 2}. \quad (40)$$

We define

$$\Sigma_{\text{pp}} \equiv \frac{\mu_p m_p}{3\eta_{\text{pp}} \sigma_{\text{pp}}} \simeq \frac{33 \text{ g cm}^{-2}}{(\eta_{\text{pp}}/0.5)(\sigma_{\text{pp}}/40 \text{ mbarn})} \simeq 1.6 \times 10^5 M_{\odot}/\text{pc}^2 \quad (41)$$

as the characteristic column for hadronic losses, i.e., the CR flux is decreased by one  $e$ -folding after passage through a matter column  $\Sigma_{\text{pp}}$ <sup>7</sup>. Using this, for future convenience we

<sup>7</sup> Note the subtlety that, with respect to losses, it is actually the *path-integrated* column that is relevant and, of course, for diffusive propagation, motion is not in general rectilinear.

can define the (in principle) optical depth *for absorption* for rectilinear<sup>8</sup> propagation through the half-column via

$$\tau_{\text{pp}} \equiv \frac{\Sigma_{\text{gas}}}{2\Sigma_{\text{pp}}} \simeq 6.4 \times 10^{-6} \Sigma_{\text{gas},0}. \quad (42)$$

Inserting the quantities above into [equation 35](#), and with some minor re-arrangement, we arrive at the following form of the dimensionless cosmic ray transport equation:

$$\frac{d}{d\xi} \left[ - \left( \frac{ds}{d\xi} \right)^{-\beta} \frac{dp_c}{d\xi} \right] = -\tau_{\text{path}} \frac{ds}{d\xi} p_c + \tau_s \frac{dp_c}{d\xi} \quad (43)$$

where we have now dropped the second order Fermi acceleration term based on the arguments above, and we have defined

$$\tau_{\text{path}} \equiv \frac{\tau_s}{\beta_{A,i}} \tau_{\text{pp}} \\ \simeq 0.02 \left( \frac{M_A}{2} \right)^3 \Sigma_{\text{gas},0} \sqrt{\chi-3} \delta v_1^{-1} \quad (44)$$

The physical meaning of the first equation is simple: it just asserts that the change in CR flux with respect to height (the LHS) is equal to the rate at which CRs are lost due to collisions (the first term on the RHS) and dissipation of CR energy into Alfvén waves via the streaming instability (the second term on the RHS). The coefficient in front of the collisional loss term is  $\tau_{\text{path}}$  rather than  $\tau_{\text{pp}}$  because the column of matter through which a CR passes in the process of escaping the galactic disc is larger than the rectilinear column by a factor  $\tau_s/\beta_{A,i}$ . This factor contains two distinct effects: the denominator accounts for the microscopic scattering of CRs off Alfvén waves as they follow the field lines, which increases their total column through which they must pass in order to propagate a given distance by a factor  $1/\beta_{A,i}$  compared to the case of free-streaming along the field lines at  $c$ . The numerator accounts for macroscopic “scattering” due to the fact that the field lines themselves are not straight, and thus CRs must follow a curved, winding trajectory to escape the galactic disc. **On the basis of the second near-equality in [equation 44](#), over the physically-relevant parameter space, we expect  $10^{-1} \lesssim \tau_{\text{path}} \lesssim 10$**  (see [Figure 4](#)).

Repeating these procedures for the equation of momentum balance, [equation 2](#), yields the non-dimensionalised equation

$$\frac{dp_c}{d\xi} + \xi_{\text{turb}} \frac{d^2 s}{d\xi^2} = - (1 - f_{\text{gas}}) \frac{ds}{d\xi} - f_{\text{gas}} s \frac{ds}{d\xi}, \quad (45)$$

where

$$\xi_{\text{turb}} = \frac{P_* + P_{B_*} - 2P_{B_*,z}}{P_*} \\ = 1 + \frac{1}{6M_A^2} - \frac{1}{3M_{A,z}^2}. \quad (46)$$

Here  $B_*$  is a reference magnetic field amplitude<sup>9</sup>,  $B_*^2 \equiv B^2/(ds/d\xi)$ , and we have defined  $M_{A,z}$  in analogy to  $M_A$  for

<sup>8</sup> Again, note that while the limiting case of rectilinear propagation provides a useful reference quantity, it is physically unrealistic; this is why we introduce  $\tau_{\text{path}}$ .

<sup>9</sup> Explicitly,  $B_*^2 \equiv 4\pi\rho_* \left( \frac{\delta v}{M_A} \right)^2$

the  $z$  component of the field only.<sup>10</sup> The terms in equation 45 are, from left to right, the pressure gradient due to CRs, the pressure gradient due to combined turbulence plus magnetic support, the gravitational acceleration due to stellar gravity, and the acceleration due to gas self-gravity.

Finally, our system of equation 43 and equation 45 is fourth order in total, and thus requires four boundary conditions. Two of these are

$$s(0) = 0 \quad (47)$$

$$\lim_{\xi \rightarrow \infty} s(\xi) = 1, \quad (48)$$

which amount to asserting that the gas half column is zero at the midplane, and that  $\lim_{z \rightarrow \infty} \Sigma_{\text{gas},1/2}(z) = 1/2 \Sigma_{\text{gas}}$ . For the boundary conditions on the CR pressure, we can rearrange the dimensionless cosmic ray flux equation 39 and evaluate it at  $\xi = 0$  which generates a third boundary condition as

$$-\left(\frac{ds}{d\xi}\right)^{-\beta} \frac{dp_c}{d\xi} \Big|_{\xi=0} = \frac{\tau_s}{\beta_{A,i}} \frac{F_{c,0}}{F_*} \equiv f_{\text{Edd}}, \quad (49)$$

where the quantity  $f_{\text{Edd}}$  is the ratio of the incoming CR flux to the Eddington flux<sup>11</sup>, defined here as the flux for which the momentum flux carried in the  $+z$  direction by the cosmic rays matches the momentum flux in the  $-z$  direction due to gravity. Note here that  $F_{c,0}$  is enhanced by the factor  $\tau_s/\beta_{A,i}$  that accounts for the diffusive nature of the CR transport (c.f., [Socrates et al. 2008](#)).

To obtain the final boundary condition, we follow [Krumholz et al. \(2019\)](#) and demand that the solution of CR propagation within the disc join smoothly to the solution for free-streaming CRs as  $z \rightarrow \infty$ , on the basis that, once one is sufficiently high above the disc, field lines should straighten out and CRs should be able to free-stream to infinity. This condition requires that the CR enthalpy flux obey

$$\lim_{z \rightarrow \infty} \frac{F_c}{u_c + P_c} = v_{A,i}. \quad (51)$$

In terms of the dimensionless parameters, this becomes

$$\lim_{\xi \rightarrow \infty} \frac{1}{\tau_s} \left(\frac{ds}{d\xi}\right)^{-\beta} \frac{dp_c}{d\xi} = \lim_{z \rightarrow \infty} 4 \text{sign}\left(\frac{dp_c}{d\xi}\right) p_c(\xi). \quad (52)$$

### 2.3 Validity of approximations

Our formulation of cosmic ray transport uses the diffusion approximation. Here we check the conditions under which this approximation is valid.

First, to be in the diffusive regime, we require that CRs

<sup>10</sup> Note that we have  $0 \leq \xi_{\text{turb}} \leq 2$ , with values of  $\xi_{\text{turb}} > 1$  corresponding to the case of a disc where magnetic pressure supports the disc more than magnetic tension confines it, and  $\xi_{\text{turb}} < 1$  corresponding to the reverse. If the field is isotropic,  $B_z = |\mathbf{B}|/\sqrt{3}$ , then  $\xi_{\text{turb}} = (18M_A^2 + 1)/18M_A^2$ , which evaluates numerically to 1.01 for our fiducial choice  $M_A = 2$ .

<sup>11</sup> A useful estimate for  $f_{\text{Edd}}$  given in terms of quantities defined in Section 4.1 is:

$$f_{\text{Edd}} \approx 3.6 \frac{f_{\text{gas}} \epsilon_{c,*}^{1/2} \dot{\Sigma}_{*, -2} \sqrt{\chi_{-3}}}{\delta v_1 \Sigma_{\text{gas},1}^2} \left(\frac{M_A}{2}\right)^3, \quad (50)$$

where we have normalised to gas surface and star formation rate surface densities similar to those of the local MW disc.

scatter at least once before escaping the matter column, i.e.,  $\tau_s \geq 1$  or  $M_A \geq 1$ ; this will be true by assumption for the dense, star-forming gas layer with which we concern ourselves. Observations and simulations (as briefly reviewed by [Krumholz et al. 2019](#)) also bear out that the turbulence in this gas phase is super- or, at least, trans-Alfvénic.

A second requirement of the diffusion approximation is that the scattering length exceed the CR gyroradius  $r_L$ , or, equivalently, that the diffusion coefficient  $\kappa$  we have calculated for FLRW be larger than the Bohm diffusion coefficient

$$\kappa_{\text{Bohm}} \equiv \frac{r_L c}{3}. \quad (53)$$

This yields a formal constraint that

$$\delta v \gtrsim \frac{\sqrt{2\chi} M_A^4 r_L c}{3z_*} \approx 2 \text{ km/s} \frac{\sqrt{f_{\text{gas}} \chi_{-3}} E_{c,3} \Sigma_{\text{gas},0}}{z_{*,2}} \left(\frac{M_A}{2}\right)^4, \quad (54)$$

where  $E_c$  is the CR energy and  $E_{c,3} = E_c/10^3$  GeV. This condition is clearly satisfied over all plausible galaxy parameters up to  $E_c = \text{few} \times \text{TeV}$ .

A third requirement for the validity of our treatment is that CR transport be primarily via diffusion and/or streaming rather than bulk flows. While we exclude systematic bulk flows by construction in our hydrostatic treatment, allowing for gas turbulence opens up the possibility for turbulent mixing – i.e., small-scale turbulent transport – of the cosmic rays ([Lacki 2013](#), and references therein). This can be treated with an effective, energy-independent diffusion coefficient ([Tennekes & Lumley 1972](#)) given by

$$\kappa_{\text{mix}} \approx l_{\text{out}} \delta v. \quad (55)$$

We are justified in neglecting turbulent transport compared to FLRW if  $\kappa_{\text{mix}} \lesssim \kappa$ . Because we restrict ourselves to the physically-motivated case that diffusivity increases with distance from the plane, this condition will be satisfied if  $\kappa_{\text{mix}} \lesssim \kappa_*$ . This condition reduces to

$$\chi_* \lesssim \frac{1}{3M_A^8} \approx 1.3 \times 10^{-3} \left(\frac{M_A}{2}\right)^{-8} \equiv \chi_{\text{max}} \quad (56)$$

In fact, in the volume-filling warm neutral phase of the ISM in the Milky Way and similar galaxies, this condition is *not satisfied*, because ionisation by the diffuse X-ray background gives  $\chi \sim 10^{-2}$  (e.g., [Wolfire et al. 2003](#), fig. 10). As shown in [Krumholz et al. \(2019\)](#), however, the condition is increasingly well-met as we move to denser, more gas-rich galaxies, which have lower ionisation fractions due to their higher recombination rates. In any case, because convection – like FLRW – is responsible for transport that may be modelled via an energy-independent diffusion term, we can treat it as though it simply places a lower limit on how slow diffusion can be. In other words, there is an upper limit on the effective  $\chi$  (given by  $\chi_{\text{max}}$  defined above); further ionising the dense, star-forming gas above  $\sim 1.3 \times 10^{-3}$  does not result in slower FLRW nor permit larger CR pressure gradients to build up. In the numerical calculations that follow, we will enforce this limit.

A final requirement we must check is causality: the CRs cannot diffuse faster than the speed of light. This requires that

$$\frac{F_c}{c(u_c + P_c)} < 1 \quad (57)$$



Making use of equation 39, this condition can be expressed as

$$\frac{1}{4\tau_s p_c} \left( \frac{ds}{d\xi} \right)^{-\beta} \left| \frac{dp_c}{d\xi} \right| \leq 1. \quad (58)$$

Since  $1/\tau_s = M_A^{-3} = 0.125 (M_A/2)^{-3}$ , while the remaining terms are all of order unity or smaller inside the main body of the disc, this condition will be satisfied. Our boundary conditions ensure that this constraint is also obeyed as  $\xi \rightarrow \infty$ .

### 3 COSMIC RAY EQUILIBRIA

Having obtained our dimensionless equations and shown that the assumptions underlying them are reasonable, we now proceed to explore numerical solutions. Throughout this section we adopt the fiducial parameter choices  $\tau_s = M_A^3 = 8$  (cf. Section 2.1.4) and  $\beta = 1/4$  to describe CR transport, and  $\xi_{\text{turb}} = 73/72$  (cf. equation 46) to describe turbulent support.

#### 3.1 Gas density and cosmic ray pressure profiles

Our first step is to develop some intuition for the behaviour of solutions to the system, and how they change as we vary the effective optical depth  $\tau_{\text{path}}$  (equation 44) and the Eddington ratio  $f_{\text{Edd}}$  (equation 49) that describe it. To this end, we must solve equation 43 and equation 45 numerically. Because the boundary conditions for the system, equation 48 - equation 52, are specified at different locations, the system forms a boundary value problem, which we solve using a shooting algorithm as follows: we have  $s(0) = 0$  from equation 48, and we start with an initial guess for the mid-plane density  $s'(0)$  and pressure  $p_c(0)$ . These choices together with equation 49 allow us to compute the midplane CR pressure gradient  $p'_c(0)$ , so that we now have a set of four initial values at  $s = 0$  and can integrate outwards until  $s(\xi)$  and  $p_c(\xi)$  approach constant values at large  $\xi$ . In general our guess will not satisfy equation 48, i.e.,  $s(\xi)$  will go to a value other than unity as  $\xi \rightarrow \infty$ . We therefore iteratively adjust  $s'(0)$  while holding  $p_c(0)$  fixed, until equation 48 is satisfied. In general, however, this choice will not obey equation 52, i.e., the CR flux will not go to the correct value as  $\xi \rightarrow \infty$ . We therefore now iteratively adjust our guess for  $p_c(0)$ . We continue to iterate between our guesses for  $s'(0)$  and  $p_c(0)$  until the system converges and all boundary conditions are satisfied, or until convergence fails (see below).

We plot dimensionless gas density and CR pressure profiles determined via this procedure for various representative values of  $\tau_{\text{path}}$  (the effective optical depth of the galaxy to CRs) and  $f_{\text{Edd}}$  (the ratio of the CR momentum flux to the gravitational momentum flux) in Figure 1. The example shown uses  $f_{\text{gas}} = 0.9$ , but other values of  $f_{\text{gas}}$  give qualitatively similar behaviour. Note that the two panels show two different values of  $\tau_{\text{path}}$ ; the lower of these two,  $\tau_{\text{path}} = 10^{-3}$ , is a value typical of a dwarf galaxy, while the larger,  $\tau_{\text{path}} = 1$ , might be representative of a dense starburst or gas-rich disc in the early Universe. The figure shows that as the CR Eddington ratio increases (i.e., as the CR flux entering at the midplane is increased) from 0, to an intermediate value, to a critical value  $f_{\text{Edd},c}$  (described below), the gas density profile goes from quasi-exponential (and monotonically decreasing)

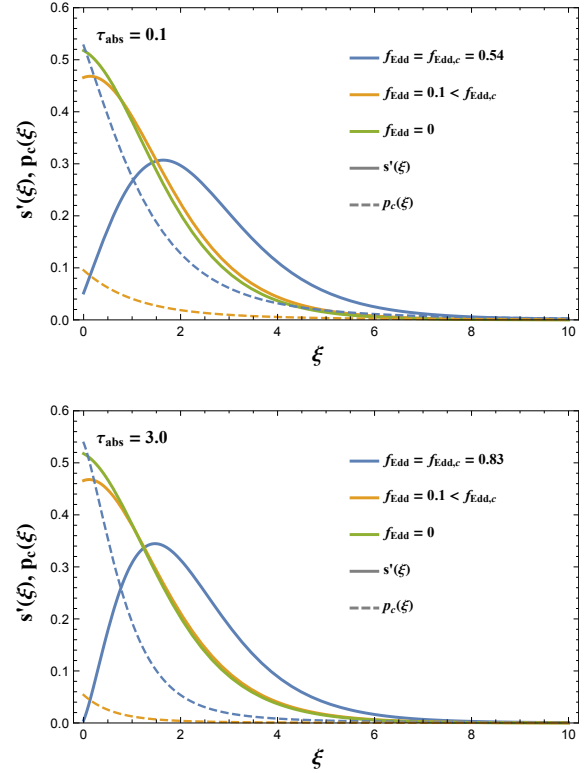


**Figure 1.** Profiles of (dimensionless) volumetric density  $s'(\xi)$  (solid) and (dimensionless) CR pressure  $p_c(\xi)$  (dashed) for various representative cases as indicated in the legend. The upper panel is for  $\tau_{\text{path}} = 10^{-3}$ , the lower is for  $\tau_{\text{path}} = 0.3$  (over the physically-relevant parameter space  $10^{-3} \leq \tau_{\text{path}} \leq 1$ ); otherwise, parameters common between the panels are  $\beta = 1/4$ ,  $M_A = 1$ ,  $f_{\text{gas}} = 0.9$ ,  $\xi_{\text{turb}} \approx 1$ . In both panels, the blue curves are evaluated for the critical  $f_{\text{Edd}}$  case and the yellow curves are for a sub-critical  $f_{\text{Edd}}$  value; the solid green curve is the density profile of a gas column supported purely by turbulence (with  $\xi_{\text{turb}} = 73/72$ ). Note that because  $\delta v$  is constant,  $s'(\xi)$  is equivalent to the dimensionless turbulent pressure, and thus the ratio of the solid and dashed curves is also the ratio of turbulent to CR pressure.

as expected for a turbulence supported atmosphere, to increasingly inverted. The midplane CR pressure also increases monotonically. We show in Appendix B that all the profiles illustrated are formally Parker unstable close to the midplane and at large heights.

Figure 2 shows the ratio of CR to turbulent pressure in the column for the same cases as shown in Figure 1. Clearly, as  $f_{\text{Edd}}$  is dialled upwards, the CRs thus tend to push the gas away from the midplane (thus reducing the turbulent

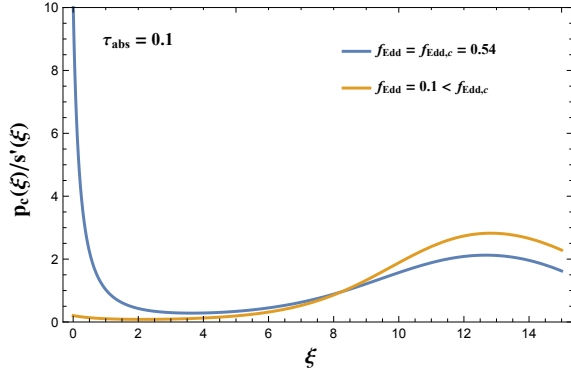


**Figure 2.** Ratio of CR pressure to turbulent pressure  $p_c(\xi)/s'(\xi) = P_c/P_{\text{turb}}$  for the same sample parameters as shown in the upper panel of Figure 1.

pressure); this ratio becomes  $\gg 1$  for the two  $f_{\text{Edd}} \approx f_{\text{Edd},c}$  cases illustrated<sup>12</sup>.

### 3.2 Critical cosmic ray Eddington ratio

Importantly, for the system of equations we have written down, the existence of an equilibrium solution is not guaranteed for an arbitrary combination of parameters. Rather, for any specified  $\tau_{\text{path}}$ ,  $\tau_s$ , and  $f_{\text{gas}}$ , there will exist a critical, CR Eddington ratio, which we denote  $f_{\text{Edd},c}$ , above which CR pressure is too strong for a hydrostatic atmosphere to form. In passing we note that, as we do not require convective (or Parker) stability, our determination of  $f_{\text{Edd},c}$  is conservatively generous.

#### 3.2.1 Expected behaviour of $f_{\text{Edd},c}$

Before proceeding with the numerical evaluation of  $f_{\text{Edd},c}$ , we predict its qualitative behaviour in various limiting cases. Roughly speaking, CRs will have a significant dynamical effect when their midplane pressure becomes significant in comparison to the pressure required to keep the column in hydrostatic equilibrium. In steady state, the midplane CR pressure, in turn, will be set by the product of the CR energy injection rate – set by star formation – and a dwell time  $t_c$  for the CRs which is essentially set by the minimum of the energy loss (via collisional,  $t_{\text{col}}$ , or streaming losses,  $t_{\text{stream}}$ ) and transport timescales, where, in the dense gas, the latter

is given by diffusion:

$$t_{\text{diff}} \approx \frac{z_*^2}{\kappa} = \frac{3z_*^2}{\beta_{A,i} c \lambda_*} \left( \frac{ds}{d\xi} \right)^{-\beta} = \frac{3\tau_s z_*}{\beta_{A,i} c} \left( \frac{ds}{d\xi} \right)^{-\beta} \quad (59)$$

In symbols, the midplane ratio of the cosmic ray to hydrostatic pressures is

$$\begin{aligned} \left. \frac{P_c}{P_{\text{turb}}} \right|_0 &\sim \left. \frac{1}{3} \frac{\dot{E}_c t_c}{V P_{\text{turb}}} \right|_0 \approx \left. \frac{1}{3} \frac{\dot{E}_c}{A z_*} \frac{(t_{\text{col}}^{-1} + t_{\text{stream}}^{-1} + t_{\text{diff}}^{-1})^{-1}}{P_* s'(\xi)} \right|_0 \\ &= \left. \frac{f_{\text{Edd}} F_* \beta_{A,i}}{3\tau_s z_*} \frac{(t_{\text{col}}^{-1} + t_{\text{stream}}^{-1} + t_{\text{diff}}^{-1})^{-1}}{P_* s'(\xi)} \right|_0, \end{aligned} \quad (60)$$

where in the last line we used equation 49. If we now drop all  $O(1)$  factors, we find

$$\begin{aligned} \left. \frac{P_c}{P_{\text{turb}}} \right|_0 &\sim \frac{f_{\text{Edd}} F_* \beta_{A,i}}{\tau_s P_*} \left( \tau_{\text{pp}} + \beta_{A,i} + \frac{\beta_{A,i}}{\tau_s} \right)^{-1} \\ &= f_{\text{Edd}} \times (\tau_{\text{path}} + \tau_s + 1)^{-1} \end{aligned} \quad (61)$$

At the critical Eddington ratio, we expect the ratio of pressures to be  $\sim 1$ , thus

$$f_{\text{Edd},c} \sim (\tau_{\text{path}} + \tau_s + 1). \quad (62)$$

#### 3.2.2 Numerical evaluation of $f_{\text{Edd},c}$

Following Krumholz & Thompson (2012, 2013) and Crocker et al. (2018a), we use the following numerical procedure to determine the locus,  $f_{\text{Edd},c}(\tau_{\text{path}})$ , of this instability curve in the  $(\tau_{\text{path}}, f_{\text{Edd}})$  plane. For each value of  $\tau_{\text{path}}$ , we start with a small value of  $f_{\text{Edd}}$ , for which a solution is guaranteed to exist because in the limit  $f_{\text{Edd}} \rightarrow 0$ , equation 45 and equation 43 are completely decoupled; the former just reduces to the equation for an isothermal atmosphere, and the latter to a nonlinear diffusion equation with losses, the analytic solution for which is given by Krumholz et al. (2019). We use the shooting procedure described Section 3.1 to obtain the numerical solution for this small value of  $f_{\text{Edd}}$ . We then progressively increase  $f_{\text{Edd}}$  and solve again, using the solution for the previous value as a starting guess. Eventually we reach a value of  $f_{\text{Edd}}$  for which the shooting method fails to converge, and no solution exists. Once we find this value, we iteratively decrease and increase  $f_{\text{Edd}}$  in order to narrow down the value  $f_{\text{Edd},c}$  for which a solution ceases to exist. We iterate in this manner until we have determined  $f_{\text{Edd},c}$  for a given  $\tau_{\text{path}}$  to some desired tolerance, and we then move on to the next value of  $\tau_{\text{path}}$ .

We show the value of  $f_{\text{Edd},c}(\tau_{\text{path}})$  determined via this procedure for various values of  $f_{\text{gas}}$  in Figure 3. These curves exhibit the qualitatively expected behaviour with respect to  $\tau_{\text{path}}$ : at small  $\tau_{\text{path}}$  they approach a fixed,  $O(1)$  value; at large  $\tau_{\text{path}}$  they begin to scale  $\propto \tau_{\text{path}}$ . They also display the qualitatively expected dependence on  $f_{\text{gas}}$ , viz. increasing  $f_{\text{gas}}$  renders the column less stable for other parameters held fixed; this is as expected given that gas self-gravity must vanish in the midplane.

It will be convenient for the remainder of this paper to provide an approximate analytic fit that we can use in lieu of the full, numerically-determined solution. We inform

<sup>12</sup> For extremal conditions – i.e., close to the midplane, close to the onset of CR instability, and for very large  $\delta v$  – the conditions for exciting the hybrid, non-resonant CR Bell (2004) instability might, in principle, be satisfied (see Section F). This could lead to local amplification of the magnetic field. While, however, this instability can generate sufficient small scale magnetic turbulence to slow diffusion down to the Bohm level in certain environments, we do not expect to see the effect of this on CR transport in our scenario because of competition from CR convective transport.

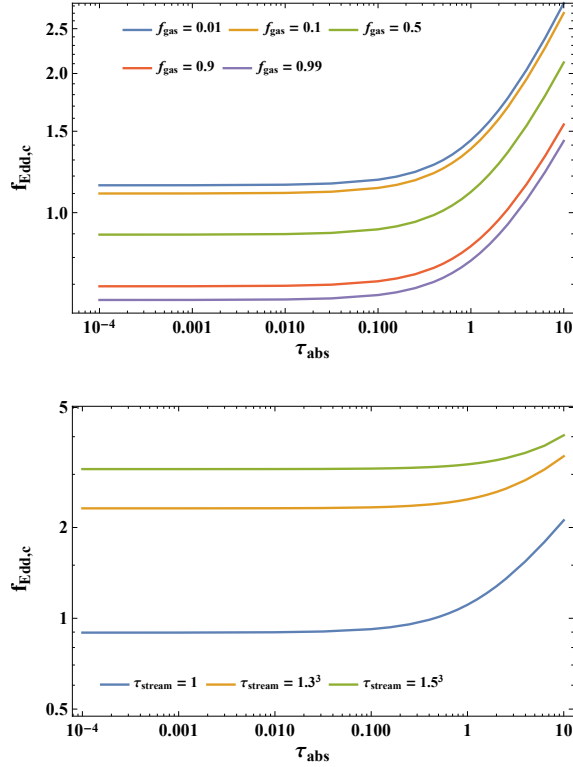


**Figure 3.** CR Eddington limit  $f_{\text{Edd},c}$  as a function of effective optical depth  $\tau_{\text{path}}$ . **Upper panel:**  $\tau_s = 1$  and the colours range over different gas fractions  $f_{\text{gas}}$  as indicated in the legend; a higher  $f_{\text{gas}}$  renders the column less stable (i.e., reduces  $f_{\text{Edd},c}$ ). **Lower panel:**  $f_{\text{gas}} = 0.5$  and the colours range over different  $\tau_s$  as indicated in the legend; a higher  $\tau_s$  renders the column more stable

our fit by analytic solutions that we can obtain to the system in a variety of limiting regimes, which we detail in [Appendix D](#). Combining these limiting solutions with some numerical experimentation, we find that the following approximation for  $f_{\text{Edd},c}$  is accurate to  $\sim 10$  percent<sup>13</sup> for  $\tau_{\text{path}} < 10$  and  $f_{\text{gas}} = 0.01 - 0.99$ :

$$f_{\text{Edd},c,\text{fit}} = \left(s'_{f_{\text{Edd}} \rightarrow 0}\right)^{0.67} \left(\frac{\tau_{\text{path}}}{6.3} + \frac{\tau_s}{0.8}\right), \quad (63)$$

where

$$s'_{f_{\text{Edd}} \rightarrow 0} = \frac{1 - f_{\text{gas}}^2 + \sqrt{1 + 2f_{\text{gas}} + f_{\text{gas}}^4}}{2(1 + f_{\text{gas}})\xi_{\text{turb}}}. \quad (64)$$

is the analytic solution for the midplane density in the limit  $f_{\text{Edd}} \rightarrow 0$ , as we show in [Appendix D](#).

<sup>13</sup> We show the relative error between the fit given by [equation 63](#) and the full numerical solutions in [Figure E1](#) in [Appendix E](#), which confirms the accuracy of the approximation.

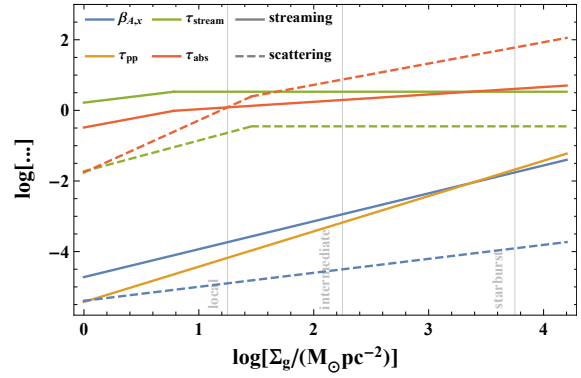


**Figure 4.** (Approximate) dependence of controlling, dimensionless parameters on gas surface density. To calculate  $\beta_{A,i}$  and  $\tau_{\text{path}}$  we need to assume models for  $\delta v(\Sigma_{\text{gas}})$  and  $\chi(\Sigma_{\text{gas}}, M_A)$ ; these are explained in [Appendix A](#). The inflexions in  $\beta_{A,i}$  and  $\tau_{\text{path}}$  correspond to where the  $\chi$  saturates at  $\chi_{\text{max}}$ .

#### 4 IMPLICATIONS FOR STAR-FORMING SYSTEMS

We have now determined, for a galactic disc of a specified gas fraction and cosmic ray scattering *and* absorption optical depths,  $\tau_s$  and  $\tau_{\text{path}}$ , the critical Eddington ratio  $f_{\text{Edd},c}$  above which hydrostatic equilibrium is no longer possible. Our next step is to translate this critical line in dimensionless space into the space of gas and star formation rate surface density, the observable quantities used most often to characterise star-forming systems. For reference, the functional dependence of the controlling, dimensionless parameters  $\tau_{\text{pp}} = \Sigma_{\text{gas}}/(2\Sigma_{\text{pp}})$ ,  $\tau_s = M_A^3/\beta_{A,i} = \delta v/(\sqrt{\chi}M_A)$ , and  $\tau_{\text{path}} = \tau_{\text{pp}}\tau_s/\beta_{A,i}$  are shown in [Figure 4](#).

##### 4.1 From dimensionless to physical quantities

To map our curves into this new parameter space, we note that the combination of [equation 42](#) and [equation 44](#) may be inverted to give

$$\begin{aligned} \Sigma_{\text{gas}} &= \frac{2\Sigma_{\text{pp}}\tau_{\text{path}}\beta_{A,i}}{\tau_s} \\ &\approx 5.6 \delta v_1 \left(\frac{M_A}{2}\right)^{-4} \chi_{-2}^{-1/2} M_{\odot} \text{ pc}^{-2} \end{aligned} \quad (65)$$

Then substitution of [equation 65](#) into [equation 33](#) determines that the reference CR flux becomes

$$\begin{aligned} F_* &= 4\pi G c \Sigma_{\text{pp}}^2 \frac{\tau_{\text{path}}^2 \beta_{A,i}^2}{f_{\text{gas}} \tau_s^2} \\ &\approx 5.3 \tau_{\text{path}}^2 \left(\frac{M_A}{2}\right)^{-8} \chi_{-2}^{-1} f_{\text{gas}}^{-1} \delta v_1^2 \text{ GeV cm}^{-2} \text{ s}^{-1}. \end{aligned} \quad (66)$$

We may also invert [equation 49](#) to express the midplane CR flux in terms of the dimensionless Eddington ratio and set this equal to the CR flux expected from star formation

$$F_{c,0} = F_* \frac{f_{\text{Edd}} \beta_{A,i}}{\tau_s} \equiv \epsilon_{c,1/2} \dot{\Sigma}_{\star} \quad (67)$$

where  $\epsilon_{c,1/2}$  is the mean total energy in relativistic CR released into each galactic hemisphere per unit mass star formation. Inverting [equation 67](#) and substituting in [equation 66](#) we obtain

$$\begin{aligned}\dot{\Sigma}_{\star} &= \frac{F_{\star}}{\epsilon_{c,1/2}} \frac{f_{\text{Edd}} \beta_{A,i}}{\tau_s} \\ &= \frac{4\pi G c \Sigma_{\text{pp}}^2}{\epsilon_c} \frac{\tau_{\text{path}}^2 \beta_{A,i}^3}{f_{\text{gas}} \tau_s^3} f_{\text{Edd}}\end{aligned}\quad (68)$$

With [equation 65](#) and [equation 68](#) we now have the mapping  $(\tau_{\text{path}}, f_{\text{Edd}}) \rightarrow (\Sigma_{\text{gas}}, \dot{\Sigma}_{\star})$  at fixed  $\tau_s, f_{\text{gas}}, \beta_{A,i}$ , and  $\beta$ . In particular, with this mapping, we can find the critical star formation rate surface density  $\dot{\Sigma}_{\star,c}$  that corresponds to the critical Eddington ratio  $f_{\text{Edd},c}$ .

Accounting only for CR acceleration associated with core collapse supernovae, a reference value for the CR energy release per unit mass of star formation into each Galactic hemisphere,  $\epsilon_{c,1/2}$ , can be defined as

$$\begin{aligned}\epsilon_{c,1/2} &\simeq \frac{1}{2} \frac{\eta_c E_{\text{SN}}}{M_{\star,\text{SN}}} \\ &\equiv \epsilon_{c,*,1/2} \left( \frac{\eta_c}{0.1} \right) \left( \frac{E_{\text{SN}}}{10^{51} \text{ erg}} \right) \left( \frac{90 M_{\odot}}{M_{\star,\text{SN}}} \right)\end{aligned}\quad (69)$$

where  $\eta_c \sim 0.1$  is a rough (e.g., [Drury et al. 1989](#); [Hillas 2005](#); [Strong et al. 2010](#); [Paglione & Abrahams 2012](#); [Peng et al. 2016](#)) calibration for the fraction of the total core collapse supernova kinetic energy release that ends up in CRs, and, for a [Chabrier \(2005\)](#) IMF, one core collapse supernova requires the formation of  $M_{\star,\text{SN}} \simeq 90 M_{\odot}$  of stars assuming that all stars born with masses of  $8 M_{\odot}$  or above end their lives of core collapse supernovae. Numerically, the normalising cosmic ray efficiency is

$$\epsilon_{c,*,1/2} \equiv 5.6 \times 10^{47} \text{ erg } M_{\odot}^{-1}.\quad (70)$$

Note that this normalisation for  $\epsilon_{c,1/2}$  may be too conservative as it ignores other sources of mechanical power that may end up in CRs including stellar wind shocks, pulsar winds, and thermonuclear supernovae. It also neglects the possibility, for which there is some evidence ([Nomoto et al. 2006](#)), that the mean mechanical energy per core collapse supernova might exceed by a factor of a few the canonical  $10^{51}$  erg. Ignoring this complication and adopting fiducial values in [equation 68](#), we find

$$\begin{aligned}\dot{\Sigma}_{\star} &\simeq 3.8 \times 10^{-3} M_{\odot} \text{ pc}^{-2} \text{ Myr}^{-1} \frac{\tau_{\text{path}}^2 f_{\text{Edd}}}{f_{\text{gas}}} \\ &\times \delta v_1^3 \left( \frac{\epsilon_{c,1/2}}{\epsilon_{c,*,1/2}} \right)^{-1} \left( \frac{M_A}{2} \right)^{-12} \chi^{-3/2},\end{aligned}\quad (71)$$

where, note, we have normalized  $\chi$  to  $\chi_{\text{max}}$ .

## 4.2 Stability region for star-forming systems

We are now ready to determine the locus of the cosmic ray stability curve,  $\dot{\Sigma}_{\star,c}$ , in the observable plane of star formation rate surface density versus gas surface density. Mathematically this locus is defined by the replacement of  $f_{\text{Edd}}$  in [equation 71](#) with our numerically-determined  $f_{\text{Edd},c} = f_{\text{Edd},c}(\tau_{\text{path}})$ . We show in [Figure 5](#) select curves for the locus of the critical star formation rate at our fiducial parameter

values ( $\tau_s = M_A^3 = 8$ ,  $\beta = 1/4$ ) for a range of values of  $f_{\text{gas}}$ ,  $\delta v$ , and  $\chi$ . The stable region is below and to the right of the curves, while the unstable region is above and to the left. The three sets of parameter values we have adopted for the blue, green, and red curves ( $\{\delta v, f_{\text{gas}}, \chi\} = \{10 \text{ km/s}, 0.1, 1.3 \times 10^{-3}\}$ ,  $\{30 \text{ km/s}, 0.5, 3 \times 10^{-3}\}$ , and  $\{100 \text{ km/s}, 0.7, 10^{-4}\}$ , respectively) correspond to typical values encountered in the ISM of i) local disc galaxies (*blue*; e.g., Milky Way local ISM), ii) either weak circumnuclear starbursts on the local universe or high-redshift main sequence galaxies (*green*; e.g., M82, NGC253, BzK galaxies), and iii) strong starbursts, ULIRGS, or sub-mm galaxies (*red*; e.g., Arp 220); cf. the data compilation in [Krumholz et al. \(2019\)](#). Following the discussion surrounding [equation 56](#), we adopt the saturated value (as informed by the competition between FLRW and turbulent transport) of  $\chi \rightarrow \chi_{\text{max}} \sim 1.3 \times 10^{-3}$  for the local spiral case. [Figure 5](#) also shows a selection of observed galaxies culled from the literature (with the archetypal examples of each ISM type identified above shown as red points).

The primary point to take from the comparison of the distribution of real galaxies and the location of the stability curves in the figure is that, for physically-plausible values of the parameters, the (blue and green) stability curves patrol a region very close to the top of the occupied part of the  $(\Sigma_{\text{gas}}, \dot{\Sigma}_{\star})$  plane for star-forming galaxies with surface mass densities  $\Sigma_{\text{gas}} \lesssim 10^{2.5} M_{\odot} \text{ pc}^{-2}$ . This correspondence strongly suggests that CR feedback may be an important mechanism in such galaxies. It might limit the ability of galaxies to make excursions above the locus where most of them like, or it might be responsible for launching winds and ejecting gas in galaxies that do wander upwards to higher star formation rates.

On the other hand, much above  $\Sigma_{\text{gas}} \sim 10^{2.5} M_{\odot} \text{ pc}^{-2}$  the (green and red) critical curves diverge away from the observed distribution of galaxies (which tend to fall into the starburst or ULIRG category) indicating that CRs do not play an important dynamical role in these systems. Mathematically, such a divergence must occur for the following reason: from [equation 68](#), for the range of  $\tau_{\text{path}}$  for which  $f_{\text{Edd},c} \sim \text{const}$  at fixed  $\tau_s$  (cf. [Figure 3](#)) we have shown that the critical star formation rate surface density scales approximately as  $\dot{\Sigma}_{\star,c} \propto \tau_{\text{path}}^2 \propto \Sigma_{\text{gas}}^2$ . On the other hand, the observed surface density of star formation rises with gas surface density with an index  $< 2$ . Physically, the divergence occurs because the high gas number densities in starburst systems kill CRs quickly, meaning that the energy density/pressure they represent cannot build up to be anything comparable to hydrostatic pressures. This is confirmed by the underlying contours/colour shading in the figure which shows the logarithm of the midplane, steady state cosmic ray pressure divided by the midplane pressure required for hydrostatic equilibrium; in Arp 220, for instance, this quantity is  $\leq 10^{-3}$ . On the other hand, such a situation constitutes a recipe for CR calorimetry, so these systems are expected – indeed, directly inferred, in a limited number of cases – to be good hadronic  $\gamma$ -ray sources (cf. [Krumholz et al. 2019](#)).

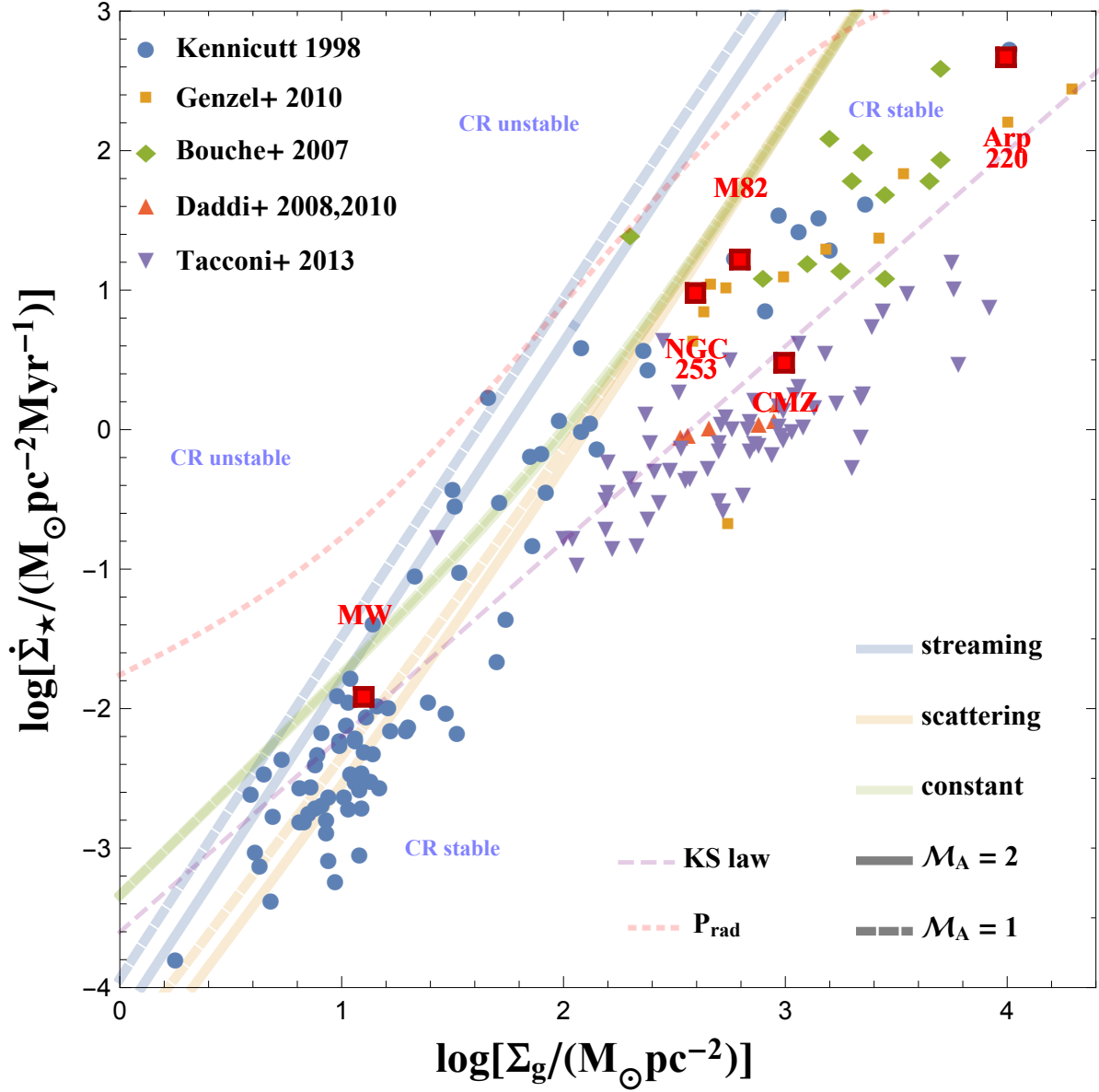


**Figure 5.** Coloured lines show critical stability curves  $\dot{\Sigma}_{\star,c}$  shows the star formation rate per unit area at which CR pressure precludes hydrostatic equilibrium, computed using our fiducial parameter choices ( $\beta = 1/4$ ,  $M_A = 2$ ,  $\epsilon_{c,1/2} = 5.6 \times 10^{47} \text{ erg}/M_\odot$ ), for three different combinations of ISM turbulent velocity dispersion  $\delta v$ , gas fraction  $f_{\text{gas}}$ , and neutral gas ionisation fraction  $\chi$ , as indicated in the legend (the critical curves are only plotted over the  $\Sigma_{\text{gas}}$  range where the parameters assumed in generating each are physically plausible). Contours and underlying colour shading show the ratio of the midplane CR pressure  $P_c$  (equation 72) to  $P_*$  (equation 32), which is approximately equal to the hydrostatic pressure. Contours are labelled by the value of  $\log(P_c/P_*)$  to which they correspond, and are in steps of 1 dex. The dashed, diagonal, purple line is the Kennicutt (1998) star formation scaling. Finally, points show observations drawn from the following sources: local galaxies from Kennicutt (1998),  $z \sim 2$  sub-mm galaxies from Bouché et al. (2007), and galaxies on and somewhat above the star-forming main sequence at  $z \sim 1-3$  from Daddi et al. (2008, 2010b); Genzel et al. (2010); Tacconi et al. (2013). The red data points show the Solar neighborhood in the Milky Way, together with three, local starbursts whose  $\gamma$ -ray emission is modelled in Krumholz et al. (2019). The observations have been homogenised to a Chabrier (2005) IMF and the convention for  $\alpha_{\text{CO}}$  suggested by Daddi et al. (2010a); see Krumholz et al. (2012) for details.



#### 4.2.1 Insensitivity of conclusions to $M_A$ and consequent insensitivity to CR diffusion coefficient

One concern the reader might have is that the coloured critical stability curves in Figure 5 are determined by equation 71 which is very sensitive to  $M_A$  ( $M_A^{12}$  appears in the denominator) and, what is more,  $M_A$  is somewhat poorly constrained. In fact, it turns out that the position of a constraint curve is rather insensitive to  $M_A$  (so long as  $M_A > 1$ ) because of a corresponding strong dependence of  $\Sigma_{\text{gas}}$  on  $M_A^{-4}$  (equation 65) and because  $f_{\text{Edd}} \propto \tau_s = M_A^3$  (for  $M_A \sim \text{few}$  and  $\tau_{\text{path}} \lesssim 1$ ); the gross effect of tuning  $M_A$  up or down is simply to slide the constraint curve south-west/north-east parallel to its length (cf. Appendix C). Thus our claim that the critical CR curve patrols the top of the observed distribution of galaxies for  $\Sigma_{\text{gas}} \lesssim 10^{2.5} M_{\odot}/\text{pc}^2$  holds irrespective of the precise value of  $M_A$ , so long as  $M_A > 1$ .

The fact that our qualitative results are insensitive to the exact value of  $M_A$  carries the further and more general implication that they are also insensitive to the fine details of our transport model, in particular, the diffusion coefficient we assume (as given by equation 29). This can be seen from the form of the dimensionless transport equation we derive (equation 43): Imagine that the true diffusion coefficient were different from that given in equation 29 by some factor  $\alpha$ . Then the LHS of equation 43 would be multiplied by  $\alpha$ . But, dividing through by  $\alpha$ , this could be soaked up by redefinitions  $\tau_{\text{path}} \equiv \tau_{\text{pp}}\tau_s/\beta_{A,i} \rightarrow \tau'_{\text{path}} \equiv \tau_{\text{path}}/\alpha$  and  $\tau_s \equiv M_A^3 \rightarrow \tau'_s \equiv \tau_s/\alpha$ . Moreover, as we have shown, our CR stability line is physically relevant when we are in the optically-thin, streaming loss dominated region of the parameter, i.e., when  $\tau_s$  (or equivalently  $M_A$ ) sets  $f_{\text{Edd},c}$ . Given we have demonstrated qualitative insensitivity to the value of  $M_A$  above and in Appendix C, our results are thus likewise insensitive to the precise details of the diffusion coefficient, provided only that its normalisation is within  $\sim$  an order of magnitude of that which we derive, it is not very strongly energy dependent, and its behaviour is such that diffusivity is smaller the denser the gas. For instance, the local Milky Way disc diffusion coefficient, as derived from observations of the locally observed cosmic rays, would satisfy all these requirements (see footnote 5).

#### 4.3 Predicted cosmic ray energy density in star-forming galaxies

Within the context of our model, we can predict midplane cosmic ray energy densities in star-forming galaxies as follows. Following from equation 60 and developments in the

previous section, we have that the CR midplane pressure is

$$\begin{aligned} P_c|_0 &\equiv \frac{1}{3} u_c|_0 \\ &\simeq \epsilon_{c,1/2} \dot{\Sigma}_{\star} \frac{\tau_s}{c \beta_{A,i}} \left( \tau_{\text{path}} + \tau_s + 1 \right)^{-1} \\ &= \epsilon_{c,1/2} \dot{\Sigma}_{\star} \frac{M_A^4 \sqrt{\chi}}{\delta v} \left( \tau_{\text{path}} + M_A^3 + 1 \right)^{-1} \\ &\simeq 1.1 \left( \frac{M_A}{2} \right)^4 \left( \frac{\epsilon_{c,1/2}}{\epsilon_{c,*,1/2}} \right) \frac{\dot{\Sigma}_{\star,-2\sqrt{\chi-3}}}{\Sigma_{\text{gas},1}^{0.37}} \\ &\quad \times \left( \frac{\tau_{\text{path}}}{8} + \left( \frac{M_A}{2} \right)^3 + \frac{1}{8} \right)^{-1} \text{ eV cm}^{-3}, \quad (72) \end{aligned}$$

where, for the last line, we have normalised to gas and star formation rate surface densities similar to the local MW disc values and we have employed a heuristic scaling of the turbulent velocity dispersion with surface mass density that approximately reproduces the observed velocity dispersions in a limited sample of galaxies from Krumholz et al. (2019),  $\delta v \propto \Sigma_{\text{gas},1}^{0.37}$  (see equation A3 in Appendix Section A). With respect to equation 72 we remind the reader that the three terms appearing in the final parentheses parameterise modifications to the CR energy density due to  $pp$  losses, streaming losses, and diffusive escape. Comparing these terms<sup>14</sup>, it is clear that within our model CRs inside the neutral gas layer are always in a loss (rather than escape) dominated regime: for  $\tau_{\text{path}}/M_A^3 = \tau_{\text{pp}}/\beta_{A,i} \gg 1$  they are in a  $pp$  collisionally-dominated, calorimetric regime, in which case

$$\begin{aligned} P_c|_0 \rightarrow P_{c,\text{cal}}|_0 &\equiv \frac{\epsilon_{c,1/2}}{c} \frac{\dot{\Sigma}_{\star}}{\tau_{\text{pp}}} = \frac{2\epsilon_{c,1/2}}{c} \frac{\Sigma_{\text{pp}}}{\Sigma_{\text{gas}}} \frac{\dot{\Sigma}_{\star}}{\Sigma_{\text{gas}}} \\ &\simeq 5.1 \left( \frac{\dot{\Sigma}_{\star,-2}}{\Sigma_{\text{gas},1}} \right) \text{ eV cm}^{-3}, \quad (73) \end{aligned}$$

and, in the opposite limit, the streaming losses that accompany their transport along the field lines are dominant, in which case

$$\begin{aligned} P_c|_0 \rightarrow P_{c,\text{stream}}|_0 &\equiv \epsilon_{c,1/2} \frac{\dot{\Sigma}_{\star} M_A \sqrt{\chi}}{\delta v} \\ &\simeq 0.7 \left( \frac{\dot{\Sigma}_{\star,-2\sqrt{\chi-3}}}{\delta v_1} \right) \left( \frac{M_A}{2} \right) \text{ eV cm}^{-3}. \quad (74) \end{aligned}$$

If we now further adopt heuristic models for the scaling of  $\chi$  and  $f_{\text{gas}}$  (see Appendix Section A), and use equation 44 to replace  $\tau_{\text{path}}$  in equation 72 we can generate contours of CR energy density across the Kenicutt-Schmidt plane; see Figure 6, upper panel. Finally, if we assume the empirical Kennicutt (1998)-Schmidt star formation law,  $\Sigma_{\star} \propto \Sigma_{\text{gas}}$ , we can collapse the 2-parameter dependence presented in the upper panel down into our model's predicting for the mean, midplane CR energy density in star-forming galaxies as a pure function of gas surface density: this is shown in Figure 6, lower panel. Note that the units of  $\Sigma_{\text{gas}}$  here are  $\text{g cm}^{-2}$  to facilitate comparison against the results of Lacki et al. (2010) fig. 16. Note that for each curve there is an inflexion at  $\tau_{\text{path}}/M_A^3 = \tau_{\text{pp}}/\beta_{A,i} \sim 1$  in scaling of the CR pressure with  $\Sigma_{\text{gas}}$ . Here the CR energy density transitions

<sup>14</sup> And given the understanding that the neutral gas layer is in the super-Alfvénic regime.

from  $\propto \dot{\Sigma}_\star/\delta v \lesssim \Sigma_{\text{gas}}^{1.4}$  for the optically-thin, streaming-loss dominated regime to  $\propto \dot{\Sigma}_\star/\Sigma_{\text{gas}} \lesssim \Sigma_{\text{gas}}^{0.4}$  for the optically-thick, calorimetric regime. Clearly, as previously found by Lacki et al. (2010) and known (Boulares & Cox 1990) to be the case for the local Milky Way disc (cf. red datum in Figure 6, lower panel), the predicted (as distinct from the maximum) mid-plane CR pressure for star-forming galaxies cannot support their gaseous discs in hydrostatic equilibrium.

## 5 DISCUSSION AND CONCLUSIONS

In this paper we analyse the stability of galactic discs against cosmic ray (CR) pressure, using an idealised model of a disc as a plane-parallel slab of gas confined by stellar and gas self-gravity, and supported by a combination of turbulent and CR pressure. This system is characterised primarily by two dimensionless numbers: the effective optical depth of the disc to CRs (including both the effects of CR scattering and losses to  $\pi$  production), and the CR Eddington ratio (defined by the ratio of the CR momentum flux to the gravitational momentum flux). The primary result of our analysis is that such a system possesses a stability limit: for a given effective optical depth, there exists a maximum CR Eddington ratio above which the system cannot remain hydrostatic. While the nature of the non-linear development of the resulting instability is uncertain, studies of the analogous instability driven by radiation suggests that the result is likely to be a wind that removes mass until the system is driven back below the stability limit.

Given standard estimates for the efficiency with which SNe inject CRs into galaxies, together with characteristic numbers describing the magnetohydrodynamic turbulence in the ISM, we can translate our stability limit directly into a line in the space of gas surface density and star formation rate, the so-called Kennicutt-Schmidt (KS) plane. The result of doing so is both surprising and suggestive. We find that the stability limit projected onto the KS plane is close to a line of slope 2, which closely matches the upper envelope of observed systems with the surface densities characteristic of modern spiral and dwarf galaxies,  $\Sigma_{\text{gas}} \lesssim 300 M_\odot \text{pc}^{-2}$ . We emphasize that there is no *a priori* reason why our calculation should have produced such a coincidence: in the dimensionless parameter space of  $\tau_s$ ,  $\tau_{\text{path}}$ , and  $f_{\text{Edd}}$  that defines our system, the critical value of  $f_{\text{Edd}}$  above which the gas column is rendered hydrostatically unstable follows purely from the mathematical form of our ODEs. The only astrophysical inputs required to map this to the KS plane are fundamental constants (e.g., the  $pp$  cross-section), quantities describing general physical processes that are unrelated to galaxies (e.g., the saturation field strength of turbulent dynamos), and quantities describing microphysical processes such as the conversion efficiency from supernova kinetic energy to CR energy. The only complex modeling needed is that required to estimate the ionization fraction, which is determined at least partly by the CRs themselves. Thus the similarity of the CR stability limit to the observed galaxy distribution seems unlikely to be a coincidence.

In contrast, we find that galaxies with higher gas and star formation surface densities lie well below the CR stability limit. Fundamentally, this is due to the increasing importance of pion losses, which prevent the CR energy density

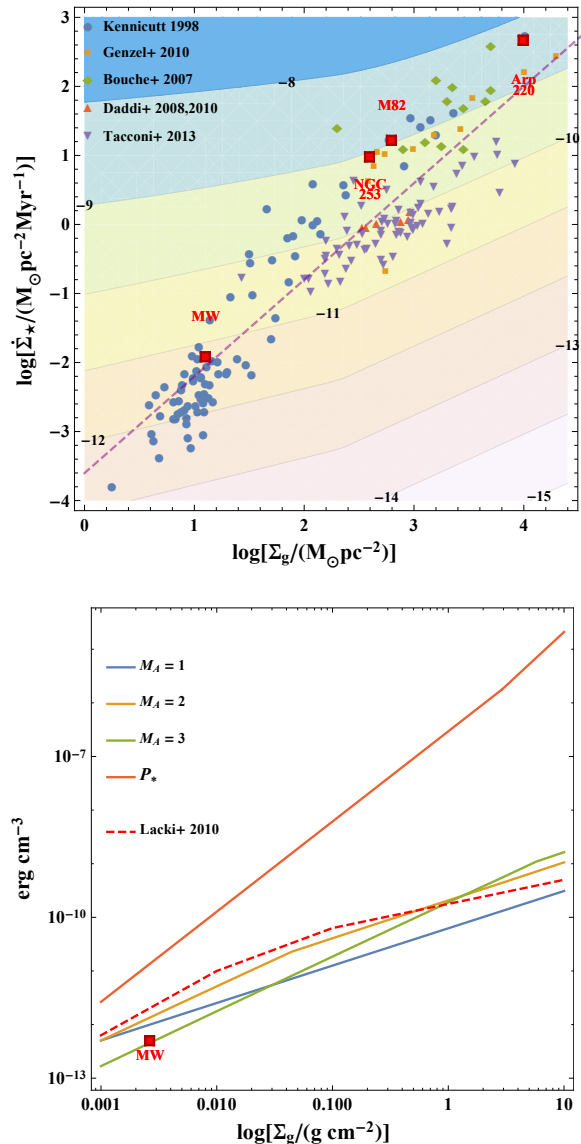


**Figure 6.** Midplane CR energy densities and pressures predicted by our model. **Upper panel:** Contours and underlying colour shading show predicted midplane CR energy densities  $u_c(0) = 3P_c(0)$  in  $\text{erg cm}^{-3}$ . Contours are labelled by the value of  $\log(u_c)$  to which they correspond, and are in steps of 1 dex. The dashed, diagonal, purple line is the Kennicutt (1998) star formation scaling. Data points for individual galaxies are as explained in the caption to Figure 5. **Lower panel:** Midplane CR pressures in  $\text{erg cm}^{-3}$  given by equation 72 for three different values of  $M_A$  and adopting the Kennicutt (1998)-Schmidt relation  $\dot{\Sigma}_\star(\Sigma_{\text{gas}}) \propto \Sigma_{\text{gas}}^{1.4}$  compared against the approximate hydrostatic equilibrium pressure  $P_{\text{hydro,eqm}}$  as calculated assuming a heuristic model for the running of the mean gas fraction of galaxies with  $\Sigma_{\text{gas}}$  (see equation A2). The dashed red curve reproduces the CR pressure determined in the model by Lacki et al. (2010). Note the units of  $\Sigma_{\text{gas}}$  here are  $\text{g cm}^{-2}$ . The red datum is for the local disc of the Milky Way adopting assuming a total energy density in relativistic CRs of  $1 \text{ eV cm}^{-3}$ .

from rising fast enough to compete with the gravitational energy density. Thus we conclude that CRs cannot be dynamically important in these galaxies. Conversely, however, due to the importance of pion losses, these galaxies are good CR calorimeters **and, therefore,  $\gamma$ -ray sources** (cf. [Torres et al. 2004](#); [Thompson et al. 2007](#); [Lacki et al. 2010, 2011](#); [Yoast-Hull et al. 2016](#)).

In future work we intend to explore the consequences of the picture set out here and in ([Krumholz et al. 2019](#)) for understanding the far infrared–radio continuum correlation and the emerging far infrared– $\gamma$ -ray correlation, and to delimit the possible contribution of hadronic  $\gamma$ -ray emission from ordinary galaxies to the isotropic  $\gamma$ -ray flux as predicted by our model.

## ACKNOWLEDGEMENTS

This research was funded by the Australian Government through the Australian Research Council, awards FT180100375 (MRK) and DP190101258 (RMC and MRK). RMC gratefully acknowledges conversations with Felix Aharonian, Geoff Bicknell, Yuval Birnboim, Luke Drury, Alex Lazarian, Chris McKee, Christoph Pfrommer, Heinz Völk, and Siyao Xu. MRK and TAT acknowledge support from the Simons Foundation through the Simons Symposium Series “Galactic Superwinds: Beyond Phenomenology”, during which this work was planned.

## REFERENCES

- Abdo, A. A., Ackermann, M., Ajello, M., et al. 2010, *ApJ*, 709, L152
- Acero, F., Aharonian, F., Akhperjanian, A. G., et al. 2009, *Science*, 326, 1080
- Beck, R. 2015, *A&ARv*, 24, 4
- Behroozi, P. S., Wechsler, R. H., & Conroy, C. 2013, *ApJ*, 762, L31
- Bell, A. R. 1978, *MNRAS*, 182, 147
- Bell, A. R. 2004, *MNRAS*, 353, 550
- Blasi, P. 2019, *Galaxies*, 7, 64
- Boettcher, E., Zweibel, E. G., Gallagher, J. S., III, & Benjamin, R. A. 2016, *ApJ*, 832, 118
- Booth, C. M., Agertz, O., Kravtsov, A. V., & Gnedin, N. Y. 2013, *ApJ*, 777, L16
- Bouché, N., Cresci, G., Davies, R., et al. 2007, *ApJ*, 671, 303
- Boulares, A., & Cox, D. P. 1990, *ApJ*, 365, 544
- Breitschwerdt, D., McKenzie, J. F., & Voelk, H. J. 1991, *A&A*, 245, 79
- Breitschwerdt, D., McKenzie, J. F., & Voelk, H. J. 1993, *A&A*, 269, 54
- Buck, T., Pfrommer, C., Pakmor, R., et al. 2019, *arXiv e-prints*, [arXiv:1911.00019](#)
- Chabrier, G. 2005, *The Initial Mass Function 50 Years Later*, 327, 41
- Chan, T. K., Kereš, D., Hopkins, P. F., et al. 2019, *MNRAS*, 488, 3716
- Cho, J., & Lazarian, A. 2002, *Phys. Rev. Lett.*, 88, 245001
- Cho, J., & Lazarian, A. 2003, *MNRAS*, 345, 325
- Ceverino, D., Klypin, A., Klimek, E. S., et al. 2014, *MNRAS*, 442, 1545
- Condon, J. J. 1992, *ARA&A*, 30, 575
- Crocker, R. M., Jones, D. I., Aharonian, F., et al. 2011, *MNRAS*, 411, L11
- Crocker, R. M. 2012, *MNRAS*, 423, 3512
- Crocker, R. M., Krumholz, M. R., Thompson, T. A., & Clutterbuck, J. 2018 (**CKTC18**), *MNRAS*, 478, 81
- Crocker, R. M., Krumholz, M. R., Thompson, T. A., Baumgardt, H., & Mackey, D. 2018, *MNRAS*, 481, 4895
- Crutcher, R. M. 1999, *ApJ*, 520, 706
- Daddi, E., Dannerbauer, H., Elbaz, D., et al. 2008, *ApJ*, 673, L21
- Daddi, E., Bournaud, F., Walter, F., et al. 2010, *ApJ*, 713, 686
- Daddi, E., Elbaz, D., Walter, F., et al. 2010, *ApJ*, 714, L118
- Davis, S. W., Jiang, Y. F., Stone, J. M., & Murray, N. 2014, *ApJ*, 796, 107
- Dekel, A., Sarkar, K. C., Jiang, F., Bournaud, F., Krumholz, M. R., Ceverino, D., & Primack, J. 2019, *MNRAS*, 4, 4753
- Domingo-Santamaría, E., & Torres, D. F. 2005, *A&A*, 444, 403
- Dorfi, E. A., & Breitschwerdt, D. 2012, *A&A*, 540, A77
- Drury, L. O., Markiewicz, W. J., & Voelk, H. J. 1989, *A&A*, 225, 179
- Drury, L. O. ’., & Strong, A. W. 2017, *A&A*, 597, A117
- Everett, J. E., Zweibel, E. G., Benjamin, R. A., et al. 2008, *ApJ*, 674, 258
- Faerman, Y., Sternberg, A., & McKee, C. F. 2017, *ApJ*, 835, 52
- Fall, S. M., Krumholz, M. R., & Matzner, C. D. 2010, *ApJ*, 710, L142
- Federrath, C. 2016, *J. Plasm. Phys.*, 82, 535820601
- Federrath, C., Schober, J., Bovino, S., & Schleicher, D. R. G. 2014, *ApJ*, 797, L19
- Fermi-LAT collaboration, et al. 2012, *ApJ*, 755, 164
- Fermi-LAT collaboration, et al. 2019, submitted to *ApJS*, [arXiv:1902.10045](#)
- Funk, S. 2015, *Annual Review of Nuclear and Particle Science*, 65, 245
- Gabici, S., Aharonian, F. A., & Blasi, P. 2007, *Ap&SS*, 309, 365
- Gentry, E. S., Krumholz, M. R., Dekel, A., & Madau, P. 2017, *MNRAS*, 465, 2471
- Genzel, R., Tacconi, L. J., Gracia-Carpio, J., et al. 2010, *MNRAS*, 407, 2091
- Ginzburg, V. L., & Syrovatskii, S. I. 1964, *The Origin of Cosmic Rays*
- Hanasz, M., Lesch, H., Naab, T., et al. 2013, *ApJ*, 777, L38
- Heckman, T. M., Armus, L., & Miley, G. K. 1990, *ApJS*, 74, 833
- Heckman, T. M. 2002, *Extragalactic Gas at Low Redshift*, 254, 292
- Heintz, E., & Zweibel, E. G. 2018, *ApJ*, 860, 97
- Hill, A. S., Joung, M. R., Mac Low, M.-M., et al. 2012, *ApJ*, 750, 104
- Hillas, A. M. 2005, *JPGNP*, 31, 95
- Hopkins, P. F., Quataert, E., & Murray, N. 2011, *MNRAS*, 417, 950
- Ipavich, F. M. 1975, *ApJ*, 196, 107
- Jiang, Y.-F., & Oh, S. P. 2018, *ApJ*, 854, 5
- Jubelgas, M., Springel, V., Enßlin, T., & Pfrommer, C. 2008, *A&A*, 481, 33
- Kafexhiu, E., Aharonian, F., Taylor, A. M., & Vila, G. S. 2014, *Phys. Rev. D*, 90, 123014
- Kalberla, P. M. W., & Kerp, J. 2009, *ARA&A*, 47, 27
- Kennicutt, R. C., Jr. 1998, *ApJ*, 498, 541
- Kennicutt, R. C., Jr., & Evans, N. J. E., II. 2012, *ARA&A*, 50, 531
- Kim, C.-G., & Ostriker, E. C. 2015, *ApJ*, 802, 99
- Kroupa, P. 2001, *MNRAS*, 322, 231
- Krumholz, M. R., & Dekel, A. 2010, *MNRAS*, 406, 112
- Krumholz, M. R., & Thompson, T. A. 2012, *ApJ*, 760, 155
- Krumholz, M. R., Dekel, A., & McKee, C. F. 2012, *ApJ*, 745, 69
- Krumholz, M. R., & Thompson, T. A. 2013, *MNRAS*, 434, 2329
- Krumholz, M. R., Kruijssen, J. M. D., & Crocker, R. M. 2017, *MNRAS*, 466, 1213
- Krumholz, M. R., Burkhardt, B., Forbes, J. C., & Crocker, R. M. 2018, *MNRAS*, 477, 2716

- Krumholz, M. R., Crocker, R. M. et al. 2019, *in submission*, (*arXiv:1911.09774*)
- Kulsrud, R. M. 2005, Plasma physics for astrophysics / Russell M. Kulsrud. Princeton, N.J. : Princeton University Press, c2005. (Princeton series in astrophysics),
- Lacki, B. C., Thompson, T. A., & Quataert, E. 2010, *ApJ*, 717, 1
- Lacki, B. C., Thompson, T. A., Quataert, E., Loeb, A., & Waxman, E. 2011, *ApJ*, 734, 107
- Lacki, B. C. 2013, *arXiv:1308.5232*
- Levermore, C. D., & Pomraning, G. C. 1981, *ApJ*, 248, 321
- Levermore, C. D. 1984, *J. Quant. Spectrosc. Radiat. Transfer*, 31, 149
- Martin, P. 2014, *A&A*, 564, A61
- Martizzi, D., Faucher-Giguère, C.-A., & Quataert, E. 2015, *MNRAS*, 450, 504
- McKee, C. F., & Ostriker, J. P. 1977, *ApJ*, 218, 148
- McKee, C. F., Parravano, A., & Hollenbach, D. J. 2015, *ApJ*, 814, 13
- Muratov, A. L., Kereš, D., Faucher-Giguère, C.-A., et al. 2015, *MNRAS*, 454, 2691
- Nomoto, K., Tominaga, N., Umeda, H., et al. 2006, *Nuclear Phys. A*, 777, 424
- Paglione, T. A. D., & Abrahams, R. D. 2012, *ApJ*, 755, 106
- Pakmor, R., Pfrommer, C., Simpson, C. M., & Springel, V. 2016, *ApJ*, 824, L30
- Parker, E. N. 1966, *ApJ*, 145, 811
- Peng, F.-K., Wang, X.-Y., Liu, R.-Y., Tang, Q.-W., & Wang, J.-F. 2016, *ApJ*, 821, L20
- Persic, M., Rephaeli, Y., & Arieli, Y. 2008, *A&A*, 486, 143
- Pfrommer, C., Pakmor, R., Simpson, C. M., & Springel, V. 2017, *ApJ*, 847, L13
- Protheroe, R. J., Ott, J., Ekers, R. D., et al. 2008, *MNRAS*, 390, 683
- Recchia, S., Blasi, P., & Morlino, G. 2016, *MNRAS*, 462, 4227
- Recchia, S., Blasi, P., & Morlino, G. 2017, *MNRAS*, 470, 865
- Rosdahl, J., Schaye, J., Teyssier, R., & Agertz, O. 2015, *MNRAS*, 451, 34
- Ruszkowski, M., Yang, H.-Y. K., & Zweibel, E. 2017, *ApJ*, 834, 208
- Rybicki, G. B., & Lightman, A. P. 1979, *A Wiley-Interscience Publication*
- Salem, M., & Bryan, G. L. 2014, *MNRAS*, 437, 3312
- Salem, M., Bryan, G. L., & Corlies, L. 2016, *MNRAS*, 456, 582
- Samui, S., Subramanian, K., & Srikanth, R. 2010, *MNRAS*, 402, 2778
- Schlickeiser, R. 2002, *Cosmic ray astrophysics / Reinhard Schlickeiser, Astronomy and Astrophysics Library; Physics and Astronomy Online Library. Berlin: Springer. ISBN 3-540-66465-3, 2002, XV + 519 pp.*
- Simpson, C. M., Pakmor, R., Marinacci, F., et al. 2016, *ApJ*, 827, L29
- Socrates, A., Davis, S. W., & Ramirez-Ruiz, E. 2008, *ApJ*, 687, 202-215
- Strong, A. W., Porter, T. A., Digel, S. W., et al. 2010, *ApJ*, 722, L58
- Tacconi, L. J., Neri, R., Genzel, R., et al. 2013, *ApJ*, 768, 74
- Tennekes, H., & Lumley, J. L. 1972, *First Course in Turbulence*, Cambridge: MIT Press, 1972,
- Thomas, T., & Pfrommer, C. 2019, *MNRAS*,
- Thompson, T. A., Quataert, E., & Murray, N. 2005, *ApJ*, 630, 167
- Thompson, T. A., Quataert, E., Waxman, E., et al. 2006, *ApJ*, 645, 186
- Thompson, T. A., Quataert, E., & Waxman, E. 2007, *ApJ*, 654, 219
- Thornton, K., Gaudlitz, M., Janka, H.-T., & Steinmetz, M. 1998, *ApJ*, 500, 95
- Torres, D. F., Reimer, O., Domingo-Santamaría, E., et al. 2004, *ApJ*, 607, L99
- Tsang, B. T. H., & Milosavljević, M. 2015, *MNRAS*, 453, 1108-1120
- Uhlig, M., Pfrommer, C., Sharma, M., et al. 2012, *MNRAS*, 423, 2374
- VERITAS Collaboration, Acciari, V. A., Aliu, E., et al. 2009, *Nature*, 462, 770
- Vogelsberger, M., Genel, S., Springel, V., et al. 2014, *MNRAS*, 444, 1518
- Völk, H. J., Aharonian, F. A., & Breitschwerdt, D. 1996, *Space Sci. Rev.*, 75, 279
- Wadepuhl, M., & Springel, V. 2011, *MNRAS*, 410, 1975
- Wentzel, D. G. 1974, *ARA&A*, 12, 71
- Wibking, B. D., Thompson, T. A., & Krumholz, M. R. 2018, *MNRAS*, 477, 4665
- Wiener, J., Pfrommer, C., & Oh, S. P. 2017, *MNRAS*, 467, 906
- Wolfire, M. G., McKee, C. F., Hollenbach, D., et al. 2003, *ApJ*, 587, 278
- Xu S., & Lazarian A., 2017, *New Journal of Physics*, 19, 065005
- Yan, H., & Lazarian, A. 2008, *ApJ*, 673, 942
- Yeast-Hull, T. M., Gallagher, J. S., & Zweibel, E. G. 2016, *MNRAS*, 457, L29
- Zirakashvili, V. N., Breitschwerdt, D., Ptuskin, V. S., et al. 1996, *A&A*, 311, 113
- Zweibel, E. G. 2013, *Physics of Plasmas*, 20, 055501
- Zweibel, E. G. 2017, *Physics of Plasmas*, 24, 055402

## APPENDIX A: CHARACTERISTIC ENERGY FOR ONSET OF ENERGY-DEPENDENT DIFFUSION

Here we show that it is reasonable to adopt an energy-independent  $\kappa_{\text{FLRW}}$  everywhere over our parameter space. Ultimately we do this by demonstrating that the streaming velocity is close to the  $v_{A,i}$  for the energetically-dominant CRs near  $\sim \text{GeV}$ .

The volume filling factor of supernova remnants (SNRs) is  $f_{\text{SNR}} \approx 1 - e^{-Q_{\text{SNR}}}$  (McKee, & Ostriker 1977; Heckman et al. 1990; Lacki 2013), where

$$Q_{\text{SNR}} \approx 3.4 E_{51}^{1.28} \left( \frac{\rho_{\text{SN}}}{10 \text{ kpc}^{-3} \text{ yr}^{-1}} \right) \left( \frac{n_{\text{H}}}{100 \text{ cm}^{-3}} \right)^{-0.14} \left( \frac{P/k_{\text{B}}}{10^7 \text{ K cm}^{-3}} \right)^{-1.3}. \quad (\text{A1})$$

Here  $E_{51}$  is the mechanical energy released per core collapse supernova,  $\rho_{\text{SN}}$  is the density of supernovae, and  $P$  is the gas pressure. The density of supernovae near the midplane is  $\rho_{\text{SN}} \approx \dot{\Sigma}_*/hm_{\text{SN}}$ , where  $\dot{\Sigma}_*$  is the star formation rate per unit area, and  $m_{\text{SN}}$  is the mean mass of stars that must be formed to eventually yield one supernova. We evaluate  $f_{\text{SNR}}$  over the Kennicutt-Schmidt plane in Figure A2 using a heuristic estimate of  $f_{\text{gas}}$  as a function of  $\Sigma_{\text{gas}}$  (see equation A2 below). Note that while  $f_{\text{SNR}} \gtrsim 0.5$  is unphysical (given equation A1 implicitly assumes that there is some dense gas surrounding the SNR into which the shell is expanding), few galaxies are binned into  $f_{\text{SNR}} > 0.5$ .

Given an estimate of  $f_{\text{SNR}}$  and given  $\Sigma_{\text{gas}}, f_{\text{gas}}, \delta v, z_*$  and  $\chi$ , we may further calculate the number density of the dense gas phase (Figure A3) and the consequent characteristic energy  $E_{\text{char}}$  at which the streaming velocity (and resultant, effective diffusion coefficient) starts to exhibit energy dependence. We define this implicitly via  $v_s(E_{\text{char}}) \equiv 2v_{A,i}$  (see

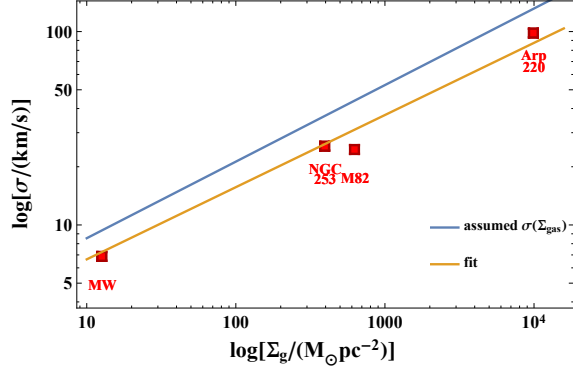


Figure A1. Observed velocity dispersions of the local Milky Way disc plus the three local starbursts modelled by Krumholz et al. (2019) together with the power-law fit to these data.

Krumholz et al. (2019) for the full expression for the energy dependent streaming velocity  $v_s(E_c)$ .

To deal with the complications around the determination of  $f_{\text{gas}}$ ,  $z_*$ , and  $\chi$ , for the purposes of generating the plots in this section we introduce phenomenological scalings for these given by

$$\begin{aligned} f_{\text{gas}}(\Sigma_{\text{gas}}) &\equiv \Sigma_{\text{gas},1}^{0.32} \\ z_*(\Sigma_{\text{gas}}) &\equiv (150 - 10.9 \log \Sigma_{\text{gas},1}) \text{ pc} \\ \chi_{\text{phen}}(\Sigma_{\text{gas}}) &\equiv 10^{-4/3} \Sigma_{\text{gas},1}^{-2/3}. \end{aligned} \quad (\text{A2})$$

The ionisation fraction  $\chi_{\text{phen}}$  is taken to be uniform over the gas column. We further assume that the gas velocity dispersion is a power law in gas surface density which is given by fitting to the observed velocity dispersion of the Milky Way plus the three starbursts modelled by Krumholz et al. (2019, viz. NGC 253, M82 and Arp 220):

$$\delta v_{\text{heur}} = 6.6 \Sigma_{\text{gas},1}^{0.37} \text{ km/s}. \quad (\text{A3})$$

## APPENDIX B: PARKER STABILITY CRITERION

The criterion for Parker (1966) stability may be written (e.g., Zweibel 2017) as

$$-\frac{d\rho_g}{dz} > \frac{\rho_g^2 g z}{\gamma_g P_g + \gamma_c P_c}. \quad (\text{B1})$$

Using our dimensionless parameters, this criterion becomes

$$\frac{d^2 s}{d\xi^2} < \frac{d^2 s}{d\xi^2} \Big|_{\text{P.c.}} \equiv - \left( \frac{ds}{d\xi} \right)^2 \frac{1 - f_{\text{gas}}}{\xi_{\text{turb}} \frac{ds}{d\xi} + \gamma_c P_c}, \quad (\text{B2})$$

where ‘P.c.’ denotes *Parker critical* and for which we have taken  $P_g \rightarrow P_* \xi_{\text{turb}} ds/d\xi$ .

We plot the ratio of  $s''(\xi, \text{P.c.})/s''(\xi)$  in Figure B1 for three representative examples from Section 3.1. Note that all profiles are formally Parker unstable in the midplane and at large  $\xi$ , even the case of  $f_{\text{Edd}} < f_{\text{Edd},c}$ .

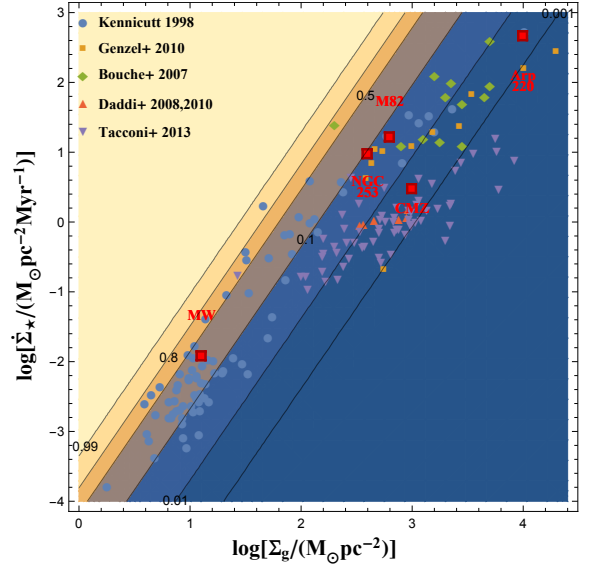


Figure A2. Filling factor of supernova remnants in a galaxy's disc in the Kennicutt-Schmidt plane. For the purposes of this plot, a heuristic scaling of the gas fraction  $f_{\text{gas}}$  is assumed as given by equation A2. Values  $f_{\text{SNR}} \gtrsim 0.5$  are likely unphysical for the reason explained in the main text.

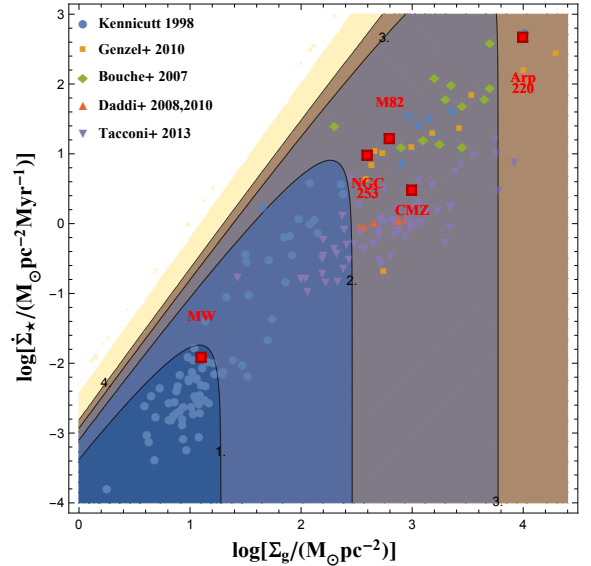
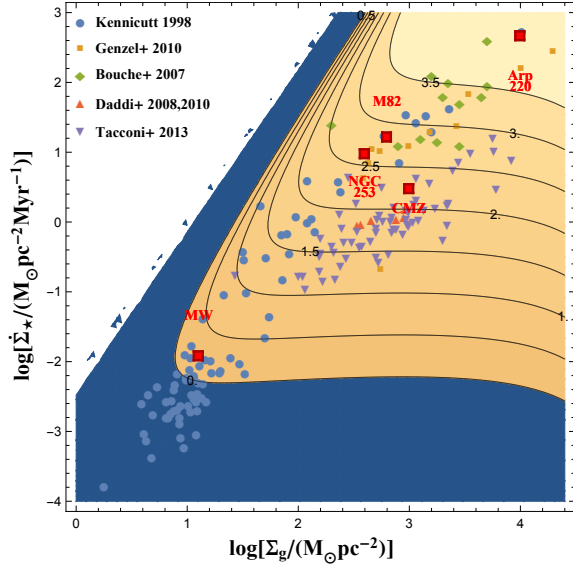
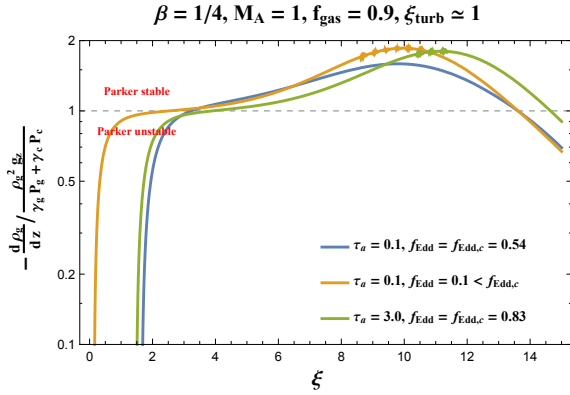


Figure A3. Log of the nucleon number density of the dense ISM gas phase in the Kennicutt-Schmidt plane accounting for  $f_{\text{SNR}}$ . For the purposes of this plot, heuristic scalings of the gas fraction  $f_{\text{gas}}$  and the galactic scale height, as given by equation A2, and the turbulent velocity dispersion as given by equation A3 are assumed.





**Figure A4.** Log of the characteristic energy (in GeV) where diffusion effectively becomes energy dependent. This characteristic energy is defined implicitly via  $v_s(E_{\text{char}}) \equiv 2v_{A,i}$  (see Krumholz et al. (2019) for the full expression for the energy dependent streaming velocity  $v_s(E_c)$ ). For the purposes of this plot, heuristic scalings of the gas fraction  $f_{\text{gas}}$ , the galactic scale height, and ionization fraction, as given by equation A2, are assumed. The plot also assumes that the population of CRs is governed by a power-law in Lorentz  $\gamma$ :  $dN/d\gamma \propto \gamma^{-p}$  where  $p = 2.6$  (matching the Milky Way value; taking harder values of  $p$  closer to 2 moves the characteristic energy higher at fixed position in the Kennicutt-Schmidt plane); and that the overall normalization of the CR flux scales with the star formation rate surface density. This plot demonstrates that it is a reasonable approximation to neglect the energy-dependence of CR transport for the energetically dominant  $\sim$  GeV CRs everywhere in our parameter space.



**Figure B1.** Parker stability criterion for three example cases.

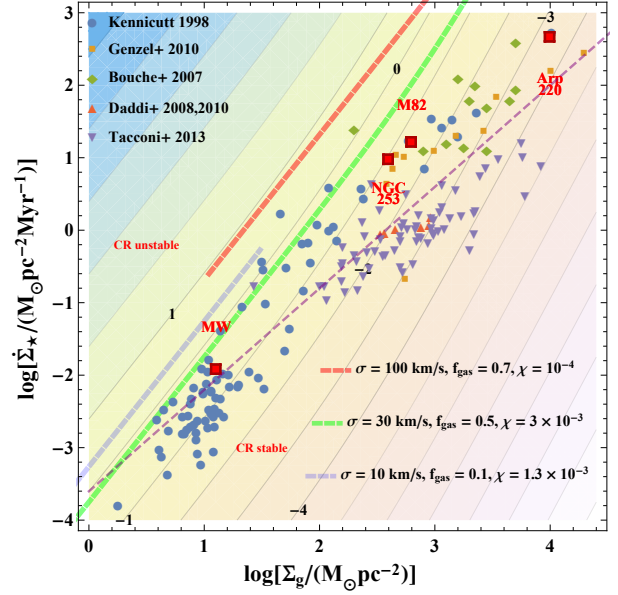


**Figure C1.** Hydrodynamic stability curves for  $M_A = 3$  accounting for cosmic ray pressure in the physical parameter space of star formation rate surface density vs. gas surface mass density. All curves are for  $\beta = 1/4$ ,  $M_A = 3$  ( $\Rightarrow \tau_s = M_A^3 = 27$ ), and  $\epsilon_c = \epsilon_{c,*} = 1/2 \times 10^{50} \text{ erg}/(90 M_\odot) = 5.6 \times 10^{47} \text{ erg}/M_\odot$ . All other details are as explained in the caption to Figure 5.

## APPENDIX C: (ABSENCE OF) EFFECT ON CR STABILITY CURVE OF VARYING $M_A$

As emphasised in the main text, the true value of  $M_A$  in star-forming neutral gas is somewhat uncertain but our results are not too sensitive to this parameter despite the large  $\propto M_A^{12}$  scaling of equation 71. The reason for this is that the factors of  $M_A$  appearing in equation 63, equation 65, and equation 71 conspire such that  $\Sigma_{\text{gas}} \propto \tau_{\text{path}} M_A^{-4}$  while  $\dot{\Sigma}_\star \propto \tau_{\text{path}}^2 M_A^{-9}$ , thus, rescaling  $M_A \rightarrow M'_A$  while performing the mapping from  $(\tau_{\text{path}}, f_{\text{Edd}}) \rightarrow (\Sigma_{\text{gas}}, \dot{\Sigma}_\star)$  shifts points in the stability curve leftwards by a factor  $(M'_A/M_A)^{-4}$  and downwards by a factor  $(M'_A/M_A)^9$  (for  $M'_A > M_A$  in this example), which because the stability curves are  $f_{\text{Edd}} \propto \Sigma_{\text{gas}}^2$  essentially means sliding the stability curve south-west along its length and rescaling it by  $M_A/M'_A$ .

This is demonstrated explicitly via comparison of Figure 5 and Figure C1; to reasonable accuracy, dialling  $M_A$  up from 2 to 3 here simply slides the constraint curves in a south-west direction along their own lengths and rescales them by a factor of 2/3, maintaining the validity of our conclusion that the cosmic ray stability line patrols the upper envelope of the occupied region in the Kennicutt-Schmidt parameter space.

## APPENDIX D: ANALYTICAL SOLUTIONS FOR TURBULENCE-SUPPORTED ATMOSPHERE

For reference, we present here the analytical solution for the dimensionless gas column in the limit that  $f_{\text{Edd}} \rightarrow 0$ . In this situation, the cosmic ray flux entering at the midplane vanishes,  $p_c \rightarrow 0$  everywhere, and the gas column must then be supported solely by the dynamical pressure represented by the turbulent velocity dispersion as parameterised by  $\xi_{\text{turb}}$ . Given we assume a fixed  $\xi_{\text{turb}}$  the gas column is akin to an isothermal atmosphere whose profile is determined by

$$\xi_{\text{turb}} \frac{d^2 s}{d\xi^2}(\xi) = - (1 - (1 - s(\xi)) f_{\text{gas}}) \frac{ds}{d\xi}(\xi), \quad (\text{D1})$$

for which we can obtain simple solutions for  $f_{\text{gas}} \rightarrow 0$  (fixed, external  $g$ ) and  $f_{\text{gas}} \rightarrow 1$  as, respectively:

$$s(\xi) = 1 - \exp\left(-\frac{\xi}{\xi_{\text{turb}}}\right) \quad ; \quad f_{\text{Edd},c} \rightarrow 0, f_{\text{gas}} = 0 \quad (\text{D2})$$

$$s(\xi) = \tanh\left(\frac{\xi}{2\xi_{\text{turb}}}\right) \quad ; \quad f_{\text{Edd},c} \rightarrow 0, f_{\text{gas}} = 1 \quad (\text{D3})$$

Note that these two solutions have dimensionless, midplane number densities of, respectively

$$s'(0) = \frac{1}{\xi_{\text{turb}}} \quad ; \quad f_{\text{Edd},c} \rightarrow 0, f_{\text{gas}} = 0 \quad (\text{D4})$$

$$s'(0) = \frac{1}{2\xi_{\text{turb}}} \quad ; \quad f_{\text{Edd},c} \rightarrow 0, f_{\text{gas}} = 1. \quad (\text{D5})$$

Thus a gas column subject to a constant, external gravitational field and a dimensionless turbulence parameter  $\xi_{\text{turb}} = 1$ , has a midplane density of  $s'(0) = 1$ . For  $0 < f_{\text{gas}} < 1$  the analytic solution to [equation D1](#) may also be found:

$$s'(0, f_{\text{gas}}, \xi_{\text{turb}}) = \frac{1 - f_{\text{gas}}^2 + \sqrt{1 + 2f_{\text{gas}} + f_{\text{gas}}^4}}{2(1 + f_{\text{gas}})\xi_{\text{turb}}} \quad (\text{D6})$$

## APPENDIX E: FIT TO CRITICAL COSMIC RAY STABILITY CURVE

In [Figure E1](#) we display our optimised analytic approximation to the full numerically-determined critical CR stability curve. We obtain this analytic approximation using the FindFit intrinsic function within MATHEMATICA. Over the relevant region of the parameter space, the analytic approximation reproduces the true value to within  $\lesssim 10\%$ ; this is demonstrated in [Figure E1](#) where

$$\text{rel. err.} \equiv \frac{|f_{\text{Edd},c} - f_{\text{Edd},c,\text{fit}}|}{f_{\text{Edd},c}}. \quad (\text{E1})$$

## APPENDIX F: HYBRID, NON-RESONANT (BELL) INSTABILITY

The condition for exciting the hybrid, non-resonant CR instability is  $u_c/u_B \gtrsim 2c/v_d$  where, in our case, the draft velocity will be  $v_d \sim v_{A,i}$  ([Bell 2004](#)). In our dimensionless parameters, this condition for exciting the instability can be written

$$\frac{9}{2} \frac{M_A}{\sqrt{\chi}} \frac{\delta v}{c} \frac{p_c(\xi)}{s'(\xi)} \gtrsim 1. \quad (\text{F1})$$

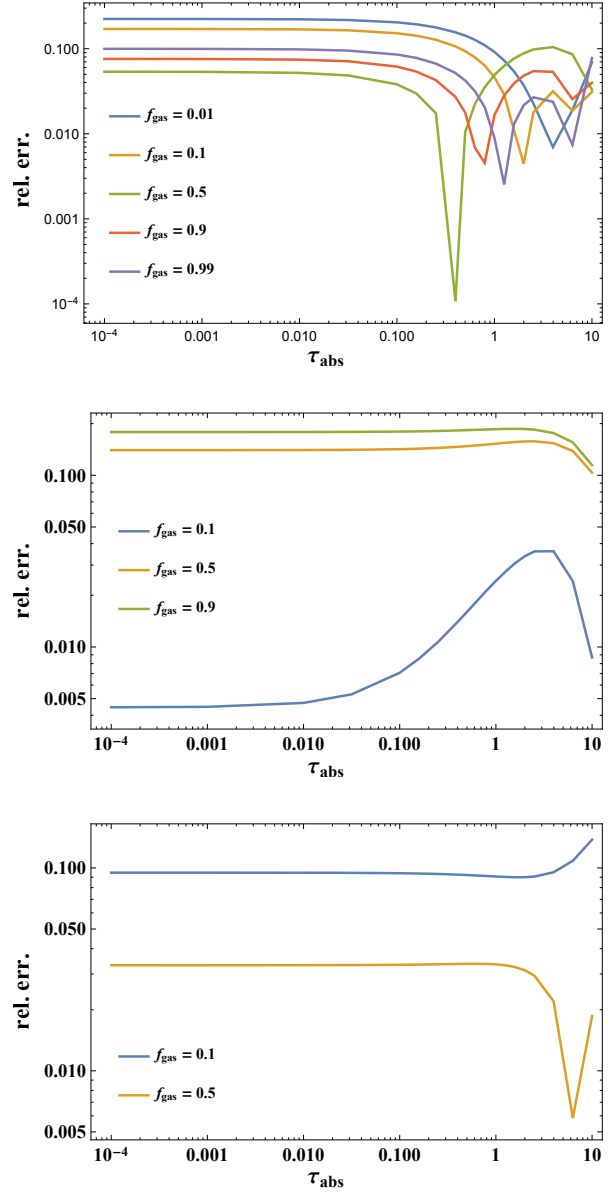


**Figure E1. Relative error between the analytic approximation and the full numerically-determined CR critical Eddington ratio.** From top to bottom, the panels are for  $\tau_s = \{1^3, 1.3^3, 1.5^3\}$ ; gas fractions are as labelled in each panel's legend.

If we now adopt extremal parameters as might pertain in the most vigorous starbursts ( $\chi \rightarrow 10^{-4}$ ,  $\delta v \rightarrow 100$  km/s) this becomes

$$\frac{p_c(\xi)}{s'(\xi)} \gtrsim 10/3, \quad (\text{F2})$$

which might be met close to the midplane for and close to the onset of CR instability (cf. [Figure 2](#)). In principle, the operation of this instability can reduce the diffusivity down

to the Bohm level. Given, however, convective transport imposes a (competitive) lower limit on the effective energy-independent diffusion coefficient for galactic environments, we do not expect any significant from this in-principle occurrence.

This paper has been typeset from a  $\text{\TeX/L\AA\TeX}$  file prepared by the author.